Cellular Mechanics and Intracellular Organization

Yaron R. Silberberg

A thesis submitted for the degree of

Doctor of Philosophy

University College London
London Centre for Nanotechnology
17-19 Gordon Street, London, WC1H 0AH, UK

I, Yaron R. Silberberg, confirm that the work presented in this thesis is my own. Where information has been derived from other sources, I confirm that this has been indicated in the thesis.

Abstract

Mechanical signals affect and regulate many aspects of the cell behaviour, including growth, differentiation, gene expression and cell death. This thesis investigates the manner by which mechanical stress perturbs the intracellular structures of the cell and induces mechanical responses. In order to correlate mechanical perturbations to cellular responses, a combined fluorescence-atomic force microscope (AFM) was used to produce well defined nanomechanical perturbations while simultaneously tracking the real-time motion of fluorescently labelled intracellular organelles in live cells.

By tracking instantaneous displacements of mitochondria far from the point of indentation, insights can be gained into the long-distance propagation of forces and the role of the cytoskeleton in force transmission. Quantitative analysis and tracking of mitochondria, using several image registration and tracking techniques, revealed an increase of approximately 40% in the mean mitochondrial displacement following AFM perturbation. Furthermore, when either the actin cytoskeleton or microtubules were disrupted using anti-cytoskeletal drugs, no significant change in mitochondrial displacement was observed following indentation, revealing the crucial role of both cytoskeletal networks in the long-distance transmission of forces through the cell.

In addition, the effect of retinol and conjugated linoleic acid (CLA), compounds that have diverse effects on various cellular processes, on the mechanical behaviour of the cell was examined: both compounds were found to have a significant detrimental effect on the formation of focal adhesions, which was directly correlated to the measured cell elasticity (Young's modulus) of the cell. Furthermore, quantification of mitochondrial displacements in response to applied AFM perturbations showed force

propagation through the cytoskeleton to be blunted. Treatment of the two compounds in combination showed an additive effect. These results may broaden our understanding of the interplay between cell mechanics and cellular contact with the external microenvironment, and help to shed light on the important role of retinoids and CLA in health and disease.

to Ima and Aba

Acknowledgements

First of all, I would like to thank my supervisor Prof. Mike Horton for giving me this amazing opportunity to work under his supervision in such a unique and inspiring environment, and for providing me with the freedom and resources that allowed me to gain scientific experience both here and in conferences and workshops abroad.

I would like to thank my co-supervisor Dr. Andrew Pelling who was always here to answer any question that I had and to guide me through these three years, and whose positive approach always cheered me up, even when things went tough.

I would like to thank Dr. Gleb Yakubov for the many meetings, fruitful discussions and free (for me at least) lunches, both in London and at Unilever's Colworth Science Park.

For the funding, I would like to thank Unilever and the BBSRC for a CASE studentship, and also the 'Dr. Mortimer and Mrs. Theresa Sackler Trust' and the Wellcome Trust for programme grant support.

Special thanks go to all my friends and colleagues at the London Centre for Nanotechnology, who are either still here or have already left: Marco, Belinda, Steve, Guillaume, Brian, Laurent, Martina, Jenny, Lorenzo, Alastair and anyone I might have forgot to mention - thank you all for being there for me. I will certainly miss all those deep conversations about the meaning of life, over a 99p-pint of beer at the Union Bar.

But most of all, I owe my deepest gratitude to my mom and dad - the best parents in the world - without their unconditional love and support I wouldn't be where I am now.

Table of Contents

Table of Figures

Chapter 1

Introduction

1.1 Overview

The living cell is embedded in a complex mechanical environment, in which its behaviour is constantly influenced by mechanical cues arriving from the extracellular matrix and from neighbouring cells. These signals regulate various cellular processes including differentiation, gene expression and apoptosis. Hence, understanding the mechanisms that are involved in cellular transduction of forces are crucial for understanding how those forces affect the living cell. Recent advances in live cell staining and imaging techniques allow the observation of intracellular structures in high temporal and spatial resolution. In addition, the development of new techniques such as atomic force microscopy allow for the high-precision measurement and application of forces in the nano- and even pico-Newton scale. The ability to visualise changes in the intracellular architecture of the living cell in real time, in response to locally applied extracellular perturbations, together with quantified measurements of changes in cell elasticity, can provide insights into the immediate effect of stress on the behaviour of the cell and on the mechanism in which forces are transmitted through the cell.

This introduction will first provide a background on the use of atomic force microscopy in cell biology, together with a short overview of other techniques used in the investigation of single cell mechanics. Second, it will give a brief description of the cytoskeleton, the mitochondria and the interaction between them. Third, the current models used for describing the mechanical behaviour of the living cell will be discussed. Finally, an outline of the thesis will be given.

1.2 Atomic force microscopy in cell biology

Atomic Force Microscopy (AFM) (Binnig, G. *et al.*, 1986), is a technique which utilizes a fabricated cantilever with a typical length of 100-400 μm is used to raster scan a sample (in the case of imaging), measure nano-scale interaction forces between the tip and the sample, or manipulate an object (Figure 1-1). The tip of the cantilever is usually a pyramid of about 3 μm high, possessing an apex with a diameter ranging typically from 1-60 nm (Figure 1-1b).

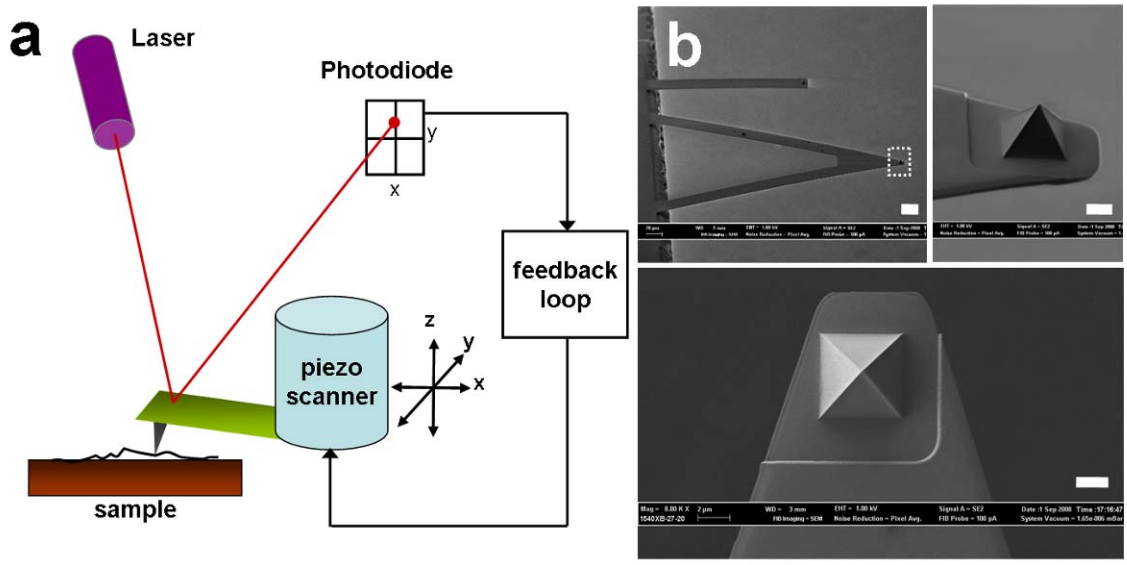

Figure 1-1. AFM diagram and cantilever images.

(a) In imaging, the cantilever raster scans the sample line by line, and topography changes in the sample result in deflection of the cantilever. This leads to changes in the intensity distribution of the laser beam between the 4 segments of the photodiode. The resulted voltage change can then be translated into force units for a known cantilever sensitivity and spring constant, using Hooke's Law: F=-*k*d. (b) Scanning electron microscope (SEM) images of an MSCT cantilever. Scale bars: upper-left: 20 μm, upper-right and bottom: 2 μm.

Cantilevers are usually batch microfabricated from single crystal silicon or silicon-nitride and often coated with a reflective metal such as gold or aluminium. The cantilever is mounted on a piezo-electric ceramic crystal (in the case of the JPK microscope used in these experiments), which can accurately control its position in a three dimensional space under controlled feedback; Some AFM setups, though, use a fixed cantilever, while having the sample mounted on the piezo-scanner instead. A laser beam is reflected from the top side of the cantilever to a four-quadrant photo-detector, which detects both the lateral and vertical deflection of the laser (Figure 1-1a) with a sub-nm vertical resolution limited by the thermal fluctuations of the surrounding medium.

The cantilever can be modelled as a spring, and if the spring constant (k) and the deflection of cantilever (d) are known, the applied force can be calculated using Hooke's Law:

(Eq. 1.1) $$F = -k \cdot d$$

Although the manufacturer usually specifies the k value of the cantilever, the exact value can vary due to the difficulty in controlling the geometry and thickness of the fabricated cantilevers (Levy, R. & Maaloum, M., 2002). There are several methods that can be used to determine k of an AFM cantilever. In this study, k was determined using the 'thermal fluctuation' method (Levy, R. & Maaloum, M., 2002). In this method, the cantilever is modelled as a harmonic oscillator with one degree of freedom that is in equilibrium with its surrounding and will fluctuate in response to thermal noise (Hutter, J.L. & Bechhoefer, J., 1993). The Hamiltonian for this system is:

(Eq. 1.2) $$H = \frac{p^2}{2m} + \frac{1}{2} m \omega_0^2 d^2$$

Here, d is the displacement of the oscillator, m is the oscillating mass, p is the momentum and ω_0 is the resonant frequency. From the equipartition theorem (Hutter, J.L. & Bechhoefer, J., 1993), the average value of each quadratic term in the Hamiltonian is equal to $k_BT/2$, where k_B is the Boltzmann constant and T is the temperature:

(Eq. 1.3) $$\left\langle \frac{1}{2} m \omega_0^2 d^2 \right\rangle = \frac{1}{2} k_B T$$

As $\omega_0^2 = k/m$, the spring constant can be solved from the mean squared displacement:

(Eq. 1.4) $$k = \frac{k_B T}{\left\langle d^2 \right\rangle}$$

This implies that the spring constant of a freely fluctuating cantilever can be estimated when the average square of vertical displacements (d) are sampled at the Nyquist frequency or higher (as determined by its resonant frequency) and the average mean square displacements $<d^2>$ are determined. It is important to note that as there are other sources of noise beside of thermal oscillations, the data should be examined in the frequency domain, in order to isolate their contribution. Then, the spring constant can be calculated by integrating the cantilever resonance in the measured power spectrum, which equals the mean square of the fluctuations (Hutter, J.L. & Bechhoefer, J., 1993). This method is easy to implement, and was found to be an accurate approach for evaluating the spring constant of both rectangular and triangular cantilevers used here and in the majority of modern AFM studies (Levy, R. & Maaloum, M., 2002).

Due to its high resolution capabilities, AFM imaging enables structures to be resolved in the sub-nanometre level and forces in the piconewton range. In addition, the ability to work in an aqueous environment, without the need for sample treatment (such as a special coating or fixation) prior to experiments has made the AFM ideal for use in

investigating biological samples such as live tissues, cells and even single molecules, under physiological conditions. This has facilitated both nanoscale imaging of live cells (Putman, C.A. *et al.*, 1994) and the measurement of various mechanical and material properties of living cells, such as elasticity (Charras, G. & Horton, M.A., 2001; Radmacher, M. *et al.*, 1992) and mechanical dynamics (Pelling, A.E. *et al.*, 2004; Rotsch, C. *et al.*, 1999).

The AFM has become an attractive tool for investigating mechanical and material properties of biological samples in their native conditions. These include the investigation of cellular strain distribution and cytoskeleton disruption in response to stress (Charras, G.T. & Horton, M.A., 2002a), and the extraction of Young's modulus and determination of elasticity properties (Radmacher, M. *et al.*, 1996; Vinckier, A. & Semenza, G., 1998; Wu, H.W. *et al.*, 1998). During such experiments, living cells can be kept at physiological conditions by heating of the stage on which the culture dish is mounted or having the whole microscope apparatus inside a controlled incubator. pH levels can be monitored and adjusted during the experiment using buffered culture media. Recent technical developments have integrated traditional microscopy methods, such as fluorescence and laser scanning confocal microscopes with AFM systems. This has enabled the simultaneous measurement of material properties of living cells and their biological responses and signalling pathways to be made (Charras, G.T. & Horton, M.A., 2002a; Haupt, B.J. *et al.*, 2006; Lehenkari, P.P. *et al.*, 2000). The combined AFM-fluorescence apparatus can also be used to apply controlled mechanical perturbations on the living cell, while imaging the real-time deformations and/or displacements that occur inside the cell, as was done here. Figure 1-2 shows the AFM head mounted on top of an

Olympus IX71 fluorescence microscope (a), and an overlay of optical and florescent images, where mitochondria dyed with MitoTracker Red (Invitrogen) can be seen as red spherical particles (Figure 1-2b). The triangular cantilever of the AFM can be seen on the top-right corner. During the application of predefined forces via the AFM cantilever (Figure 1-2c) both optical and fluorescent images can be acquired.

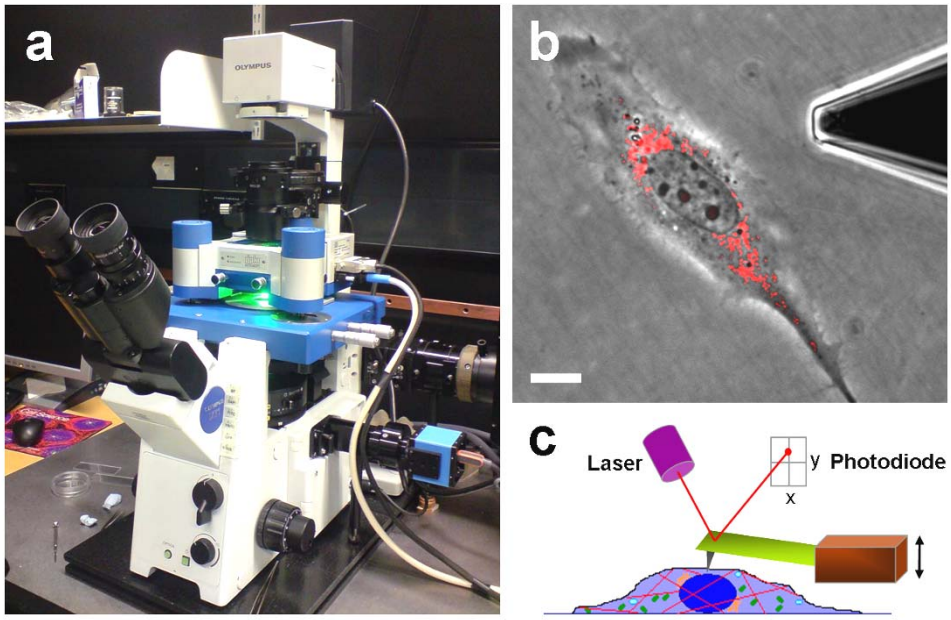

Figure 1-2. AFM-fluorescence microscopy setup for live-cell measurements

The AFM-fluorescence combined microscopy used in our study. (a) The AFM head mounted on Olympus IX71 fluorescence microscope. (b) Overlay of optical and fluorescence images of a NIH-3T3 cell stained with the live-cell mitochondria-specific dye MitoTracker Red (Invitrogen). The top side of the AFM cantilever can be seen on the top-right corner. Scale bar: 10 μm. (c) side-view of the cell with the AFM cantilever indenting from above.

1.2.1 Operation modes of AFM

The most straightforward mode of work is *contact mode*, where the AFM tip is kept in constant contact with the sample throughout the operation. The cantilever is scanned over a predefined area, line by line, in a raster scan fashion. As the cantilever traces the surface topography, it is deflected vertically and causes the reflected laser beam to move

up and down, resulting in voltage changes on the photodiode. This voltage change is fed back to the z-component of the piezo scanner, which control the vertical positioning of the cantilever. This allows one to maintain a set force ('setpoint') between the tip and the sample. This line-by-line scanning reveals the topography of the surface by using the height change of the piezo ('height signal') to map the surface. Another channel that is often recorded during a scan is the 'error signal' (or 'vertical deflection'), which represents the difference between the setpoint and the cantilever deflection. This deflection image, being close to the first derivative of the topography image, emphasizes the edges of surface features and often reveals more subtle information than the topography image does. The disadvantage of this mode is the strong lateral forces exerted by the tip on soft samples such as cells, where the indentation into the probed sample limits the achieved resolution.

In order to overcome the problem of lateral drag forces exerted on the sample, *tapping mode* method can be used (Hansma, P.K. *et al.*, 1994). In this mode, the base of the cantilever is sinusoidally driven at a frequency that is close to the cantilever resonance frequency. Rather than recording the deflection of the cantilever, the amplitude of the resulting cantilever oscillation is recorded and maintained by the feedback system. When the oscillating tip reaches the sample, the amplitude is dampened. The feedback system adjusts the height accordingly, to maintain constant amplitude, and the recorded piezo height represents the surface topography. This method greatly reduces the lateral forces and can achieve resolutions down to the nanometre level, allowing imaging of cells (Putman, C.A. *et al.*, 1994) and single molecules (San Paulo, A. & García, R., 2000). In addition to amplitude detection, it is possible to detect the phase change, i.e., the phase

lag of the cantilever oscillation relative to the signal sent to the piezo scanner. This allows one to gain information about tip-sample interactions and determination of material properties such as elasticity (Chen, X. *et al.*, 1998).

In the study presented here, the focus was mainly on employing the AFM probe as a local indenter rather than a tool for topographical imaging. In addition, the AFM was used to extract mechanical properties of living cells. By analysing the indentation of the tip into the sample as a function of force, the elasticity, or Young's modulus, of the sample can be determined from so-called force-distance curves.

1.2.2 Force curve analysis and Young's modulus derivation

A 'force-distance' curve is obtained by recording the force acting on the AFM cantilever as it lowered into contact with a sample and until it reaches a predetermined setpoint ('approach curve'). At this point the piezo is retracted back to its original point ('retract curve'). The cantilever deflection is recorded as a function of the distance travelled by the piezo. For a rigid surface, such as glass, where there is negligible indentation into the surface, the relationship between the bending of the cantilever and the movement of the piezo is linear (assuming no non-linear time or voltage-dependent behaviour of the photodetector and cantilever). This is normally used for calibration of the deflection sensitivity, converting the photodiode voltage signal (V) into cantilever deflection units (nm). When the cantilever tip is retracted from the surface, surface-tip adhesion forces will cause downwards bending of the cantilever (showing as negative force) and a rupture event that occurs when the tip detaches and leaps back to the non-contact position of zero force (Figure 1-3A).

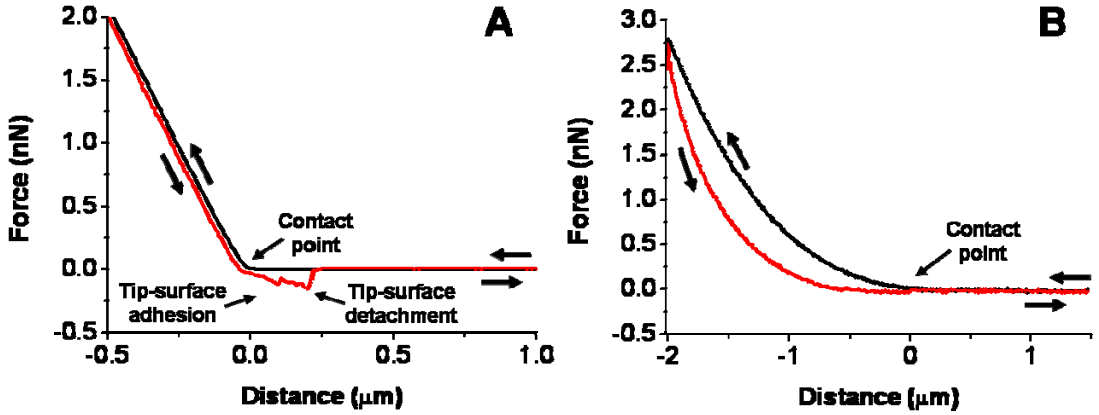

Figure 1-3. AFM force curves obtained on rigid and soft surfaces.

The approach of the cantilever towards the surface starts at the right side of the curve and is represented by a black line. When the cantilever reaches a set force it begins to retract from the sample (red line). (A) A force-distance curve obtained on glass dish in liquid. The contact point between the tip and the rigid surface is easy to locate, and the slope of the curve is linear, as every displacement in the piezo is directly translated to cantilever deflection. Unspecific adhesion event between the tip and the surface can occur and result in what seems as a negative force as the cantilever bends downwards. A rupture events occurs as the tip detaches from the surface and return to its original state. (B) A force-distance curve obtai1ned on a live cell. Here, the contact point is difficult to determine exactly, and the slope of the curve is non-linear due to indentation of the AFM tip into the soft sample.

While for rigid surfaces the slope of the force-distance curve is linear in the contact region (Figure 1-3A), in soft samples such as cells the slope is non-linear due to indentation of the tip into the sample (Figure 1-3B). By analysing the shape of the force-distance curve, materials properties of the sample such as stiffness, or Young's modulus (E), can be determined by using the Hertz model for either a conical (Eq. 1.5) or spherical (Eq. 1.6) indenter (Hertz, H., 1882; Radmacher, M. *et al.*, 1995). Figure 1-4 shows the two types of indenters.

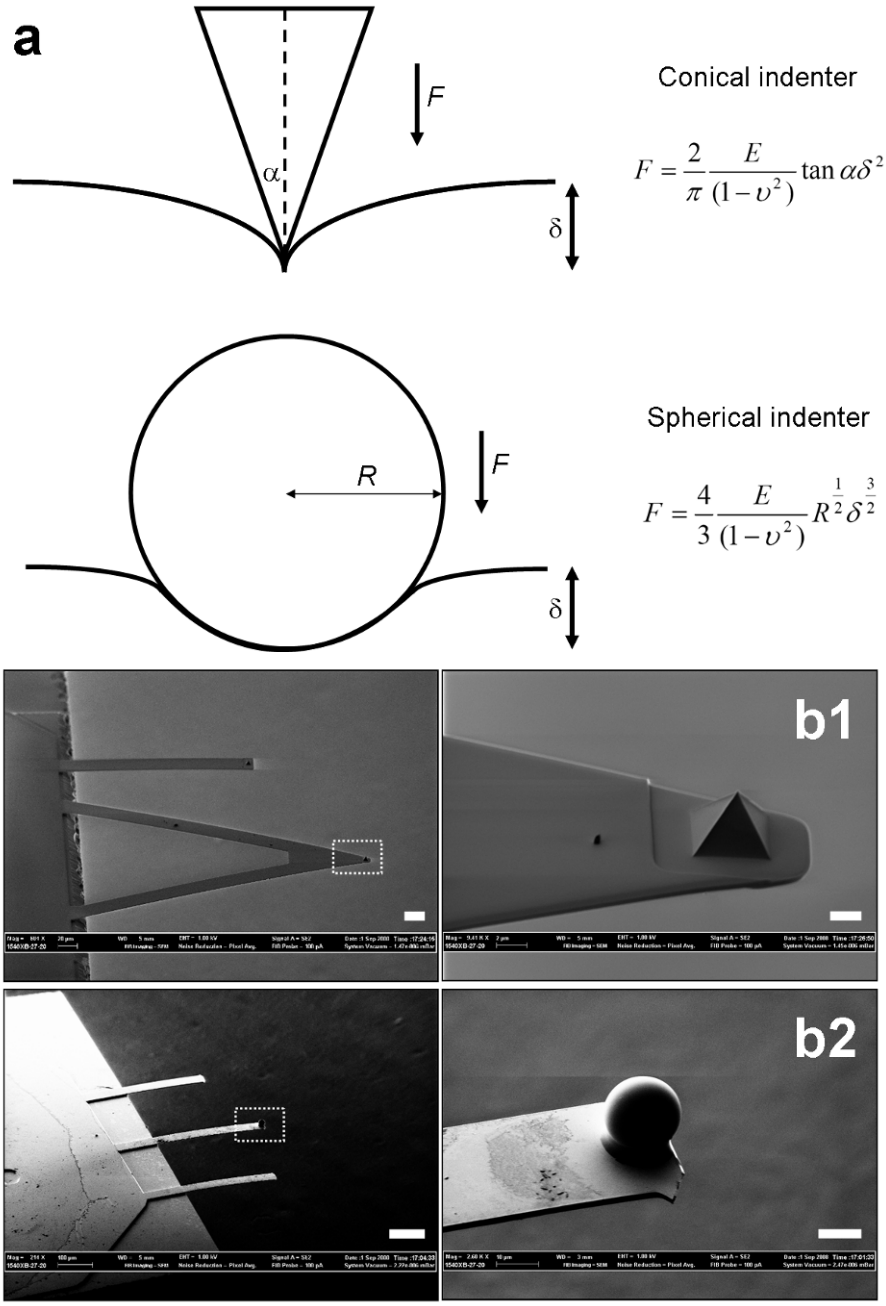

Figure 1-4. Conical and spherical indenters.

(a) Relationships between the force applied (F), Young's modulus of the sample (E) and indentation depth (δ). ν is Poisson's ratio of the sample, α is half the opening angle of the conical indenter, and R is the radius of the spherical indenter. (b) Scanning Electron Microscope (SEM) images of conical (b1) and spherical (b2) indenter. The latter is a Polystyrene microsphere of ~19 μm diameter. Scale bars are: b1, 20 μm (left) and 2 μm (right); b2, 100 μm (left) and 10 μm (right).

(Eq. 1.5) $$F_{cone} = \frac{2}{\pi}\frac{E}{(1-\nu^2)}\tan(\alpha)\delta^2$$

(Eq. 1.6) $$F_{sphere} = \frac{4}{3}\frac{E}{(1-\nu^2)}\sqrt{R}\delta^{3/2}$$

These equations relate between the force (F) that is applied to the sample and the indentation (δ) of the tip into the sample. E is the Young's modulus of the sample. The indentation (δ) can be calculated from the known movement of the piezo (z) and the measured cantilever deflection (d):

(Eq. 1.7) $$\delta = z - d$$

On a rigid substrate, the cantilever deflection (d) equals the piezo displacement (z) and there is no indentation ($\delta = 0$), but on a soft sample such as cell membrane the deflection is reduced by the indentation (δ). The value for cantilever deflection (d) is obtained by dividing the recorded force (F) by the cantilever spring constant (k) (Eq. 1.1).

The other parameters in the equations are: α, the half opening angle of the tip for conical indentation (Eq. 1.5), and R, the sphere radius in the case of sphere indentation (Eq. 1.6). Poisson's ratio (ν) is the ratio between the contraction (the traverse strain) and the extension (axial strain that is in the direction of the applied load) of the material. It is difficult to determine ν for a complex and heterogeneous system such as a cell. Several studies have adopted the convention of assuming a Poisson ratio of 0.3-0.5 for living cells (Mahaffy, R.E. *et al.*, 2004; Maniotis, A.J. *et al.*, 1997; Trickey, W.R. *et al.*, 2006), with consistent results indicating a ν value of ~0.3 to be with agreement with YM measurements (Mahaffy, R.E. *et al.*, 2004; Trickey, W.R. *et al.*, 2006), which was the value used in this study.

A spherical indentation differs from a conical indentation in both the contact area and indentation profile, and the two can be used to compare local versus global stiffness variations (See Chapter 4). Spherical indentation has a much larger surface area (>10 μm^2 for a 200 nm indentation) when compared to a conical indentation where the contact surface area for a 200 nm indentation is < 100 nm^2. The absolute YM values obtained using conical tips are usually higher than those obtained with spherical tips (Radmacher, M. *et al.*, 1995). This is mainly due to the small contact area of the tip with the sample, where the tip is almost in direct contact with single actin filaments and is influenced by their high YM of around ~2GPa (Kojima, H. *et al.*, 1994), and thus force is dissipated directly into the cytoskeleton. On the other hand, the spherical beads have a large contact area with the cell and are more highly influenced by the cell membrane and cytoplasm as it flows through the cytoskeleton in response to the applied force, and force is mainly dissipated into the cytoplasm and membrane.

Fitting of force curves measured on live cells to the Hertz model is usually done for small indentations of <1000 nm. This is in order to minimize the contribution of the stiff substrate, to which the cell adheres, to the YM measurement (Solon, J. *et al.*, 2007). Therefore, deeper indentations will usually result in increasing calculated YM values. Figure 1-5 shows a force-indentation plot, derived from a force curve measurement with a maximum load of 2 nN. The highest calculated value for E was ~3 kPa when the full indentation of ~1.7 μm was fitted with the Hertz model. For lower indentation depths the calculated E was slightly smaller and gradually dropped down to ~2.6 kPa for an indentation of 200 nm (purple line).

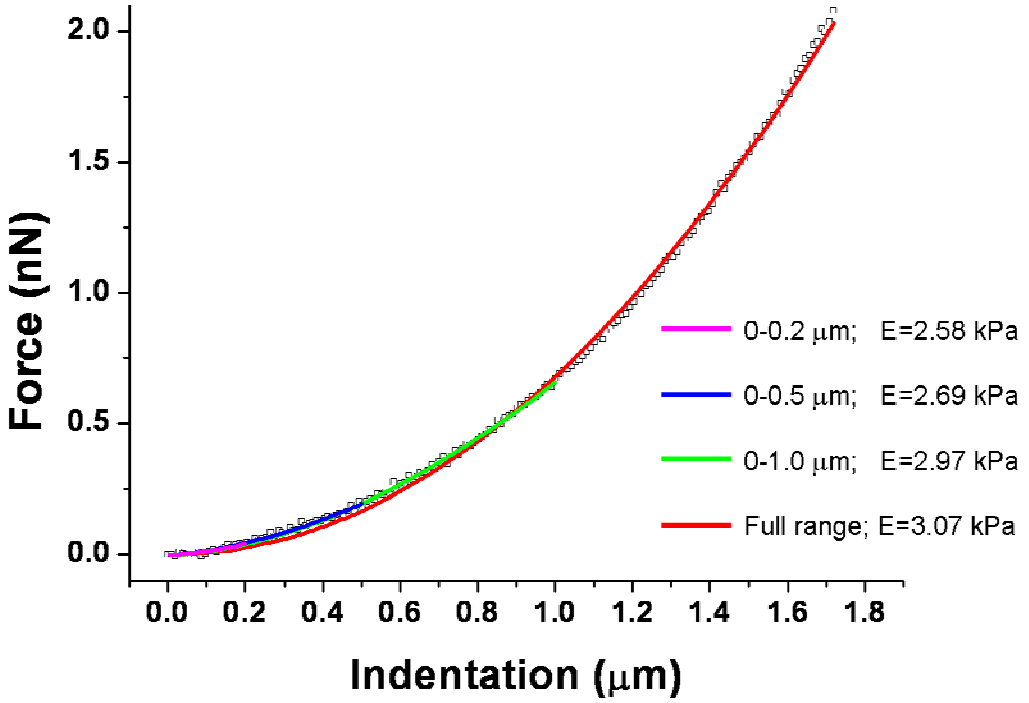

Figure 1-5. Young's modulus as a function of indentation depth fit.

The squares represent the measurement of a single force-curve with a maximum load of 2 nN obtained on a live 3T3 fibroblast cell. The data was then fitted with the Hertz model for a conical indenter, for different indentation depths: 0-200 nm, 0-500 nm, 0-1000 nm and the full 2nN indentation range that corresponded to 0~1700 nm. The corresponding calculated YM values (E) increase together with an increase in indentation.

1.3 Other techniques for investigation of single cell mechanics

This section will present a brief summary of several other important experimental techniques that have contributed to the understanding of the mechanical properties of single cells. A More comprehensive review of the different methods can be found at (Huang, H. *et al.*, 2004) and (Lim, C.T. *et al.*, 2006).

Micropipette aspiration technique involves aspiration of a portion of the cell into a tube with a diameter of a few micrometres (usually between 1-8 μm), using a known suction pressure (typically between 0.1-10^5 Pa). The geometry of the deformation and the known pressure are then used investigating the mechanical properties of the cell (Hochmuth, R.M., 2000). An early example for the use of this methods is the investigation viscoelasticity and cortical tension of red blood cells (Evans, E. & Yeung, A., 1989; Evans, E.A., 1973).

Optical tweezers (laser traps) are a highly sensitive technique in which dielectric spherical beads are trapped at the focus of a laser beam (Ashkin, A., 1997). The surface of the bead is functionalized and can be attached to a cell membrane or other molecules. The laser beam creates a field that 'traps' the bead at the focal point, allowing measurement of forces acting on the bead. Using this method, forces such as those generated by single molecules such as kinesin motors (Kuo, S. & Sheetz, M., 1993) and cytoskeleton-integrin linkage (Choquet, D. *et al.*, 1997) were successfully measured. This method was also used for stretching individual dsDNA molecules and characterising their mechanical behaviour (Smith, S.B. *et al.*, 1996).

Magnetic tweezers technique uses electromagnetic field rather than an optical one, and is used to generate forces on small paramagnetic beads with a typical size of 0.1-5 μm. Resulting displacements of the beads can then be used to deduce mechanical properties of living cell. Beads were functionalized and bound to integrin receptors on the membrane to measure local viscoelastic properties of adherent fibroblast cells (Bausch, A.R. *et al.*, 1998) and their response to deformations (Coughlin, M.F. & Stamenovic, D., 2003). In the magnetic twisting cytometry method, a modification of the above technique, a ferromagnetic bead is twisted vertically and the cell response to sinusoidal perturbations is measured. This allows to measure cell response to varying frequencies (Fabry, B. *et al.*, 2001) and to investigate integrin-cytoskeleton linkage and the transmission of extracellular forces to the cytoskeleton (Wang, N. *et al.*, 1993).

Traction force microscopy technique is useful for measuring traction forces exerted by individual cells plated on a substrate by inspection of the wrinkle formation on the substrate (Harris, A. *et al.*, 1980). Improvement of the method included embedding of beads in the substrate and tracking their displacement in order to elucidate deformation maps (Dembo, M. *et al.*, 1996). Another variation was plating the cells on an array of elastic pillars, allowing measurements local forces due to deflection of individual pillars (Tan, J.L. *et al.*, 2003).

1.4 The cytoskeleton

An elaborated network of filamentous protein fibres is spread throughout the cytoplasm in an organised fashion to form the intracellular cytoskeleton. The cytoskeleton gives cells their mechanical strength, the ability to migrate, to separate chromosomes during cell division and to transport organelles and other cargos throughout the cell. The cytoskeleton forms an elaborated network of tracks on which cargos, both membrane-bound such as the Golgi and mitochondria and non membrane-bound such as mRNA and protein, can be transported (Hirokawa, N., 1998; Vale, R.D., 2003). Three types of filaments that make the cytoskeleton include the actin filaments, intermediate filaments and microtubules. A brief summary of the three is given here (Alberts B., B.D., Lewis J., Raff M., Roberts K. and Watson J.D., 2002).

The *actin filaments* (Figure 1-6, a) are typically located below the plasma membrane and are cross-linked by a variety of proteins, including motor proteins such as myosin, which can generate forces and perform mechanical work. They are assembled from subunits called G-actin and are roughly 8 nm thick in diameter. The filaments are also linked to the plasma membrane through the membrane-spanning integrins, allowing signals from the extracellular matrix to be transmitted to the cytoskeleton, and vice versa (Burridge, K. & Chrzanowska-Wodnicka, M., 1996; Maniotis, A.J. *et al.*, 1997).

Microtubules (Figure 1-6, b) are hollow, cylindrical filaments of approximately 25 nm in diameter, which are formed by the assembly of tubulin monomers. Individual microtubules originate from the centrosome that is near the nucleus, and can span the entire cell. They play an important role in organelle transport and organization, in cell

division and chromosome distribution, and in mechanical stabilisation of the cell (Ingber, D.E., 1993).

Intermediate filaments (Figure 1-6, c), unlike actin filaments and microtubules, are not polarised and are made of elongated polypeptide rods that are arranged in a coiled-coil structure of about 8-10 nm in diameter. They are located in two separate systems, one in the nucleus and one in the cytoplasm. Their main role is believed to be that of a passive mechanical absorber and providing of structural reinforcement, particularly in cells that need to withstand strong mechanical stress such as epithelial cells (Herrmann, H. *et al.*, 2007). Apart from the structural contribution, intermediate filaments were found to have cell-type specific physiological roles and also contribute to some gene-expression programmes (Herrmann, H. *et al.*, 2007).

Various *motor proteins* are associated with actin filaments and microtubules (Vale, R.D., 2003). They act as transporters for delivering vesicles and moving organelles around the cell, and as generators of mechanical force that control functions such as cell division and migration. Three major motor classes are the myosin, dynein and kinesin. The myosins interact with actin filaments and generate contractile stresses. They can form actomyosin complexes, by interacting with neighbouring filaments, and generate relative movement and active stress within the actin network. Kinesin and dynein are microtubule-associated motor proteins and are capable of directed motion towards either the plus-end or minus-end of the microtubule, respectively. They have a crucial role in the transportation of proteins, vesicles and other organelles throughout the cell (Huang, J.D. *et al.*, 1999).

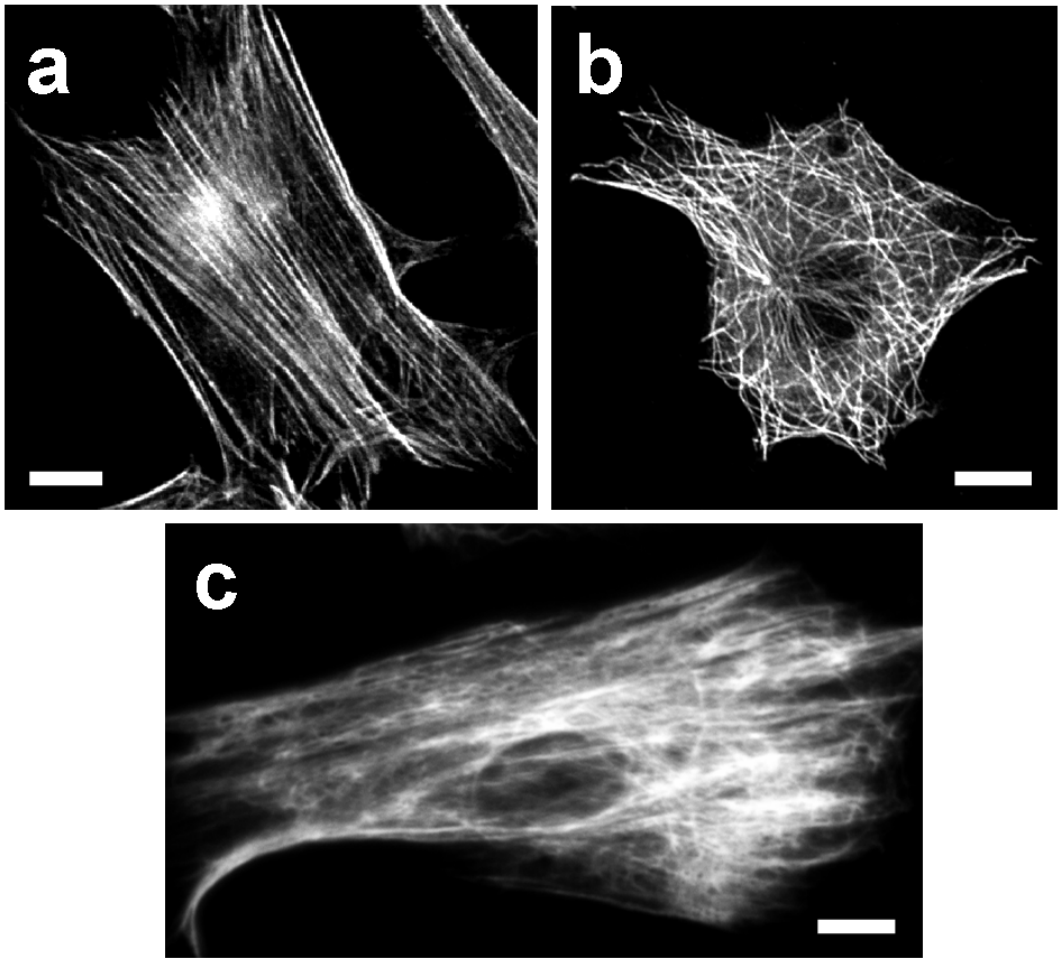

Figure 1-6. Actin filaments, microtubules and intermediate filaments.

Fluorescent images of 3T3 fibroblast cells fixed and stained for either the actin filaments (a, stained with Phalloidin Alexa Fluor 488), microtubules (b, stained with Alexa Fluor 546-conjugated α-tubulin antibodies) and intermediate filaments (Alexa Fluor 488-conjugated vimentin antibody). Scale bars are 10 μm.

1.5 The mitochondria

Mitochondria were discovered 60 years ago and are known to be the organelles in which oxidative energy metabolism takes place, generating most of the cell's supply of ATP (Kennedy, E.P. & Lehninger, A.L., 1949). Mitochondria range in size but are typically between 0.5μm to 1μm long, and there are typically hundreads to thousands of mitochondria per cell, depending on cell type, making up 15-20% of the cell volume (Bereiterhahn, J. & Voth, M., 1994). Mitochondria are highly dynamic organelles and constantly change their shape and location in the cell (Okamoto, K. & Shaw, J.M., 2005). The morphology of mitochondria varies between cell types and between cell states. Constant fusion and fission events govern the dynamic morphology of mitochondria, ranging from elaborated, branched networks (formed by fusion of individual mitochondria) to small bean-shaped individual mitochondria (due to mitochondrial fission) that are dispersed throughout the cytoplasm (Okamoto, K. & Shaw, J.M., 2005; Shaw, J.M. & Nunnari, J., 2002).

Mitochondria are transported throughout the cell on the actin and microtubule cytoskeletal networks. Microtubules were the first cytoskeletal element found to be directly associated with mitochondria (Heggeness, M.H. *et al.*, 1978) and are used by mitochondria for active transportation throughout the cell, facilitated by cargo-carrying microtubule motors dynein and kinesin, which make the predominant mechanism for mitochondrial movement (Lee A. Ligon, O.S., 2000; Vale, R.D., 2003).

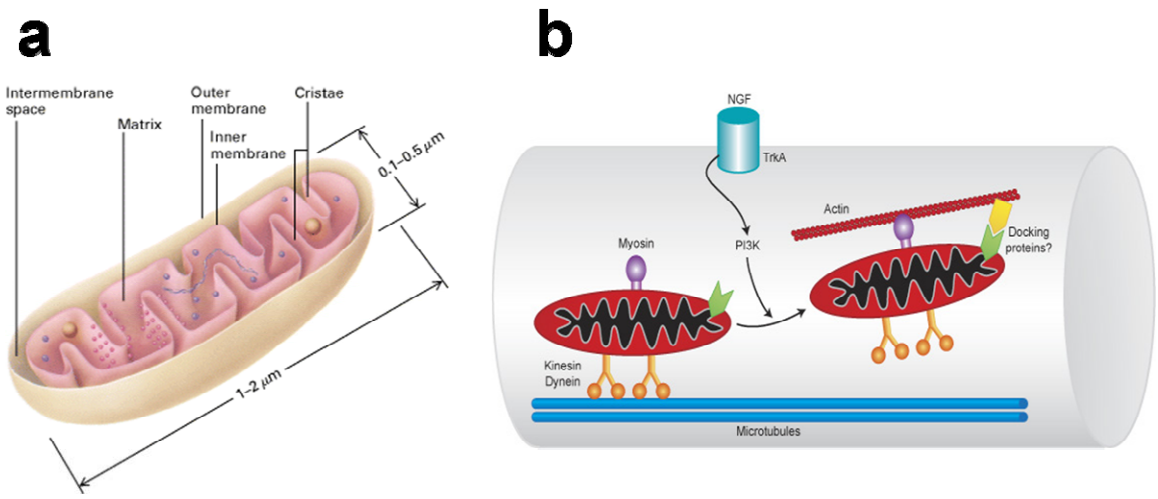

Figure 1-7. Mitochondrial structure and cytoskeleton transportation.

Mitochondria use both the actin filaments and microtubules for intracellular transportation (with the aid of motor proteins such as kinesin, dynein and myosin) and are also shown to leap from one type of filaments to the other (b). a, from (Lodish, H. *et al.*, 1995) ; b, from (Reynolds, I.J. & Rintoul, G.L., 2004).

More recent studies showed that actin filaments also have an important role in facilitating mitochondrial organization in yeast (Drubin, D. *et al.*, 1993) and vertebrate neurons (Morris, R. & Hollenbeck, P., 1995), and controlling mitochondrial movement and morphology (Rudiger Suelmann, R.F., 2000). Transportation on actin filaments is facilitated by myosins (Vale, R.D., 2003), and is usually over shorter distances, in comparison with microtubule transport (Kulik, A.V. *et al.*, 2006; Romagnoli, S. *et al.*, 2007). Leaping of mitochondria between actin filaments and microtubules, in vitro, has also been observed (Reynolds, I.J. & Rintoul, G.L., 2004; Romagnoli, S. *et al.*, 2007).

Given the direct association of mitochondria with the intracellular cytoskeleton, its abundance throughout the cytoplasm and the readily available live-cell mitochondrial dyes, this organelle was an ideal choice to be used as a natural cellular marker for investigation of force transduction in live cells (see Chapters 2 and 3).

1.6 Mechanical models of the cell

Mechanical forces affect and regulate essential cellular processes, such as gene expression, migration, protein synthesis and proliferation (Alenghat, F.J. & Ingber, D.E., 2002; Chen, K.D. *et al.*, 1999; Janmey, P.A. & McCulloch, C.A., 2007). In addition to other environmental signals, mechanical forces can induce morphological changes and affect various signalling pathways in the cell (Ingber, D.E., 1997). Examples include the effect of mechanical load on cytoskeletal stiffening (Wang, N. *et al.*, 1993), on phosphorylation of kinases (Takahashi, M. *et al.*, 1997), and on activation of growth factors (Sadoshima, J. & Izumo, S., 1997). A more recent study even shows how direct mechanical stretching of an actin stress fibre can activate mechanosensitive ion channels in eukaryotic cells (Hayakawa, K. *et al.*, 2008). Also, mechanical force was shown to regulate the expression of various genes and even block cell cycle progression in colon cancer cells (Avvisato, C.L. *et al.*, 2007). Different mechanical models have been developed, which aim to explain experimental observations and to describe the mechanical environment of the living cell. However, there is no one 'correct' model that could perfectly describe the mechanical nature of the cell. The ability of a model to describe an experimental observation is highly dependent on the type of cell, the experimental conditions, the size scale of the observation and also the time scale (Zhu, C. *et al.*, 2000).

Early studies of cell mechanics considered the cell as a homogenous continuum structure and looked at the distribution of stress and strain on the cellular level. From models simulating the cell as a viscous fluid surrounded by a cortical shell (Evans, E. & Yeung, A., 1989) and later on more complex models, which take into consideration two

different tensions of both a plasma membrane and a nuclear membrane, together with two separate viscosities for the cytoplasm and the nucleus interior (Dong, C. *et al.*, 1991; Hochmuth, R.M. *et al.*, 1993; Kan, H.C. *et al.*, 1998; Theret, D.P. *et al.*, 1988). These models were adequate in explaining some experimental observations, such as blood granulocytes flow (Evans, E. & Yeung, A., 1989) and whole-cell deformations of leukocytes (Dong, C. *et al.*, 1988) during micropipette aspiration. However, In spite of being an accurate representation of the cell, these models failed to explain certain observations, such as the recovery of cells back to their original shape after being expelled from the micropipette (Tran-Son-Tay, R. *et al.*, 1998). In addition, treating suspended cells as a continuum would suit when describing whole-cell deformations, but would not be adequate for smaller scale mechanical observations (Zhu, C. *et al.*, 2000).

In recent years it had become more and more apparent that many other observations cannot be accounted for by using the continuum approach alone. These include the non-uniformity of the distribution of strain throughout the cell (Bausch, A.R. *et al.*, 1998; Helmke, B.P. *et al.*, 2003; Helmke, B.P. *et al.*, 2001), and the propagation of forces over long distances across the cytoskeleton (Maniotis, A.J. *et al.*, 1997). The main limitation of the continuum models is not taking into account the heterogeneous interior of the cell, which includes various cellular organelles, cytoskeleton and nucleus. This idea led to the development of ‘discrete’ models, which take into consideration the role of discrete cytoskeletal structures in describing the mechanical behaviour of the cell.

The shape and the mechanical properties of tissue cells depend largely on the cytoskeleton and on the ECM to which the cells are anchored. As described in 1.4, the cytoskeleton consists of actin filaments, intermediate filaments and microtubules. These

three filamentous systems are not only believed to maintain the mechanical stability of the cell but also to provide mechanical interactions all the way from the membrane down to the nucleus (Ingber, D.E., 1993; Wang, N. *et al.*, 1993). A structural model that is based on Buckminster Fuller's theory of synergy between balanced tension and compression components is the *tensegrity model* (Ingber, D.E., 1993). This model describes a system that is made of tensile elements, cables, which are under constant tensile tension and provide the stability and shape to the structure. This is tension is often termed 'prestress'. In the cell, the actin filaments of the CSK are usually regarded as the tensed cables. The counter-balance to the tensed cables can be provided both externally (by the extracellular matrix, in the case of a cell) and internally (by compression-resistant elements of the cytoskeleton). During externally applied stress, actin filaments do not bend or twist, but rather rotate, change their spacing and length to regain equilibrium.

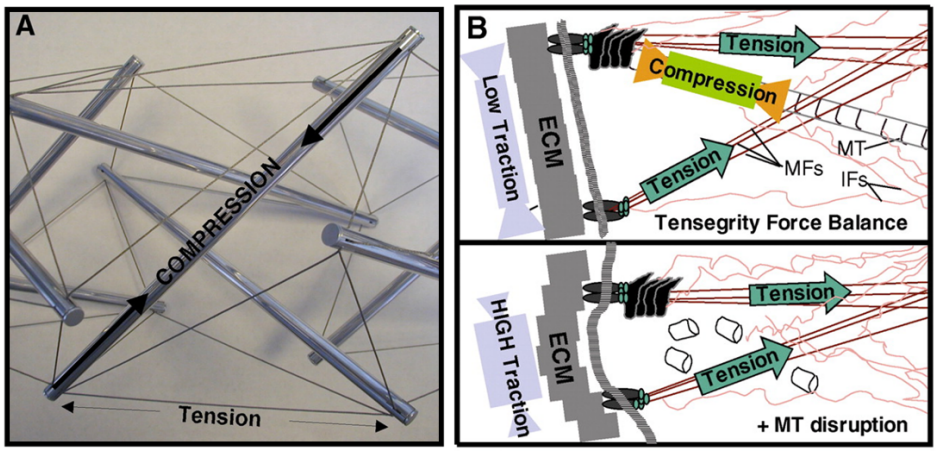

Figure 1-8. The cell as a tensegrity model.

(A) A sculpture by Kenneth Snelson that first visualised the tensegrity model. Tensed cables are supported by compression-bearing rods. (B) A diagram of the force balance between tensed actin microfilaments (MFs), intermediate filaments (IFs), compressed microtubules (MTs) and the ECM. Compressive forces borne by microtubules (top) are transferred to ECM adhesions when microtubules are disrupted (bottom) causing substrate traction (see text for details). From (Ingber, D.E., 2003a).

In the tensegrity model, as shown in Figure 1-8, the tension of the tensile elements (cables) is balanced by compressive elements (rods). This interaction between the tensile and compressive networks gives the cell its mechanical stability. In adherent cells, the actin filaments are regarded as tensile elements, while microtubules are regarded as compression elements. In addition, the extracellular matrix also balances some of the CSK tension. According to this model, therefore, the CSK works together with the extracellular matrix to form a stable, mechanical system (Ingber, D.E., 1993; Stamenovic, D. & Ingber, D.E., 2002). According to the tensegrity model, the role the actin network (combined with dynamic actin-myosin interactions) is to carry the prestress, distributing it throughout the cell to maintain shape and stability, while the role of microtubules is to carry compression to balance this prestress. When large loads are applied, the role of the intermediate filaments in tension-bearing becomes more crucial, while under small loads their contribution is negligible (Maniotis, A.J. *et al.*, 1997; Wang, N. & Stamenovic, D., 2000). The tensegrity model helped identifying the relative contributions of the different CSK components to the observed behaviours. Treatments with microtubule-disrupting drugs led to observed increase in the traction forces exerted by the cell to the underlying substrate, confirming their role as compression-bearing elements (Stamenovic, D. & Ingber, D.E., 2002; Wang, N. *et al.*, 2001). A more recent study showed the existence of tensile stress in actin filaments, where single actin stress fibres recoiled following incision with laser nanoscissors (Kumar, S. *et al.*, 2006).

However, being a rather simplistic way of describing the balance of mechanical forces in the living cell, some observations do not support the tensegrity model and there is still much debate about the validity and universality of this theory (Ingber, D.E. *et al.*,

2000). One example is the highly localized responses observed in fibroblasts in response to mechanical probing, rather than integrated, spatially broad responses that would have been predicted by the tensegrity model (Heidemann, S.R. *et al.*, 1999). Another important point of dispute is the lack of temporal dimension to the tensegrity theory, i.e. not being able to take into consideration the time-dependency of many mechanical observations (Buxbaum, R. *et al.*, 1987; Ingber, D.E. *et al.*, 2000; Thoumine, O. & Ott, A., 1997).

Other discrete models include the percolation model and the cellular solid model. These models look at the actin network for describing the mechanical behaviour of the cell. The percolation model (Forgacs, G., 1995) uses phase transitions, which are caused by intracellular changing of polymer concentration, to describe the changes in network connectivity, rather then relying on a constant prestress in the system as does the tensegrity model. The cellular solid model, suggested by Satcher and Dewey, models the cytoplasm of endothelial cells as solid foam, due to the complex interconnected network of actin filaments, and looks at the bending of actin filaments to describe the cell's resistance to deformations (Satcher, R.L. & Dewey, C.F., 1996).

Another important approach for describing the mechanical behaviour of the cell is presented by the poroelasticity model, which attempts to combine the structural and continuum approaches, and explain phenomena's such as local variations in cytoplasmic pressure, which neither continuum nor structural models can adequately account for on their own (Charras, G.T. *et al.*, 2008; Mitchison, T.J. *et al.*, 2008). According to this model, the localization of pressure, such as that involved in formation of cellular blebs (Charras, G.T. *et al.*, 2005), might be explained by modelling the cytoplasm as a porous, contractile, elastic network (consisting of cytoskeletal filaments and other organelles),

that is infiltrated with the cytoplasmic fluid (consisting of the cytosol, water, ions and proteins), in a way similar to fluid-filled sponge. Contraction of the acto-myosin cytoskeletal cortex creates a compressive stress that leads to localized hydrostatic pressure, which then results in cytosol flow and bleb formation (Charras, G.T. *et al.*, 2005; Wang, H., 2000) .

To summarize, for describing experimental observations and to better understand the cell behaviour, there is a need for a suitable model that explains the mechanism of force transmission through the cytoskeleton and throughout the cell as a whole. Different models attempt to explain and predict different observations. However, to date, no complete mechanical model of the cell has been proposed which does not contain obvious disparities with experimental data. Different models suit different circumstances and can be used to explain specific phenomena. Depending on the experimental conditions and the scale (both spatial and temporal), identical cells can be viewed as either a continuum or a discrete collection of structural elements, and be described using different mechanical models. An obvious example is when considering whole cell deformations, where a continuum model would give close approximations. However, when the force probe is on the scale of an AFM tip, and the observations include intracellular changes in the nucleus or cytoskeleton, then a model that takes into consideration the internal organisation of the filaments would be more appropriate.

1.7 Aims and motivation

Previous studies have been carried out to investigate the cell's response to mechanical stress, mainly by looking at changes in gene expression, protein synthesis patterns and signalling pathways. The main objective of the research contained in this thesis was to investigate the first step of cellular mechanotransduction, which is the deformation and displacement that occur in the cellular organelles and architecture in response to externally applied mechanical force. These immediate changes in the intracellular architecture would consequently lead to biochemical changes that go to affect various aspects of cell behaviour such as growth, differentiation, motility and apoptosis.

The ability of the atomic force microscope to be used both as a high precision micromanipulator/indenter and as a probe that allows to measure the mechanical properties of live cells in their physiological conditions made it an attractive tool for investigating the mechanical behaviour of cells. Furthermore, the ability to combine the use of the AFM with simultaneous optical and fluorescence observations allows the real-time visualisation of the changes in the intracellular architecture that follow an externally applied stress.

In this study, we aim to investigate the immediate response of the living cell to an externally applied stress, by observing and quantifying the instantaneous displacements and deformations of intracellular components. By using intracellular organelles as natural markers for the mechanical response of the cell to applied stress, we aim to better understand the way forces are transmitted through the cell and to elucidate the role of the cytoskeleton in force transmission. In addition, we aim to learn more about the interplay

between cell stiffness, adhesion to the substrate and the cellular transmission of forces through the cell.

1.8 Thesis outline

Chapter 2 will outline the techniques and methodology used for visualising displacements of intracellular organelles in response to local indentations applied by the AFM. This will follow with the particular observations of mitochondrial displacements and explanation as to the advantage of using this organelle for the study of cellular force transmission.

Chapter 3 will present two tracking algorithms that were used for quantifying mitochondrial displacements: fluid registration analysis and the feature point tracking algorithm. Quantitative results will be presented of both the natural and force-induced mitochondrial displacements in response to nanomechanical AFM perturbations. The suitability of the two registration techniques for tracking and quantifying displacements of mitochondria will be discussed.

Chapter 4 will investigate the hypothesis of the cytoskeleton's role in cellular force transmission. The effect of cytoskeletal disruption has on both force transmission and cell stiffness will be investigated. Mitochondrial displacements, both natural and force-induced, in cells treated with either the actin-disrupting drug CytD or the microtubule-disrupting drug nocodazole, will be compared with those of untreated cells.

Chapter 5 will look into the effect of two compounds – retinol and conjugated linoleic acid – on certain aspects of the mechanical behaviour of the cell. The effect of these compounds, both individually and in combination, on cell adhesion to the substrate

will be investigated together with the correlation to the measured changes in cell stiffness. The displacement of mitochondria following local indentations and the interplay between force transmission, cell stiffness and adhesion will be discussed.

The final chapter will summarize the findings of this study and will discuss their significance and the implications they have for understanding the mechanical behaviour and force transduction in cells. The advantages of combining complementary techniques for the investigation of cell biology will be discussed, together with suggestions for future experiments.

1.9 Published work

Chapters 2, 3 and 4 present data published in:

Silberberg Y.R., Pelling A.E., Yakubov G.E., Crum W.R., Hawkes D.J., Horton M.A. (2008). "Mitochondrial displacements in response to nanomechanical forces". *Journal of Molecular Recognition* 21:30-36, and

Silberberg Y.R., Pelling A.E., Yakubov G.E., Crum W.R., Hawkes D.J., Horton M.A. 2008. "Tracking displacements of intracellular organelles in response to nanomechanical forces". Biomedical Imaging: From Nano to Macro (2008). *5th IEEE International Symposium* on 14-17 May 2008. Page(s):1335 - 1338.

Chapter 5 is a version of:

Silberberg Y.R., Pelling A.E., Yakubov G.E., Horton M.A. (2009). "Cell nanomechanics and focal adhesions are regulated by retinol and conjugated linoleic acid in a dose dependent manner". *Nanotechnology* 20:285103.

1.10 References

Alberts B. B.D., Lewis J., Raff M., Roberts K. and Watson J.D. (2002). *Molecular biology of the cell*, Garland Science Publ, New York.

Alenghat F.J.,Ingber D.E. 2002. Mechanotransduction: All signals point to cytoskeleton, matrix, and integrins. *Sci. STKE* 2002:pe6-.

Ashkin A. 1997. Optical trapping and manipulation of neutral particles using lasers. *Proceedings of the National Academy of Sciences of the United States of America* 94:4853-4860.

Avvisato C.L., Yang X., Shah S., Hoxter B., Li W.Q., Gaynor R., Pestell R., Tozeren A.,Byers S.W. 2007. Mechanical force modulates global gene expression and beta-catenin signaling in colon cancer cells. *Journal of Cell Science* 120:2672-2682.

Bausch A.R., Ziemann F., Boulbitch A.A., Jacobson K.,Sackmann E. 1998. Local measurements of viscoelastic parameters of adherent cell surfaces by magnetic bead microrheometry. *Biophys. J.* 75:2038-2049.

Bereiterhahn J.,Voth M. 1994. Dynamics of mitochondria in living cells - shape changes, dislocations, fusion, and fission of mitochondria. *Microscopy Research and Technique* 27:198-219.

Binnig G., Quate C.F.,Gerber C. 1986. Atomic force microscope. *Physical Review Letters* 56:930-933.

Burridge K.,Chrzanowska-Wodnicka M. 1996. Focal adhesions, contractility, and signaling. *Annual Review of Cell and Developmental Biology* 12:463-518.

Buxbaum R., Dennerll T., Weiss S.,Heidemann, SR. 1987. F-actin and microtubule suspensions as indeterminate fluids. *Science* 235:1511-1514.

Charras G.,Horton M.A. 2001. Cellular mechanotransduction and its modulation: An atomic force microscopy study. *Biophysical Journal* 80:305A-306A.

Charras G.T., Coughlin M., Mitchison T.J.,Mahadevan L. 2008. Life and times of a cellular bleb. 94:1836-1853.

Charras G.T.,Horton M.A. 2002. Determination of cellular strains by combined atomic force microscopy and finite element modeling. *Biophys. J.* 83:858-879.

Charras G.T., Yarrow J.C., Horton M.A., Mahadevan L.,Mitchison T.J. 2005. Non-equilibration of hydrostatic pressure in blebbing cells. 435:365-369.

Chen K.D., Li Y.S., Kim M., Li S., Yuan S., Chien S.,Shyy J.Y.J. 1999. Mechanotransduction in response to shear stress - roles of receptor tyrosine kinases, integrins, and shc. *Journal of Biological Chemistry* 274:18393-18400.

Chen X., Davies M.C., Roberts C.J., Tendler S.J.B., Williams P.M., Davies J., Dawkes A.C.,Edwards J.C. 1998. Interpretation of tapping mode atomic force microscopy data using amplitude-phase-distance measurements. *Ultramicroscopy* 75:171-181.

Choquet D., Felsenfeld D.P.,Sheetz M.P. 1997. Extracellular matrix rigidity causes strengthening of integrin-cytoskeleton linkages. *Cell* 88:39-48.

Coughlin M.F.,Stamenovic D. 2003. A prestressed cable network model of the adherent cell cytoskeleton. *Biophysical Journal* 84:1328-1336.

Dembo M., Oliver T., Ishihara A.,Jacobson K. 1996. Imaging the traction stresses exerted by locomoting cells with the elastic substratum method. *Biophysical Journal* 70:2008-2022.

Dong C., Skalak R.,Sung K.L.P. 1991. Cytoplasmic rheology of passive neutrophils. *Biorheology* 28:557-567.

Dong C., Skalak R., Sung K.L.P., Schmidschonbein G.W.,Chien S. 1988. Passive deformation analysis of human-leukocytes. *Journal of Biomechanical Engineering-Transactions of the Asme* 110:27-36.

Drubin D., Jones H.,Wertman K. 1993. Actin structure and function: Roles in mitochondrial organization and morphogenesis in budding yeast and identification of the phalloidin- binding site. *Mol. Biol. Cell* 4:1277-1294.

Evans E.,Yeung A. 1989. Apparent viscosity and cortical tension of blood granulocytes determined by micropipet aspiration. *Biophysical Journal* 56:151-160.

Evans E.A. 1973. New membrane concept applied to the analysis of fluid shear- and micropipette-deformed red blood cells. *Biophysical Journal* 13:941-954.

Fabry B., Maksym G.N., Butler J.P., Glogauer M., Navajas D.,Fredberg J.J. 2001. Scaling the microrheology of living cells. *Physical Review Letters* 8714:

Forgacs G. 1995. On the possible role of cytoskeletal filamentous networks in intracellular signaling: An approach based on percolation. *J Cell Sci* 108:2131-2143.

Hansma P.K., Cleveland J.P., Radmacher M., Walters D.A., Hillner P.E., Bezanilla M., Fritz M., Vie D., Hansma H.G., Prater C.B., Massie J., Fukunaga L., Gurley J.,Elings V. 1994. Tapping mode atomic-force microscopy in liquids. *Applied Physics Letters* 64:1738-1740.

Harris A., Wild P.,Stopak D. 1980. Silicone rubber substrata: A new wrinkle in the study of cell locomotion. *Science* 208:177-179.

Haupt B.J., Pelling A.E.,Horton M.A. 2006. Integrated confocal and scanning probe microscopy for biomedical research. *TheScientificWorldJOURNAL* 6:1609-1618.

Hayakawa K., Tatsumi H.,Sokabe M. 2008. Actin stress fibers transmit and focus force to activate mechanosensitive channels. *J Cell Sci* 121:496-503.

Heggeness M.H., Simon M.,Singer S.J. 1978. Association of mitochondria with microtubules in cultured cells. *PNAS* 75:3863-3866.

Heidemann S.R., Kaech S., Buxbaum R.E.,Matus A. 1999. Direct observations of the mechanical behaviors of the cytoskeleton in living fibroblasts. *J. Cell Biol.* 145:109-122.

Helmke B.P., Rosen A.B.,Davies P.F. 2003. Mapping mechanical strain of an endogenous cytoskeletal network in living endothelial cells. *Biophys. J.* 84:2691-2699.

Helmke B.P., Thakker D.B., Goldman R.D.,Davies P.F. 2001. Spatiotemporal analysis of flow-induced intermediate filament displacement in living endothelial cells. *Biophys. J.* 80:184-194.

Herrmann H., Bar H., Kreplak L., Strelkov S.V.,Aebi U. 2007. Intermediate filaments: From cell architecture to nanomechanics. 8:562-573.

Hertz H. 1882. Über die berührung fester elastischer körper. *J. reine angewandte Matematik* 92:156-171.

Hirokawa N. 1998. Kinesin and dynein superfamily proteins and the mechanism of organelle transport. *Science* 279:519-526.

Hochmuth R.M. 2000. Micropipette aspiration of living cells. *Journal of Biomechanics* 33:15-22.

Hochmuth R.M., Tingbeall H.P., Beaty B.B., Needham D.,Transontay R. 1993. Viscosity of passive human neutrophils undergoing small deformations. *Biophysical Journal* 64:1596-1601.

Huang H., Kamm R.D.,Lee R.T. 2004. Cell mechanics and mechanotransduction: Pathways, probes, and physiology. *Am J Physiol Cell Physiol* 287:C1-11.

Huang J.D., Brady S.T., Richards B.W., Stenoien D., Resau J.H., Copeland N.G.,Jenkins N.A. 1999. Direct interaction of microtubule- and actin-based transport motors. *Nature* 397:267-270.

Hutter J.L.,Bechhoefer J. 1993. Calibration of atomic-force microscope tips. *Review of Scientific Instruments* 64:1868-1873.

Ingber D.E. 1993. Cellular tensegrity - defining new rules of biological design that govern the cytoskeleton. *Journal of Cell Science* 104:613-627.

Ingber D.E. 2003. Tensegrity i. Cell structure and hierarchical systems biology. *Journal of Cell Science* 116:1157-1173.

Ingber D.E. 1997. Tensegrity: The architectural basis of cellular mechanotransduction. *Annual Review of Physiology* 59:575-599.

Ingber D.E., Heidemann S.R., Lamoureux P.,Buxbaum R.E. 2000. Opposing views on tensegrity as a structural framework for understanding cell mechanics. *J Appl Physiol* 89:1663-1678.

Janmey P.A.,McCulloch C.A. 2007. Cell mechanics: Integrating cell responses to mechanical stimuli. *Annual Review of Biomedical Engineering* 9:1-34.

Kan H.C., Udaykumar H.S., Shyy W.,Tran-Son-Tay R. 1998. Hydrodynamics of a compound drop with application to leukocyte modeling. *Physics of Fluids* 10:760-774.

Kennedy E.P.,Lehninger A.L. 1949. Oxidation of fatty acids and tricarboxylic acid cycle intermediates by isolated rat liver mitochondria. *J. Biol. Chem.* 179:957-972.

Kojima H., Ishijima A.,Yanagida T. 1994. Direct measurement of stiffness of single actin filaments with and without tropomyosin by in vitro nanomanipulation. *Proceedings of the National Academy of Sciences of the United States of America* 91:12962-12966.

Kulik A.V., Nekrasova O.E.,Minin A.A. 2006. Mitochondria motility is regulated by f-actin. *Biologicheskie Membrany* 23:42-51.

Kumar S., Maxwell I.Z., Heisterkamp A., Polte T.R., Lele T.P., Salanga M., Mazur E.,Ingber D.E. 2006. Viscoelastic retraction of single living stress fibers and its impact on cell shape, cytoskeletal organization, and extracellular matrix mechanics. *Biophysical Journal* 90:3762-3773.

Kuo S.,Sheetz M. 1993. Force of single kinesin molecules measured with optical tweezers. *Science* 260:232-234.

Lee A. Ligon O.S. 2000. Role of microtubules and actin filaments in the movement of mitochondria in the axons and dendrites of cultured hippocampal neurons. *The Journal of Comparative Neurology* 427:351-361.

Lehenkari P.P., Charras G.T., Nykanen A.,Horton M.A. 2000. Adapting atomic force microscopy for cell biology. *Ultramicroscopy* 82:289-295.

Levy R.,Maaloum M. 2002. Measuring the spring constant of atomic force microscope cantilevers: Thermal fluctuations and other methods. *Nanotechnology* 13:33-37.

Lim C.T., Zhou E.H., Li A., Vedula S.R.K.,Fu H.X. 2006. Experimental techniques for single cell and single molecule biomechanics. *Materials Science and Engineering: Proceedings of the First TMS Symposium on Biological Materials Science* 26:1278-1288.

Lodish H., Baltimore D., Berk A., Zipursky L., Matsudaira P.,Darnell J. (1995). *Molecular cell biology*, W. H. Freeman, New York.

Mahaffy R.E., Park S., Gerde E., Käs J.,Shih C.K. 2004. Quantitative analysis of the viscoelastic properties of thin regions of fibroblasts using atomic force microscopy. 86:1777-1793.

Maniotis A.J., Chen C.S.,Ingber D.E. 1997. Demonstration of mechanical connections between integrins cytoskeletal filaments, and nucleoplasm that stabilize nuclear structure. *Proceedings of the National Academy of Sciences of the United States of America* 94:849-854.

Mitchison T.J., Charras G.T.,Mahadevan L. 2008. Implications of a poroelastic cytoplasm for the dynamics of animal cell shape. *Seminars in Cell & Developmental Biology Cell Shape and Tissue Morphogenesis* 19:215-223.

Morris R.,Hollenbeck P. 1995. Axonal transport of mitochondria along microtubules and f-actin in living vertebrate neurons. *J. Cell Biol.* 131:1315-1326.

Okamoto K.,Shaw J.M. 2005. Mitochondrial morphology and dynamics in yeast and multicellular eukaryotes. *Annual Review of Genetics* 39:503-536.

Pelling A.E., Sehati S., Gralla E.B., Valentine J.S.,Gimzewski J.K. 2004. Local nanomechanical motion of the cell wall of saccharomyces cerevisiae. *Science* 305:1147-1150.

Putman C.A., van der Werf K.O., de Grooth B.G., van Hulst N.F.,Greve J. 1994. Viscoelasticity of living cells allows high resolution imaging by tapping mode atomic force microscopy. *Biophys. J.* 67:1749-1753.

Radmacher M., Fritz M.,Hansma P.K. 1995. Imaging soft samples with the atomic-force microscope - gelatin in water and propanol. *Biophysical Journal* 69:264-270.

Radmacher M., Fritz M., Kacher C.M., Cleveland J.P.,Hansma P.K. 1996. Measuring the viscoelastic properties of human platelets with the atomic force microscope. 70:556-567.

Radmacher M., Tillmann R.W., Fritz M.,Gaub H.E. 1992. From molecules to cells - imaging soft samples with the atomic force microscope. *Science* 257:1900-1905.

Reynolds I.J.,Rintoul G.L. 2004. Mitochondrial stop and go: Signals that regulate organelle movement. *Sci. STKE* 2004:pe46-.

Romagnoli S., Cai G., Faleri C., Yokota E., Shimmen T.,Cresti M. 2007. Microtubule- and actin filament-dependent motors are distributed on pollen tube mitochondria and contribute differently to their movement. *Plant Cell Physiol.* 48:345-361.

Rotsch C., Jacobson K.,Radmacher M. 1999. Dimensional and mechanical dynamics of active and stable edges in motile fibroblasts investigated by using atomic force microscopy. *PNAS* 96:921-926.

Rudiger Suelmann R.F. 2000. Mitochondrial movement and morphology depend on an intact actin cytoskeleton in aspergillus nidulans. *Cell Motility and the Cytoskeleton* 45:42-50.

Sadoshima J.,Izumo S. 1997. The cellular and molecular response of cardiac myocytes to mechanical stress. *Annual Review of Physiology* 59:551-571.

San Paulo A.,García R. 2000. High-resolution imaging of antibodies by tapping-mode atomic force microscopy: Attractive and repulsive tip-sample interaction regimes. *Biophysical Journal* 78:1599-1605.

Satcher R.L.,Dewey C.F. 1996. Theoretical estimates of mechanical properties of the endothelial cell cytoskeleton. *Biophysical Journal* 71:109-118.

Shaw J.M.,Nunnari J. 2002. Mitochondrial dynamics and division in budding yeast. *Trends in Cell Biology* 12:178-184.

Smith S.B., Cui Y.,Bustamante C. 1996. Overstretching b-DNA: The elastic response of individual double-stranded and single-stranded DNA molecules. *Science* 271:795-799.

Solon J., Levental I., Sengupta K., Georges P.C.,Janmey P.A. 2007. Fibroblast adaptation and stiffness matching to soft elastic substrates. 93:4453-4461.

Stamenovic D.,Ingber D.E. 2002. Models of cytoskeletal mechanics of adherent cells. *Biomechanics and Modeling in Mechanobiology* 1:95-108.

Takahashi M., Ishida T., Traub O., Corson M.A.,Berk B.C. 1997. Mechanotransduction in endothelial cells: Temporal signaling events in response to shear stress. *Journal of Vascular Research* 34:212-219.

Tan J.L., Tien J., Pirone D.M., Gray D.S., Bhadriraju K.,Chen C.S. 2003. Cells lying on a bed of microneedles: An approach to isolate mechanical force. *Proceedings of the National Academy of Sciences of the United States of America* 100:1484-1489.

Theret D.P., Levesque M.J., Sato M., Nerem R.M.,Wheeler L.T. 1988. The application of a homogeneous half-space model in the analysis of endothelial-cell micropipette

measurements. *Journal of Biomechanical Engineering-Transactions of the Asme* 110:190-199.

Thoumine O.,Ott A. 1997. Time scale dependent viscoelastic and contractile regimes in fibroblasts probed by microplate manipulation. *Journal of Cell Science* 110:2109-2116.

Tran-Son-Tay R., Kan H.C., Udaykumar H.S., Damay E.,Shyy W. 1998. Rheological modelling of leukocytes. *Medical & Biological Engineering & Computing* 36:246-250.

Trickey W.R., Baaijens F.P.T., Laursen T.A., Alexopoulos L.G.,Guilak F. 2006. Determination of the poisson's ratio of the cell: Recovery properties of chondrocytes after release from complete micropipette aspiration. *Journal of Biomechanics* 39:78-87.

Vale R.D. 2003. The molecular motor toolbox for intracellular transport. *Cell* 112:467-480.

Vinckier A.,Semenza G. 1998. Measuring elasticity of biological materials by atomic force microscopy. *Febs Letters* 430:12-16.

Wang H. (2000). *Theory of linear poroelasticity with applications to geomechanics and hydrogeology*, Princeton Univ. Press, Princeton, New Jersey.

Wang N., Butler J.P.,Ingber D.E. 1993. Mechanotransduction across the cell-surface and through the cytoskeleton. *Science* 260:1124-1127.

Wang N., Naruse K., Stamenovic' D., Fredberg J.J., Mijailovich S.M., Tolic'-Norrelykke I.M., Polte T., Mannix R.,Ingber D.E. 2001. Mechanical behavior in living cells consistent with the tensegrity model. *PNAS* 98:7765-7770.

Wang N.,Stamenovic D. 2000. Contribution of intermediate filaments to cell stiffness, stiffening, and growth. *American Journal of Physiology-Cell Physiology* 279:C188-C194.

Wu H.W., Kuhn T.,Moy V.T. 1998. Mechanical properties of l929 cells measured by atomic force microscopy: Effects of anticytoskeletal drugs and membrane crosslinking. *Scanning* 20:389-397.

Zhu C., Bao G.,Wang N. 2000. Cell mechanics: Mechanical response, cell adhesion, and molecular deformation. *Annual Review of Biomedical Engineering* 2:189-226.

Chapter 2

Approaches to Visualizing Intracellular Deformations Following AFM Indentation

2.1 Introduction

Previous studies have combined fluorescence imaging techniques with force-application methods, in order to observe structural intracellular changes in response to extracellular perturbations. Among these studies are the observations of changes in the actin and microtubule cytoskeleton of live fibroblast cells in response to deformations produced by glass needles, which were visualized using GFP-tagged cytoskeletal proteins (Heidemann, S.R. *et al.*, 1999). Deformations of the intermediate filament cytoskeleton were analysed by visualizing GFP-vimentin in live endothelial cells before and after the application of shear stress in a flow chamber (Helmke, B.P. *et al.*, 2003). In another study that combined the magnetic bead twisting technique with GFP-fluorescent imaging, application of forces to focal adhesions by the use of specifically-coated beads resulted in displacements of actin filament bundles at distances of 20-30 μm from the beads (Wang, N. & Suo, Z.G., 2005). A similar technique was used to visualize displacements of intracellular organelles such as mitochondria (Hu, S. *et al.*, 2003) and to analyse the propagation of forces to the nucleus by quantifying displacements of nucleolar structures in response to load (Hu, S.H. *et al.*, 2005). Visualization of responses to extracellular perturbations is not limited to the tracking of natural organelles or cytoskeletal components: in a recent study, AFM was used to apply perturbations onto live, adherent cells, while quantifying stress propagation through the cell by tracking of integrin-bound fluorescent microspheres (Rosenbluth, M.J. *et al.*, 2008).

As described in Chapter 1, mitochondria are semi-autonomous and highly dynamic organelles, which have the ability to change their shape and their location inside the living cell (Bereiterhahn, J. & Voth, M., 1994). Localization and rearrangement of mitochondria in higher Eukaryotes is known to be dependant on the microtubule cytoskeleton (Brady, S. et al., 1982; Heggeness, M.H. et al., 1978). More recent research suggests that actin filaments have an important role as well, such as facilitating mitochondrial organization in yeast and vertebrate neurons (Morris, R. & Hollenbeck, P., 1995); (Drubin, D. *et al.*, 1993), and controlling mitochondrial movement and morphology (Rudiger Suelmann, R.F., 2000). Given the strong association of mitochondria with the cytoskeleton, it is predicted that forces locally applied via the AFM tip would affect their arrangement if the cytoskeleton is capable of mechanical transduction (Alenghat, F.J. & Ingber, D.E., 2002; Blumenfeld, R., 2006; Wang, N. *et al.*, 1993). This hypothesis is investigated later in Chapter 4.

Following live-cell staining experiments using various organelle-specific live-cell fluorescent markers (among them are the endoplasmic reticulum, Golgi apparatus and nucleus), mitochondria were found to be an ideal candidate for a natural, live-cell marker, for a number of reasons:

1) High organelle-specificity and signal-to-noise ratio of the live-cell mitochondria dye MitoTracker (Invitrogen);
2) Spherical morphology of mitochondria (such as in 3T3 fibroblasts) allows convenient tracking using various tracking techniques (described in Chapter 3);

3) Dispersion of mitochondria throughout the cell in large numbers allows to investigate stress propagation to various distances with a high number of data points;
4) Mitochondria use both microtubules and actin filaments for transport, allowing the role of the cytoskeleton in force transduction to be investigated.

The combined AFM-fluorescence microscopy methods used here allow the application well-defined perturbations, together with real-time fluorescence and confocal imaging of the intracellular structural responses. In comparison to the use of the magnetic bead method to apply force onto the cell, AFM has several advantages: first, the force is well-defined and highly localized (contact area of <100 nm^2); second, the AFM applies a static load, in comparison to the oscillating loads applied by a magnetic bead; and third, there is no specific molecular linking between the probe and the cell surface, as in the case of magnetic bead experiments, which could independently modify cell behaviour. Here, we demonstrate this approach for visualizing intracellular deformations and displacements of intracellular organelles, and in particular that of mitochondria, in live cells, in response to applied loads.

2.2 Materials and Methods

2.2.1 Cell culture

NIH-3T3 Fibroblasts were cultured in Dulbecco's modified Eagle's medium GlutaMAX I media (Invitrogen) supplemented with 10% fetal bovine serum (Sigma) and 100 IU/ml penicillin and 100 μg/ml streptomycin (Sigma), at 37 °C in 5% CO_2 atmosphere. Cells were plated on the day prior to the experiment into either 60mm plastic culture dishes (Orange Scientific) (for fluorescence imaging) or 50 mm glass-bottom FluoroDish™ culture dishes (World Precision Instruments, Inc., UK) (for confocal laser scanning imaging).

2.2.2 Actin-GFP transfections

Cells were transfected with plasmids encoding Actin-GFP using Lipofectamine 2000 (Invitrogen). 1μg of DNA was incubated with 4 μl of Lipofectamine in 50 μl Opti-MEM media (Invitrogen) for 20 min, and the mixture was then added to ~50% confluent cell culture together with 1ml of Opti-MEM media for 8 hours incubation. Then, 3ml of fresh media were added and the cells were left in the incubator for another day prior to experiment. Plasmids were a kind gift of Dr. Guillaume Charras (London Centre for Nanotechnology) and are based on Clontech GFP backbones.

2.2.3 Live-cell florescence dyes

Live-cell mitochondrial dyes were purchased from Invitrogen. MitoTracker Green and MitoTracker Red stock solutions were kept at -20^{0}C in DMSO at concentration of 1mM. Cells were incubated with either MitoTracker Green at 1 μM for 30 min or MitoTracker Red at 100 nM for 10 min, before replacing with fresh media. Nuclei were stained using Hoechst 33342 (Invitrogen) at 200 nM for 10min before replacing with fresh media.

2.2.4 AFM indentation and fluorescence imaging

For observations of intracellular deformations and displacements in response to AFM indentation, cells were first stained and/or transfected and were then mounted in the AFM (JPK NanoWizard® I) combined with either Olympus X71 fluorescence microscope or Olympus FV1000 laser scanning confocal microscope. The temperature-controlled stage was maintained at 37°C for the duration of the experiment. Images on the Olympus X71 were acquired using a Hamamatsu ORCA-ER camera. MSCT-AUWH AFM cantilevers (Veeco) with pyramidal-shaped tips were calibrated and the spring constant was experimentally determined to be 0.05 ± 0.01 N/m (Levy, R. & Maaloum, M., 2002). Single, live interphase cells were chosen optically and the AFM cantilever was positioned above the nucleus. Cells underwent indentations with forces of 10nN or less, as stated in the text. An application of 10nN force typically resulted in an indentation of ~1.7-2.0 μm.

2.3 Results and Discussion

2.3.1 Observations of cytoskeleton and nuclear deformations

Cells underwent transient transfection with actin-GFP (as described in 2.2.2). The tip was first positioned above the nucleus. Images of the cell were then acquired before and after indentation with the AFM tip at a maximum force of 10nN.

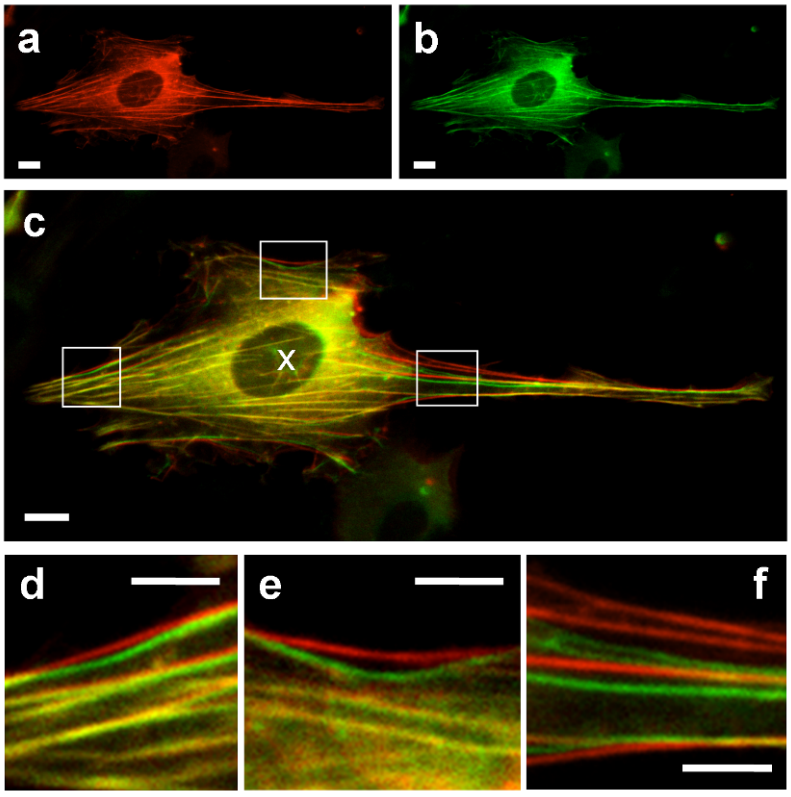

Figure 2-1. Deformations in the actin cytoskeleton following AFM indentation.
Fluorescence images of actin-GFP transfected cells were taken prior (a) and after (b) AFM indentation, with 4 second interval between the two images (images a. Images were pseudo-coloured in red (before indentation) and green (after indentation) and overlayed (c). Local deformations of the actin cytoskeleton can be clearly seen far from the indentation point (c, white cross). d, e and f are magnified areas, marked by the white squares in (c). Scale bars are: a-c, 10μm; d-f, 5μm.

Figure 2-1 shows the deformations in the actin cytoskeleton that resulted from AFM indentation. Image (c) is a results of an overlay of red (before indentation) and green (after indentation), with a 4 second interval between the two. As can be seen, changes in the actin fibres are visible at locations far from the indentation point. Comparing the natural and the indented states, some filaments at the cell edge assume a curved state following indentation (green), in comparison to their pre-indented stretched state (red) (Figure 2-1, d-f).

Nuclei of live cells were stained using Hoechst 33342 (Invitrogen). Figure 2-2c shows an overlay of florescence images taken before (red) and after (green) indentation, showing a green border surrounding the nucleus, indicating its expansion following indentation.

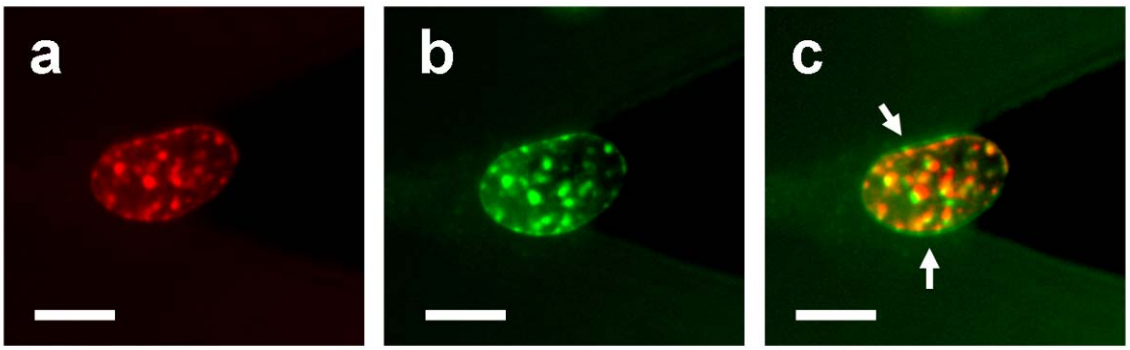

Figure 2-2. Nuclear deformation following indentation.

Fluorescent images of cells stained with the live-cell nucleus dye Hoechst 33342, before (a, pseudo-coloured red) and after (b, pseudo-coloured green) indentation with AFM (taken 4 seconds apart). A green border surrounds the nucleus in the overlay image (c) indicating an expansion caused by the indentation. Scale bars are 10μm.

2.3.2 Observations of mitochondrial displacements

As discussed in the introduction, mitochondria was found to be an ideal candidate as a live, intracellular marker, that is easy to track and can be indicative of mechanical transduction of forces through the cell, as will be discussed later on. Figure 2-3 shows indentation results for a cell stained with the mitochondria-specific dye MitoTracker Red.

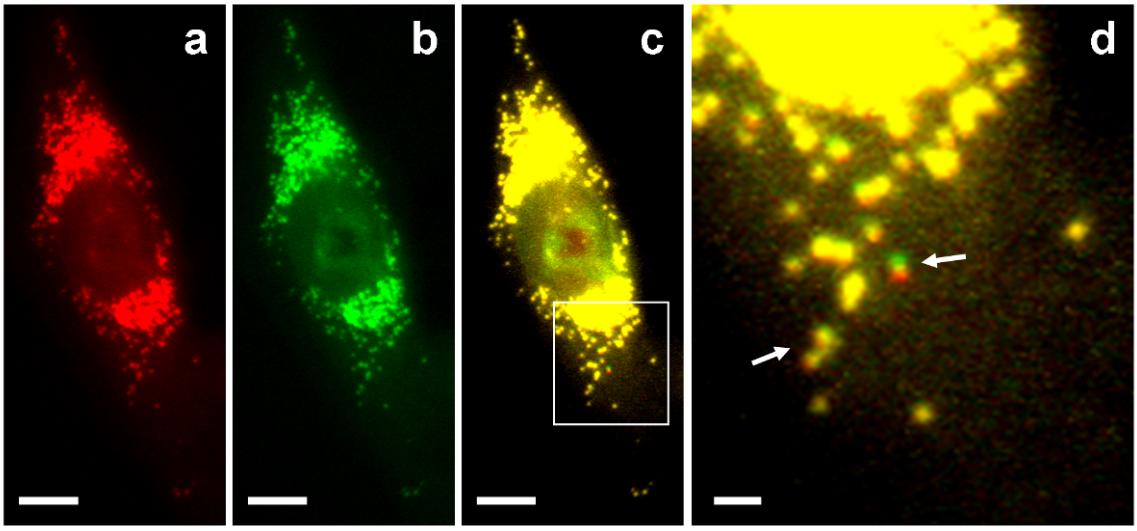

Figure 2-3. Mitochondrial displacements following indentation.
Fluorescent images of cells stained with the live-cell mitochondria dye MitoTracker Red, before (a, pseudo-coloured red) and after (b, pseudo-coloured green) indentation with AFM (taken 1 second apart). (c) An overlay of the two images. (d) A magnified section from c (white square). It is difficult to resolve individual displacements close to the centre of the cell due to overlapping of the mitochondrial mass. However, further away, where mitochondria are sparser, displacement of individual structures can be seen (d, white arrows). Scale bars are: a-c, 10μm; d, 2μm

When images pre- and post-indentation images were pseudo-coloured and overlayed, mitochondrial displacements were apparent, as seen in Figure 2-3c and d (white arrows). The focus was on mitochondria that are located further from the nucleus and closer to the cell edges. This if for two reasons: first, as mitochondria are much

sparser around the edges of the cell, it allowed us to distinguish and track individual mitochondrial structures, while it was not possible to resolve individual structures at the crowded mesh surrounding the nucleus; second, as will be further explained in Chapter 4, our interest was in examining the long-distance effect, i.e. the displacements that occur further away (> 20 μm) from the indentation point; finally, as the cell is relatively flat at the edges (< 1 μm) we can assume a 2D or near-2D displacements of the mitochondria.

Although the overlays of fluorescent pre- and post-indentation images (Figure 2-3) do not reveal significant collective movement of all mitochondria, it was evident from observing the time-laps video sequences, which clearly showed large-scale displacements of mitochondria following indentation with the AFM. The displacements observed not only covered a larger number of mitochondria but also showed a counter-intuitive movement of structures to different and often opposite directions in response to indentation, as will be discussed in the next section.

2.3.3 Natural mitochondrial displacements and force-induced displacements

Initial experiments used MitoTracker Green for staining mitochondria in live cells. However, further experiments using MitoTracker Red (CMXRos) proved this dye to be better suited due to its stronger signal-to-noise ratio and reduced photobleaching. Figure 2-4 shows fluorescence images of 3T3 cells stained with either MitoTracker Green (a) or MitoTracker Red (b). The latter gave better results with a higher signal-to-noise ratio and was more photostable. MitoTracker Green lost most of its signal after less than 10 seconds of exposure, while MitoTracker Red could still be clearly visible after 30 seconds of exposure. In addition, being membrane potential-sensitive, the MitoTracker Red would only stain live mitochondria, which would mean a higher ratio of the mitochondria stained would be associated to the cytoskeleton at any given time, thus being a better indicator for mechanical transduction driven by the cytoskeleton (as expanded in Chapter 4).

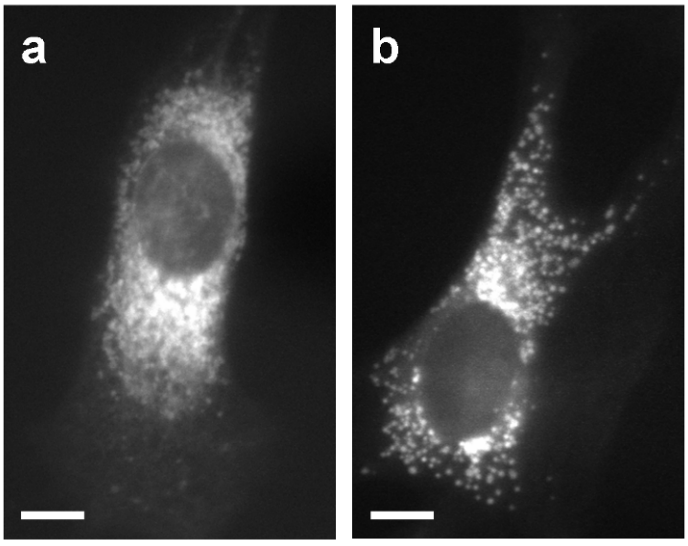

Figure 2-4. MitoTracker Green versus MitoTracker Red. (a) 3T3 cell stained with MitoTracker Green. Relatively low signal-to-noise ratio makes it difficult to resolve individual structures. (b) Staining with MitoTracker Red gave a stronger fluorescence signal making it easier to resolve individual structures. Scale bars are 10μm.

By optimising the image acquisition and AFM indentation process, the time interval between the two images was reduced to 1 second. Further improvement of the temporal resolution was not possible, as the AFM tip approach and indentation into the cell takes roughly 0.5 seconds. An additional and important point to be considered is the basal movement of mitochondria. Due to the dynamic nature of mitochondria in the living cell, natural mitochondria movements occur constantly (as described in Chapter 1). In order to distinguish basal mitochondrial movement from force-induced movement, which resulted from AFM indentation, the following experimental protocol was designed, which has a built-in control:

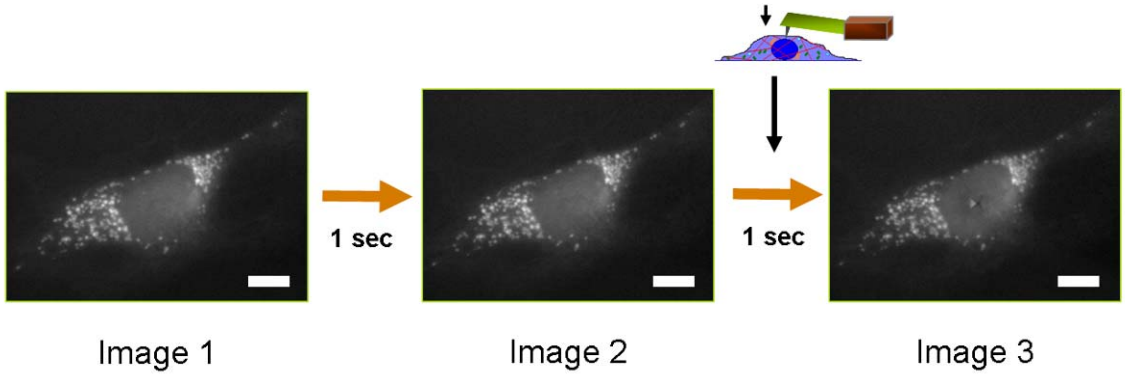

Figure 2-5. Experimental layout of image acquisition.

A sequence of images was taken at 1 second intervals. 3 images were picked for analysis: 2 images taken prior to AFM indentation (images 1 and 2) and the one image that followed the indentation (image 3). Changes between image 1 and 2 reflect basal mitochondrial movement, while changes between image 2 and image 3 reflect the basal movement together with force-induced movement that resulted from the AFM indentation. Scale bars are 10 μm.

A series of fluorescence images were captured at 1 second intervals, with the AFM indentation performed between two image acquisitions. Two pairs of images were compared: changes from image 1 to image 2, which were captured before indentation,

reflect the basal movement of mitochondria in the cell (control), and changes from image 2 to image 3, between which indentation takes place, reflect the basal movement plus the force-induce movement. Thus, this experimental layout has a built-in control that allows the normal, basal movement to be distinguished from movement resulting from indentation.

Figure 2-6 shows a comparison between basal mitochondrial movement (left column) and the displacement that followed the AFM indentation (right column). Each of the images a-d is an overlay of two consecutive fluorescence images, one red and one green. Images (a) and (c) show an overlay of Image 1 and 2, thus showing the basal movement of mitochondria. Images (b) and (d) show and overlay of Image 2 and 3, thus showing the displacement that followed AFM indentation. Further from the nucleus, at the cell periphery, mitochondria are sparser and it is possible to distinguish movement of individual mitochondria (Figure 2-6d) in response to indentation. Subtraction images (Figure 2-6, e-h) show the magnitude of displacement following indentation in comparison to basal displacements. Two important reproducible observations can be seen in Figure 2-6: One is that the magnitude of displacements between the pre- and post-indentation images (right column) is larger than that seen for the basal displacement (left column). This can be seen both in the overlay images (Figure 2-6, (d) in comparison to (c)) and in the subtraction images (more signal left after image subtraction, in (h) compared to (g)). Second, the direction of displacement following indentation is not consistent. Mitochondria appeared to move at different directions in response to indentation (Figure 2-6d, white arrows).

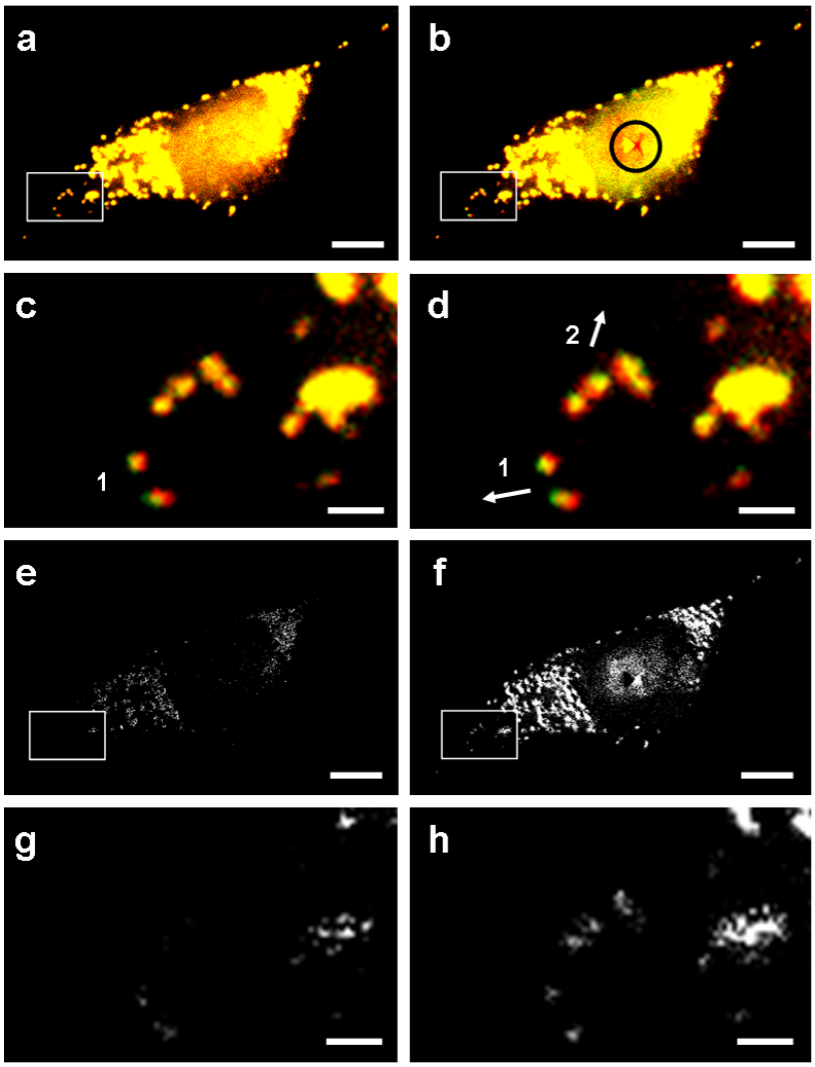

Figure 2-6. Comparison between basal and force-induced mitochondrial displacements.

The left column shows the basal displacement (control) and the right column shows the displacement following AFM indentation. (a) Overlay of consecutive fluorescent images 1 (red) and 2 (green), both acquired prior to AFM indentation. (b) Overlay of consecutive images 2 (red, before AFM indentation) and 3 (green, after perturbation). The yellow colour results from the red-green overlay, and is much denser around the nucleus where mitochondria are much sparser. The reflection image of the perturbing AFM tip can be seen in the centre of the nucleus (b, circle). (c-d) Magnified sections of the cell where motion of mitochondria in different directions can be visually observed. Arrows show direction of displacement of different mitochondrial structures (d1,2; the green colour shows the post-indentation image and thus the direction of displacement). Although some natural displacements are evident in the control image (c, 1), the displacement in the post-indentation image is higher and includes a larger number of organelles (d, 1 and 2). (e-h) Subtraction images of control (e) and post-indentation (f), and magnified images of the relevant sections (h-h). Here, the magnitude of the post-perturbation displacement can be clearly seen, in comparison with the control displacement. Scale bars are: a-b, e-f: 10 μm; c-d, g-h: 2 μm.

2.3.4 Observations of mitochondrial displacements in HFF cells

In order to validate the reproducibility of our method and to establish whether it is applicable to other cell lines, similar experiments were conducted using Human Skin Fibroblasts (HFF). Under physiological conditions, mitochondria often tend to form elongated tubular networks in HFF cells, rather than the fragmented bean-shaped morphology that appears in 3T3 fibroblasts (Figure 2-7).

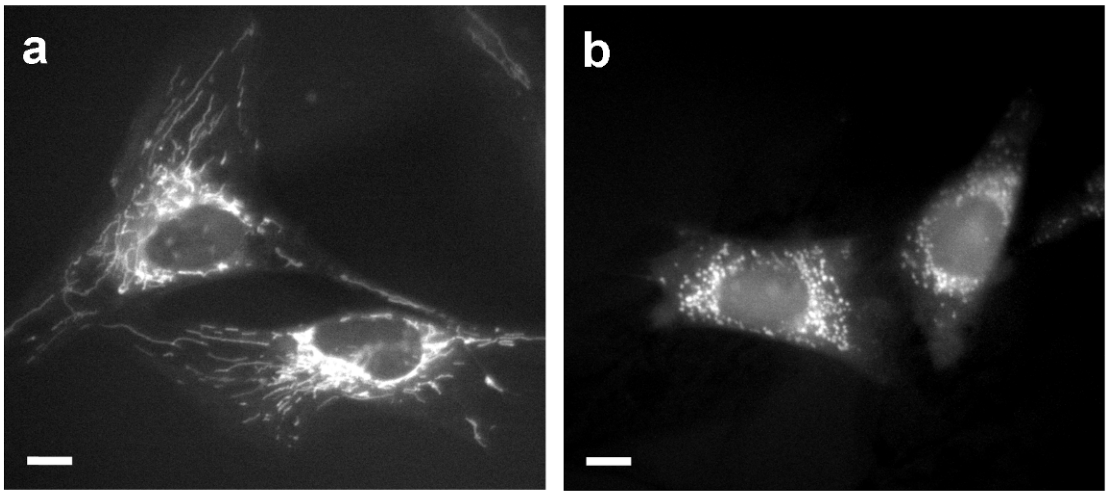

Figure 2-7. HFF and 3T3 fibroblasts stained with MitoTracker Red.
Fluorescence images of live HFF (a) and 3T3 mouse fibroblasts (b), both stained with the live mitochondrial dye MitoTracker Red. Mitochondria in HFF cells assume tubular network morphology due to dynamic mitochondria fusion, while in 3T3 mitochondria assume a much more fragmented and spherical morphology. Scale bars are 10 μm.

Figure 2-8 shows fluorescent images of HFF cells stained with MitoTracker Red. The cell culture and staining procedures were the same as those used for 3T3 fibroblasts.

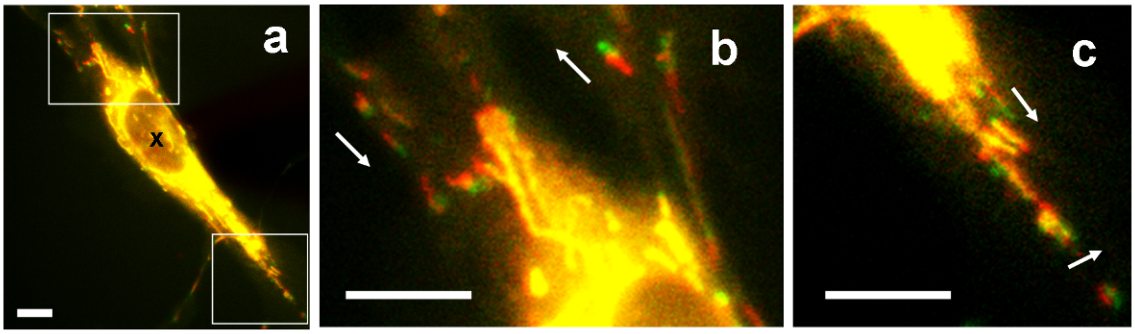

Figure 2-8. Mitochondrial displacements following AFM indentation.

(a) An overlay of images taken before (red) and after (green) indentation. (b c) magnified section of the cell, where mitochondrial structures clearly show displacements into different and, in some cases, opposite directions (b, arrows). Scale bars are 10 μm.

Although mitochondrial morphology in this cell type is different, similar unexpected displacements were observed. Again, indentation did not cause all mitochondria to be pushed away from the point of indentation, as would have been intuitively assumed. Rather, mitochondria seemed to move in unpredicted directions. Moreover, even mitochondria that were at close proximity to each other, moved in opposite directions (Figure 2-8b, white arrows). In order to better observe displacements of mitochondria, and further on to quantify their displacements (as will be discussed in Chapter 3), 3T3 fibroblasts were the preferred cell type for subsequent quantitative experiments.

2.4 Conclusion

In this chapter we presented an approach for the application of precise, well-defined extracellular perturbations to living cells, combined with the simultaneous visualisation of the resulting intracellular deformations. While keeping acquisition times to the minimum, it was possible to produce indentations and compare images taken at intervals down to 1 second apart. This led to the design of an experimental protocol that has a built-in control, allowing basal displacements of intracellular components to be distinguished from those displacements that result from the applied force. The increased magnitude of displacement that was observed following extracellular indentation with AFM suggested that forces applied at the indentation point were transmitted through the cell, leading to that observed increase, and raised the cytoskeleton as a candidate responsible for this force propagation. These examples of force propagation over relatively long distances, also termed 'action at a distance', were observed previously (Blumenfeld, R., 2006; Ingber, D.E., 1993; Wang, N. & Suo, Z.G., 2005). This will be further discussed in Chapter 4.

The reproducible observations of intracellular organelle displacements in cells that underwent perturbation with AFM also raise two important questions: first, does the indentation significantly increase the magnitude of displacements for organelles that are far from the indentation point, as suggested by visual inspection of the images? Second, which component in the cell propagates the forces that lead to these observed displacements? The prime suspect is the cytoskeleton, but other candidates could be the plasma membrane, the cytoplasm, or even undesired movement of the culture dish itself.

In Chapter 4, the hypothesis concerning the role of the cytoskeleton in force-induced displacement of mitochondria is investigated, while in Chapter 3 the observed displacement of mitochondria, both basal and force-induced, is quantified using several image registration and tracking techniques.

2.5 References

Alenghat F.J.,Ingber D.E. 2002. Mechanotransduction: All signals point to cytoskeleton, matrix, and integrins. *Sci. STKE* 2002:pe6-.

Bereiterhahn J.,Voth M. 1994. Dynamics of mitochondria in living cells - shape changes, dislocations, fusion, and fission of mitochondria. *Microscopy Research and Technique* 27:198-219.

Blumenfeld R. 2006. Isostaticity and controlled force transmission in the cytoskeleton: A model awaiting experimental evidence. *Biophysical Journal* 91:1970-1983.

Brady S., Lasek R.,Allen R. 1982. Fast axonal transport in extruded axoplasm from squid giant axon. *Science* 218:1129-1131.

Drubin D., Jones H.,Wertman K. 1993. Actin structure and function: Roles in mitochondrial organization and morphogenesis in budding yeast and identification of the phalloidin- binding site. *Mol. Biol. Cell* 4:1277-1294.

Heggeness M.H., Simon M.,Singer S.J. 1978. Association of mitochondria with microtubules in cultured cells. *PNAS* 75:3863-3866.

Heidemann S.R., Kaech S., Buxbaum R.E.,Matus A. 1999. Direct observations of the mechanical behaviors of the cytoskeleton in living fibroblasts. *J. Cell Biol.* 145:109-122.

Helmke B.P., Rosen A.B.,Davies P.F. 2003. Mapping mechanical strain of an endogenous cytoskeletal network in living endothelial cells. *Biophys. J.* 84:2691-2699.

Hu S., Chen J., Fabry B., Numaguchi Y., Gouldstone A., Ingber D.E., Fredberg J.J., Butler J.P.,Wang N. 2003. Intracellular stress tomography reveals stress focusing and structural anisotropy in cytoskeleton of living cells. *Am J Physiol Cell Physiol* 285:C1082-1090.

Hu S.H., Chen J.X., Butler J.P.,Wang N. 2005. Prestress mediates force propagation into the nucleus. *Biochemical and Biophysical Research Communications* 329:423-428.

Ingber D.E. 1993. Cellular tensegrity - defining new rules of biological design that govern the cytoskeleton. *Journal of Cell Science* 104:613-627.

Levy R.,Maaloum M. 2002. Measuring the spring constant of atomic force microscope cantilevers: Thermal fluctuations and other methods. *Nanotechnology* 13:33-37.

Morris R.,Hollenbeck P. 1995. Axonal transport of mitochondria along microtubules and f-actin in living vertebrate neurons. *J. Cell Biol.* 131:1315-1326.

Rosenbluth M.J., Crow A., Shaevitz J.W.,Fletcher D.A. 2008. Slow stress propagation in adherent cells. 95:6052-6059.

Rudiger Suelmann R.F. 2000. Mitochondrial movement and morphology depend on an intact actin cytoskeleton in aspergillus nidulans. *Cell Motility and the Cytoskeleton* 45:42-50.

Wang N., Butler J.P.,Ingber D.E. 1993. Mechanotransduction across the cell-surface and through the cytoskeleton. *Science* 260:1124-1127.

Wang N.,Suo Z.G. 2005. Long-distance propagation of forces in a cell. *Biochemical and Biophysical Research Communications* 328:1133-1138.

Chapter 3

Tracking and Quantifying Mitochondrial Displacements

3.1 Introduction

This chapter will present two tracking algorithms used for quantifying mitochondrial displacements: fluid registration analysis and the feature point tracking algorithm. Quantitative results will be presented of both natural and force-induced mitochondrial displacements in response to nanomechanical AFM perturbations. This will be followed by a discussion of the reasons for the differences in the results and the suitability of the respective registration techniques for tracking of intracellular organelle displacements.

3.1.1 Fluid registration

Image registration is a general name for the procedure that involves overlaying two images and measuring the relative change between them, when one image acts as a reference point and the second is an image of the same scene at a different time point, viewpoint or acquired by a different technique. In medicine, image registration is frequently used in diagnosis using Computer Tomography (CT) and MRI images, and for monitoring tumor growth and brain activity (Zitova, B. & Flusser, J., 2003). Fluid registration is used to determine a mapping from one image to another in the form of a displacement field (u), which is defined throughout the image. The displacement field is modeled as a time-dependent viscous fluid flow. Force vectors are derived in order to improve image similarity between the two images, and the response of the fluid to the forces is obtained by solving the Navier-Stokes equation for a compressible viscous fluid:

(Eq. 4.1) $$\mu\nabla^2 v + \mu\nabla(\nabla \cdot v) + f(u) = 0$$

The equation determines the velocity field *v* of a fluid with viscosity μ in response to an applied force *f*. The velocity field is derived from the gradient of image similarity measure and is a function of the estimated displacement field u(x). The similarity measure is the square of the intensity correlation coefficient (ICC) (Freeborough, P.A. & Fox, N.C., 1998):

(Eq. 4.2) $$ICC^2 = \frac{\left(N\sum_i T(x_i)S(x_i - u(x_i)) - \left(\sum_i T(x_i)\right)\left(\sum_i S(x_i - u(x_i))\right)\right)^2}{\left(N\sum_i T^2(x_i) - \left(\sum_i T(x_i)\right)^2\right)\left(N\sum_i S^2(x_i - u(x_i)) - \left(\sum_i S(x_i - u(x_i))\right)^2\right)}$$

In equation 4.2, T and S represent intensities of pixels at positions x and (x-u(x)) in the Target and Source images, respectively. The summation is over all *N* pixels in the target image. More information in the viscous fluid flow model can be found in (Christensen, G.E. *et al.*, 1996; Crum, W.R. *et al.*, 2005; Lester, H. *et al.*, 1999). The use of fluid registration proved successful in different medical image applications, including brain scan analysis of patients suffering from dementia (Crum, W.R. *et al.*, 2001; Freeborough, P.A. & Fox, N.C., 1998), mapping of large deformations in CT images (Christensen, G.E. *et al.*, 2001) and analysis of 3D MRI of breast tissue (Crum, W.R. *et al.*, 2005).

3.1.2 Feature-point tracking algorithm

In single particle tracking (SPT), images or video sequences captured using optical or fluorescent techniques are used to track the motion of molecules, proteins, viruses and intracellular organelles over time (Saxton, M.J. & Jacobson, K., 1997). In SPT, the centre of the particle can be indentified and tracked over time with a precision well bellow the wavelength of light, even though two particles at that separation cannot be resolved (Ghosh, R.N. & Webb, W.W., 1994; Schnapp, B.J. *et al.*, 1988). SPT is an invaluable

tool in cellular and molecular biology. The ability to extract quantitative data of particle trajectories can provide useful information, such as the velocity of the particle, direction of motion and the mode of motion (if it is random Brownian motion or a directed motion, for example)(Saxton, M.J. & Jacobson, K., 1997). Examples for the use of SPT in cell biology include the tracking of low density lipoprotein receptors on the cell membrane (Ghosh, R.N. & Webb, W.W., 1994), lateral diffusion of membrane proteins (Zhang, F. *et al.*, 1991), displacements driven by kinesin motors on microtubules (Gelles, J. *et al.*, 1988), the tracking of single intracellular proteins for the purpose of diffusion constant calculations (Goulian, M. & Simon, S.M., 2000), and Brownian dynamics analysis for elucidation of material properties (Qian, H., 2000).

Feature-point tracking is a SPT algorithm that enables an efficient, automated, two-dimensional detection and tracking analysis of particles trajectories (Sbalzarini, I.F. & Koumoutsakos, P., 2005). The method is suited to digital video and time-lapse fluorescence imaging, which typically generates low-intensity data. Feature point tracking detects particle positions in a digital video or image sequence and generates particle trajectories over time. One of its main advantages is that it does not make any assumptions regarding the smoothness of the trajectories. Thus, it is extremely useful for many biological applications where the type of motion is not explicitly known in advance, or when the motion is random and can change rapidly. Furthermore, by not assuming a motion model, the algorithm integrity is not biased when several modes of motion are incorporated by a single trajectory. Therefore, this method is useful for tracking both natural and force-induced motion (post-perturbation) of an organelle in the same time-lapse sequence, such as in our case of tracking mitochondrial displacements.

Feature point tracking has been successfully used for different biological applications, including tracking viruses and virus-like particle trajectories on or within living cells (Ewers, H. et al., 2005; Helmuth, J.A. et al., 2007; Sbalzarini, I.F. & Koumoutsakos, P., 2005); investigating individual membrane microdomains in relationship to the cytoskeleton (Langhorst, M.F. et al., 2007); analyzing cargo movement along microtubules (Brunner, C. et al., 2007); trafficking of particles during phagocytosis (Manderson, A.P. et al., 2007); and cell migration (Sengers, B.G. et al., 2007).

3.2 Materials and Methods

3.2.1 Cell culture

NIH-3T3 Fibroblasts were cultured in DMEM GlutaMAX media supplemented with 10% fetal bovine serum (both obtained from Invitrogen, Paisley, UK), 100 IU/mL penicillin and 100 μg/mL streptomycin (Invitrogen), and were maintained at 37 °C and 5% CO_2. Cells were plated into 50 mm glass-bottom FluoroDish™ culture dishes (World Precision Instruments, Inc., UK) one day prior to the experiment.

3.2.2 AFM indentation

Cells plated in cell culture dishes were placed in a combined AFM-fluorescence microscope (Olympus IX71 inverted optical microscope and JPK NanoWizard® I AFM). The temperature-controlled stage was maintained at 37°C for the duration of the experiment. MSCT-AUWH cantilevers (Veeco) with pyramidal-shaped tips were calibrated and the spring constant was experimentally determined to be 0.05 ± 0.01 N/m (Levy, R. & Maaloum, M., 2002). Single, live interphase cells were chosen optically and the AFM cantilever was positioned above the nucleus. Cells underwent indentations with forces of 10 nN (leading to indentations of ~1.7-2.0 μm).

3.2.3 Motion displacements using fluid registration

Fluid registration maximises a measure of image-similarity so that a perfect registration results in two structurally identical images with the relative motion between the image features encoded in the displacement field. The fluid registration technique, as described

earlier, allows displacements that are solutions of physics-based equations which describe the flow of a viscous fluid. These methods can recover large magnitude localised displacements while preserving a global one-to-one mapping between images (i.e. they result in a diffeomorphic transformation (a transformation that does not fold or tear) (Crum, W.R. *et al.*, 2005). In this application, we track the displacement of specific mitochondria from frame to frame and therefore require such one-to-one mapping. The registration algorithm maximises the intensity cross-correlation between the images and assumes that, at correct registration, corresponding intensities are linearly related. We expect some departures from this approximation, especially in the vicinity of the AFM probe, but in all the cases studied herein these minor intensity fluctuations did not have a serious effect on the registration.

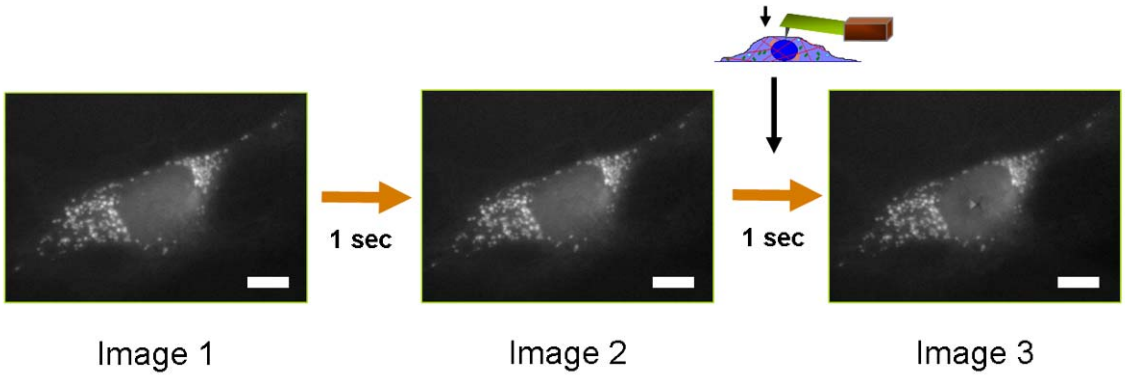

Figure 3-1. Experimental layout of image acquisition.

A sequence of images was taken at 1 second intervals. 3 images were picked for analysis: 2 images taken prior to AFM indentation (images 1 and 2) and the one image that followed the indentation (image 3). Scale bars are 10μm.

Each motion tracking experiment was conducted on three sequential images with the cell at rest in the first two images and perturbed using the AFM between the second and third image (Figure 3-1), as described in Chapter 2. In the application of the fluid

registration algorithm, all motion analysis was performed using image 2 as a reference. Therefore the pre-perturbation mitochondrial motion was estimated by registering image 1 → image 2 and the post-perturbation motion by registering image 3 → image 2. Then, a pixel-by-pixel analysis of the displacements of structures in image 2 backward (to image 1) and forward (to image 3) reveals the change in structure displacement between the images. The registrations produce displacement maps defined at every pixel in image 2. We focus attention on regions of interest away from the nucleus where the cell is relatively flat (<1 μm thick) and the motion of mitochondria is assumed to have a mainly two-dimensional component. A semi-automated analysis was used to obtain localised mitochondrial motion estimates. In the first, manual step, a circular mask is placed on image 2 to define a region of interest (ROI) (Figure 3-2b). Then, an intensity threshold is chosen, which would best distinguish foreground from background within each region (Figure 3-2c).

The remainder of the analysis was automated and in two parallel streams: (i) **regional analysis**: the displacement was weighted by pixel intensity and integrated over the whole of the chosen region (Figure 3-2b) to yield the mean displacement before (1 → 2) and after (3 → 2) perturbation. The assumption is that within the ROI high intensities correspond to mitochondria so they are given a high weighting; (ii) **cluster analysis**: each ROI was thresholded to produce a binary image of foreground (= mitochondria) and background (= noise). Figure 3-2c shows the thresholded binary image of mitochondrial structures (red) overlayed on top of the original image.

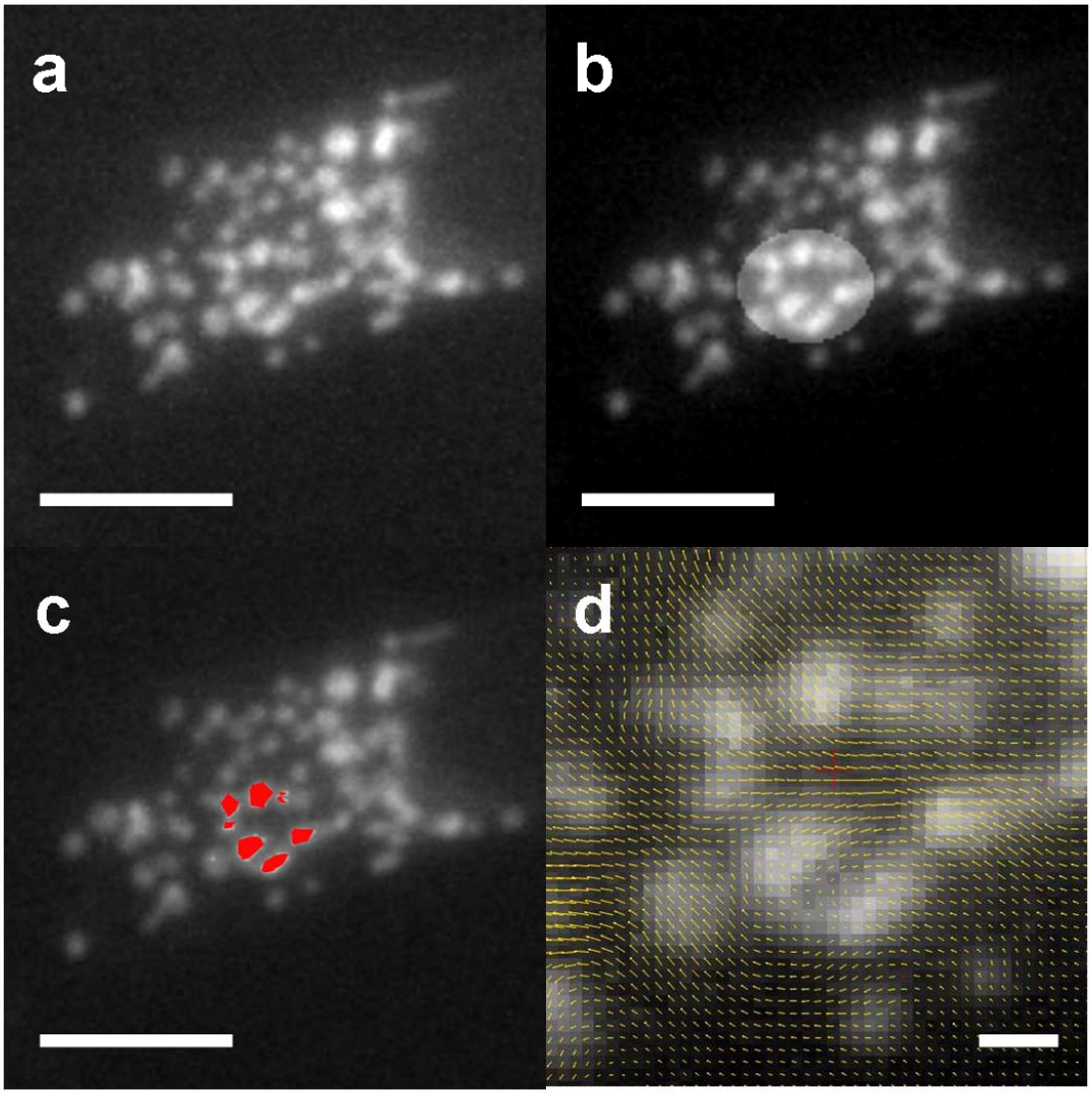

Figure 3-2. Registration of mitochondrial displacements with the fluid flow algorithm.

(a) The left-side of a cell stained with the mitochondrial dye MitoTracker Red. (b) In the first step of the registration, a region is selected for analysis. (c) A thresholded binary image for the selected region overlayed on top of the original image. The thresholded areas (red) are used as a mask for the following displacements map. (d) Displacement maps showing velocity vectors for all the pixels in the image. Scale bars: a-c, 10μm; d, 2μm.

Clusters of connected pixels in each thresholded image were automatically identified and small clusters (< 3 pixels) were discarded. The mean displacement before

(1 → 2) and after (3 → 2) perturbation was computed for each cluster without intensity-weighting. Therefore, for each region an overall intensity-weighted motion estimate could be compared with the motion of individual mitochondrial clusters within the region. By analysing differences in pre- and post- perturbation motion in the same frame, we focus on changes in displacement rather than absolute displacement.

3.2.4 Tracking displacements using the feature point tracking algorithm

The fluorescence images that were analyzed with fluid registration algorithm were also analyzed using the feature point tracking method in order to assess the appropriateness of each methodology for tracking natural and force induced mitochondrial displacements. Feature point tracking was carried out in a similar manner to fluid flow registration by analyzing a sequence of 3 images taken in 1 sec intervals, where images 1 and 2 were taken prior to AFM indentation and image 3 taken right after the indentation. ImageJ, a public-domain image processing and analysis programme developed at the National Institute of Health ([1]), was used for the analysis, together with the ParticleTracker plug-in ([2]). This plug-in is used to detect particles and calculate trajectories in an image sequence using the feature point tracking algorithm (Sbalzarini, I.F. & Koumoutsakos, P., 2005). The tracking algorithm consists of two main steps: detection of feature points in every frame and linking of these points into trajectories.

In the first step of the analysis, the three images are converted into a stack in ImageJ and a semi-automatic detection of feature points is carried out using the

[1] ImageJ, http://rsbweb.nih.gov/ij/
[2] ParticleTracker, http://weeman.inf.ethz.ch/particletracker/

ParticleTracker plug-in. The detection step itself is divided into several automated stages that include image restoration and noise reduction, estimation and refinement of point locations, and non-particle discrimination (Sbalzarini, I.F. & Koumoutsakos, P., 2005). Since image conditions, such as the intensity and noise levels, vary between each image set, several parameters needs to be adjusted manually in order to facilitate correct particle detection and avoid false detections due to background noise. These include the approximate radius of the particle (in pixels), which should be bigger than a single point radius but smaller than the distance between two separate points (usually set to 3), and a percentile (%) that determines the sensitivity of the algorithm to background noise when deciding the local maxima of featured points (i.e. how bright the particle needs to be in order to be accepted as a feature point). The percentile is the percentage of the upper end intensity range that will be considered as feature points, and is usually set between 0.2% and 1.5%. When estimating the feature point locations, the algorithm looks for local intensity maxima. This process is performed on a per-frame basis to eliminate the effect of a reduction in the overall intensity in time, such as in the case of photo-bleaching. When refining the location of the detected points, the assumption made is that a calculated local maximum is near the actual geometric centre of the object. The software then highlights all determined feature points (particles) (Figure 3-3a). The trajectories of all determined particles, along the 3-image sequence, can then be visualized (Figure 3-3b).

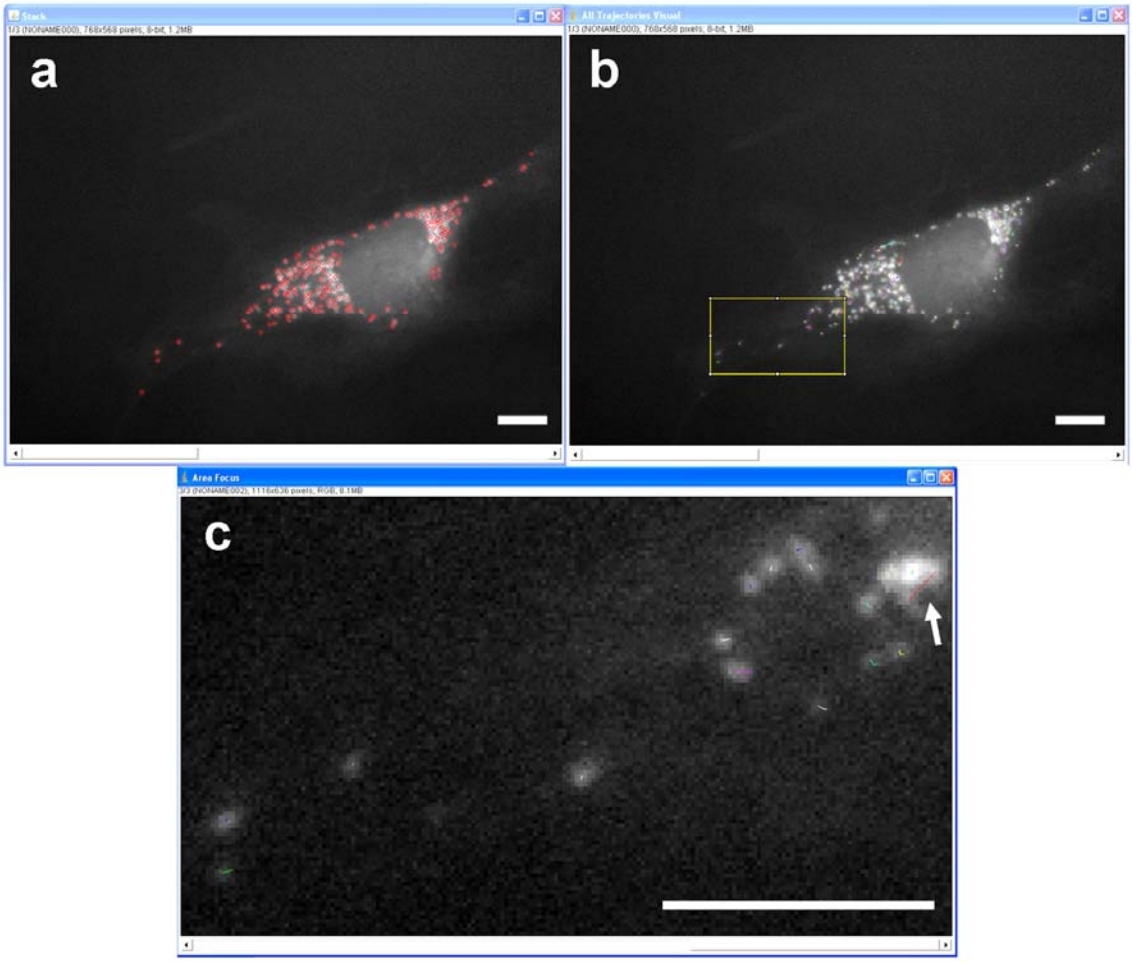

Figure 3-3. Tracking mitochondrial displacements using ParticleTracker.
After the 3 images are combined into a stack, the ParticleTracker plug-in identifies feature points according to manually entered parameters (a). A region for analysis is then chosen (b) and the trajectories in that region are shown together with coordinates of each determined feature point at each of the 3 images (c). Before processing the results, all trajectories are manually verified and false links (c, white arrow) are removed. Scale bars are 10μm.

In the next step, two regions are chosen in image 1, typically on either side of the cell, and at a distance of at least 20μm from the indentation point (Figure 3-3b, square). Data on all the trajectories in that region is extracted, including the x and y coordinates of each particle in each of the images (Figure 3-3c). This data will normally include a few invalid trajectories (around 5-10% of the total calculated trajectories), which result from

false linking of particles between two frames (Figure 3-3c, white arrow). This can happen due to close proximity between two particles, image noise or low intensity. As these invalid trajectories originate from false linking of different feature points between the frames, their magnitude can be more than 10 times higher and therefore will greatly affect the overall calculated average; hence it is important to manually validate and remove the false linking of feature points. Therefore, each trajectory is validated visually, and all false and broken links are removed. The final step involves the calculation of the absolute displacement of each particle from the extracted trajectory, using code written in Matlab. For each particle, the absolute displacement between image 1 and 2 (natural movement) and between image 2 and 3 (post-indentation movement), is calculated.

3.2.5 Statistical Methods

Data are presented as mean ± standard error of the mean (s.e.m), unless stated otherwise. Measurements were analysed using unpaired or paired Student's *t* tests with significance at $P < 0.05$ or lower, as stated in the text.

3.3 Results and Discussion

3.3.1 Quantification of displacements using the fluid registration algorithm

Results from fluid registration analysis for mitochondria displacements are shown in Figure 3-4. Two ROIs containing mitochondria were chosen for each cell, typically at opposite sides of the nucleus and close to the cell periphery. On average, the mitochondria were located at a distance of ~27 μm from the indentation point. Each ROI was then used as a mask for calculating the intensity-weighted mean displacement of the region, using fluid registration analysis, as described in Materials & Methods. A total of 44 regions were chosen in 22 individual cells. Figure 3-4 shows the mean displacement (in nm) for each region, as calculated using intensity-weighted fluid registration algorithm. Pre-indentation displacement represents the natural mitochondrial movement (control; white) and post-indentation displacement represents the displacement following the indentation (grey). The average calculated displacement was 37 ± 6 nm (mean ± s.e.m), and the average post-indentation displacement was 56 ± 9 nm (mean ± s.e.m; $*P < 0.0001$, paired Student's t-test). Thus, the average displacement of mitochondria has increased by ~50% following the application of 10 nN of force above the cell nucleus with the AFM tip.

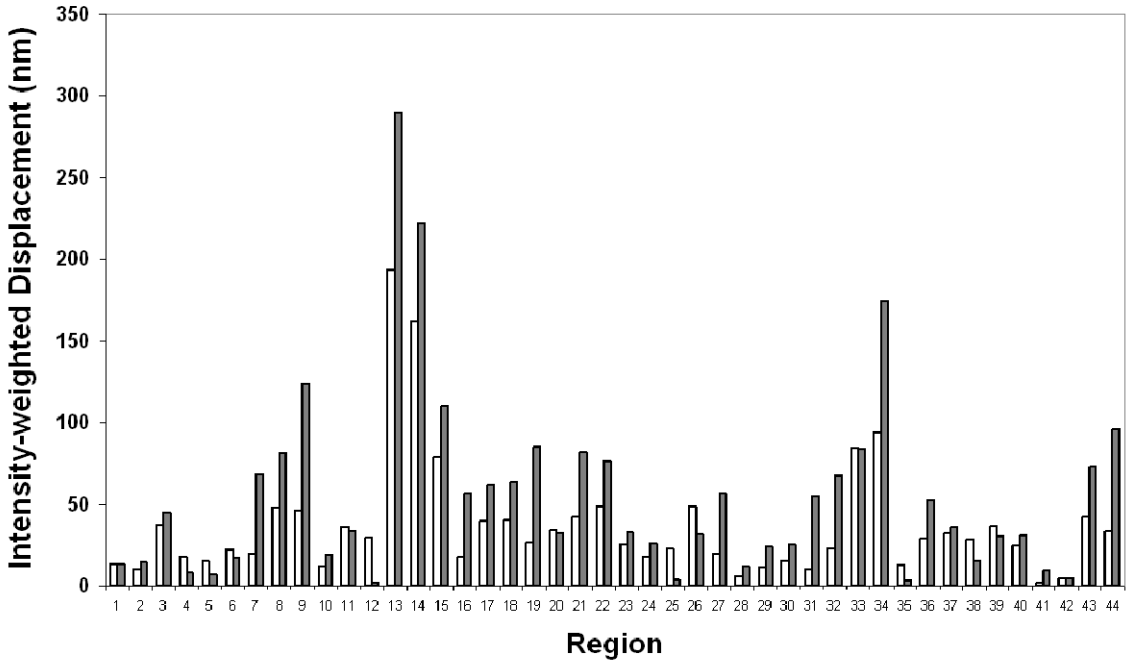

Figure 3-4. Natural and post-indentation intensity-weighted displacements for each region (fluid registration).

For each region, the graph show the natural (pre-indentation displacement, in white) and the force-induced (post-indentation, in grey) displacement, calculated in an intensity-weighted manner for each region using the fluid registration algorithm.

In order to revalidate the results, a second approach was to single out individual structures and apply the fluid registration specifically to them, rather than applying the registration over the whole region. In this approach, the image was first converted to binary and then thresholded, so that there were now multiple masks in each of the region, each representing a mitochondrial structure (see Materials & Methods, Figure 3-2). In this case, the mean displacement was calculated from the displacement map for each of the pixels that were included in the masked structure, without weighing by their intensity. It is important to note that the registration was done on the same cells and the same

chosen regions that were used at the first approach. A total of 177 individual mitochondrial structures were analysed. The mean displacement for the control was 28 ± 4 nm and the mean post-indentation displacement was 45 ± 8 (mean ± s.e.m; *P < 0.0001, paired Student's t-test). Thus, there was an increase of ~60% in mitochondrial displacement following indentation (Figure 3-5).

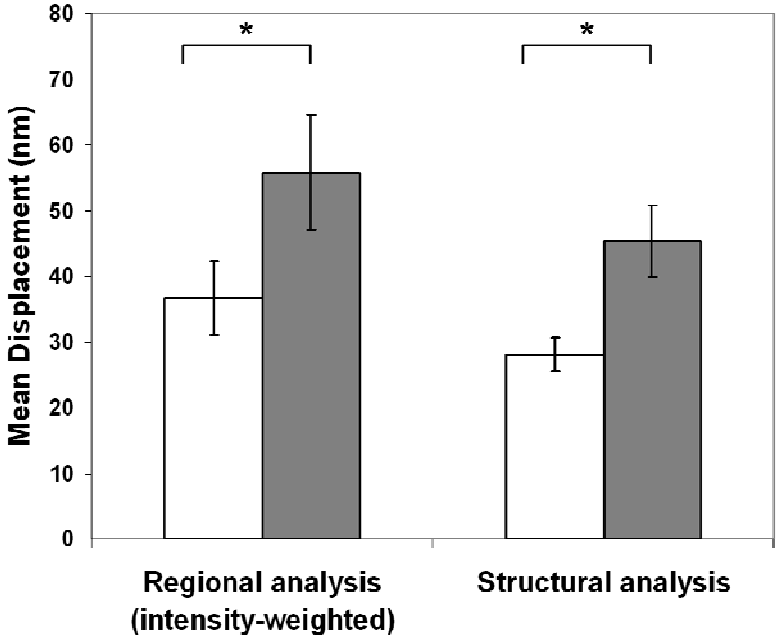

Figure 3-5. Mean mitochondrial displacement calculated with the fluid registration algorithm.

Using the regional analysis, AFM indentation resulted in an increase of ~50% in the average displacement, from 37 ± 6 nm for the control (white) to 56 ± 9 nm post-indentation (grey). Using the structural analysis method, an increase of ~60% was observed, from 28 ± 4 nm to 45 ± 8 nm (mean ± s.e.m; *P < 0.0001, paired Student's t-test).

Figure 3-5 shows both control and post-indentation mitochondrial displacements, for both registration approaches. As indicated in the graph, the mean displacements calculated using the intensity-weighted region analysis approach were slightly higher than those measured using the structural analysis approach, both for control and for post-

indentation displacements. The regional approach takes into consideration every pixel in the selected circular region, and factors the pixel's intensity into the calculation of its displacement. Thus, background noise has an effect and would increase the calculated mean displacement. In the structural approach, on the other hand, only the displacements of the thresholded mitochondrial structures are taken into account. This would explain the slightly higher absolute displacements calculated in the regional analysis, compared to the structural approach. These differences were not statistically significant, when comparing control *versus* control and post-indentation *versus* post-indentation, between the two methods ($P > 0.05$).

However, the relative change in displacement calculated in each of the methods, between the natural (control) mitochondrial movement and the force-induced (post-indentation) movement is significant for both methods: an ~50% increase following indentation for the regional analysis approach and ~60% increase for the structural approach ($^{*}P < 0.0001$ for both methods). This increase in displacement over short intervals is a strong example of an 'action at a distance' mechanism in the living cell, in which forces are instantaneously propagated through the cell, as observed in previous studies (Hayakawa, K. *et al.*, 2008; Hu, S. *et al.*, 2003; Maniotis, A.J. *et al.*, 1997). This type of force propagation is termed 'instantaneous' as it occurs in a timescale of milliseconds, in contrast to diffusion- or motor-based signal transduction mechanisms, which occur in the timescales of tens of seconds and up to minutes (Wang, N. *et al.*, 2009). This mechanism and the implications these results have on understanding the crucial role the cytoskeleton has in cellular mechanotransduction are further investigated in Chapter 4.

3.3.2 Tracking mitochondria using the feature-point tracking algorithm

Fluid registration proved to be a useful method for quantifying displacement of mitochondrial structures. However, the process is time-consuming and also highly dependent on intensity and noise conditions of the images. One of the main drawbacks of this method is that displacement vectors are calculated for each pixel in the chosen region. Thus, even though reduced by intensity-weighing, noise and autofluorescence still affect the overall calculated mean displacement for the region. And, in the structural analysis method, when images are thresholded to include only mitochondrial structures in the registration, rapid movements of mitochondria that go beyond the region's boundary are not taken into consideration. Furthermore, calculation of displacements using the fluid registration algorithm, by its nature, constrains the displacement to the Navier-Stokes equation for the description of viscous fluid flow. Hence, rapid alterations in mitochondrial displacements, which could be caused by cytoskeletal filament deformations, are not taken into consideration.

In contrast, as mitochondria in 3T3 cells typically assume a spherical form, it is computationally easy to apply a feature-point tracking algorithm in order to track displacement. In order to quantify natural and force-induced displacements of individual mitochondria, ImageJ was employed together with the Particle Tracker plug-in. The same images analysed with the fluid registration algorithm were also analysed using feature point tracking. The identification and tracking of particles was carried out as described in Materials & Methods. It is important to note that, although the identification and tracking process is semi-automatic, each one of the identified particles and every calculated trajectory were visually inspected and verified, in order to avoid false identification of

particles and false linking of displacement trajectories between sequential images. It is also important to note here that the same images were used to derive mitochondrial displacements using this approach as were previously used in the fluid registration analysis, though the selected ROIs were larger.

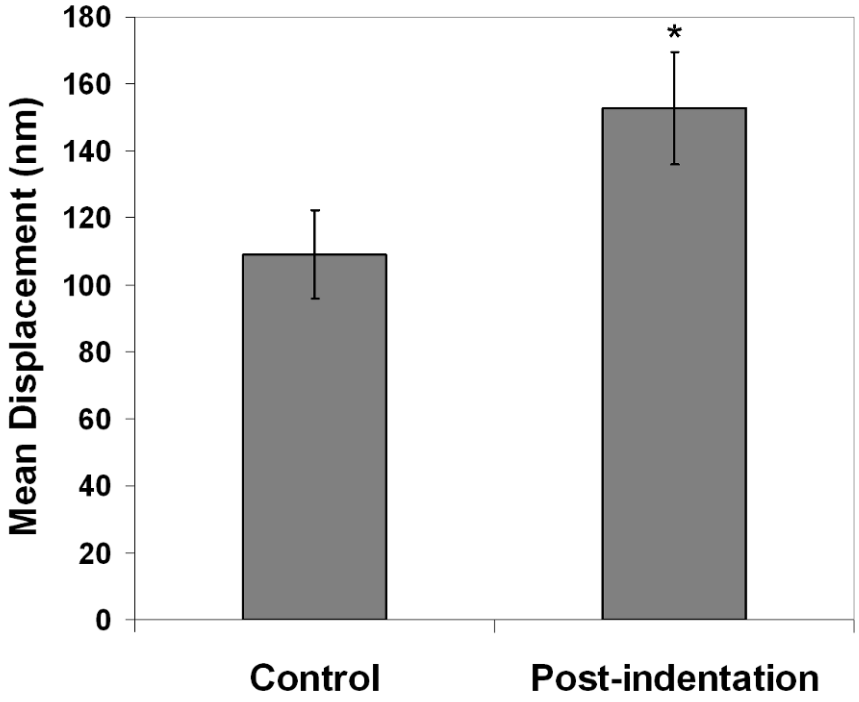

Figure 3-6. Mean mitochondrial displacement calculated with the feature-point tracking algorithm.

The average mitochondrial displacement increased in ~40% following AFM indentation, from 114 ± 6 nm for the natural displacement to 160 ± 10 nm post-indentation (mean ± s.e.m; **P* < 0.001).

Figure 3-6 shows the results for natural and post-indentation displacement of mitochondria, calculated using the feature-point tracking algorithm. A total of 323 individual mitochondria were analysed, in 42 regions for a total of 21 cells. The average natural displacement calculated to be 114 ± 6 nm, and the average post-indentation

displacement was 160 ± 10 nm (mean ± s.e.m; *P < 0.001). That is, mitochondrial displacement increased by ~40% following indentation.

The displacements measured using the feature-point particle tracking algorithm were on average ~3 times larger than the results derived from the fluid registration algorithm. This is due to the nature of displacement registration. In the fluid registration method, calculated displacements are subjected to the constraints placed by the Navier-Stocks equation. Mitochondria, however, can either freely float in the cytoplasm or be attached to actin filaments or microtubules, and thus rapid movements along filaments, both natural and those induced by indentation, are not well accounted for using fluid registration models. Therefore, a lower average displacement arises from the use of fluid registration, in comparison to feature-point tracking.

3.4 Conclusion

In this chapter, mitochondrial displacements were quantified using two separate approaches: the fluid flow registration and the feature point tracking algorithm. Although the absolute magnitude of displacement differed between the two approaches due to nature of each method, they both demonstrated a significant increase in mitochondrial displacement in response to the applied force. Due to the spherical morphology of the mitochondria in the inspected cells, the feature point tracking algorithm was found suitable to use in the following experiments. In addition, this algorithm does not impose any constraints on the tracking by trying to model the displacement; this allows more the accountability of more displacement modes, an in particular the rapid directed movement of mitochondria that can occur on cytoskeletal networks.

Both algorithms determined a significant increase of 40%-60% in the displacement of mitochondria following AFM indentation. Hence, this is a direct evidence for the physical transduction of force in the living cell: mechanical forces were observed to be transmitted over large distances of up to 40 μm in less than a second. These observations suggested the cytoskeleton as being the prime suspect for this form of 'action at a distance'. To confirm this hypothesis, further experiments were needed in order to investigate the role of the cytoskeleton in force transduction and are described in Chapter 4.

3.5 References

Brunner C., Wahnes C.,Vogel V. 2007. Cargo pick-up from engineered loading stations by kinesin driven molecular shuttles. *Lab on a Chip* 7:1263-1271.

Christensen G.E., Carlson B., Chao K.S.C., Yin P., Grigsby P.W., Nguyen K., Dempsey J.F., Lerma F.A., Bae K.T., Vannier M.W.,Williamson J.F. 2001. Image-based dose planning of intracavitary brachytherapy: Registration of serial-imaging studies using deformable anatomic templates. *International Journal of Radiation Oncology Biology Physics* 51:227-243.

Christensen G.E., Rabbitt R.D.,Miller M.I. 1996. Deformable templates using large deformation kinematics. *Ieee Transactions on Image Processing* 5:1435-1447.

Crum W.R., Scahill R.I.,Fox N.C. 2001. Automated hippocampal segmentation by regional fluid registration of serial mri: Validation and application in alzheimer's disease. *Neuroimage* 13:847-855.

Crum W.R., Tanner C.,Hawkes D.J. 2005. Anisotropic multi-scale fluid registration: Evaluation in magnetic resonance breast imaging. *Physics in Medicine and Biology* 50:5153-5174.

Ewers H., Smith A.E., Sbalzarini I.F., Lilie H., Koumoutsakos P.,Helenius A. 2005. Single-particle tracking of murine polyoma virus-like particles on live cells and artificial membranes. *Proceedings of the National Academy of Sciences of the United States of America* 102:15110-15115.

Freeborough P.A.,Fox N.C. 1998. Modeling brain deformations in alzheimer disease by fluid registration of serial 3d mr images. *Journal of Computer Assisted Tomography* 22:838-843.

Gelles J., Schnapp B.J.,Sheetz M.P. 1988. Tracking kinesin-driven movements with nanometre-scale precision. *Nature* 331:450-453.

Ghosh R.N.,Webb W.W. 1994. Automated detection and tracking of individual and clustered cell surface low density lipoprotein receptor molecules. *Biophysical Journal* 66:1301-1318.

Goulian M.,Simon S.M. 2000. Tracking single proteins within cells. *Biophysical Journal* 79:2188-2198.

Hayakawa K., Tatsumi H.,Sokabe M. 2008. Actin stress fibers transmit and focus force to activate mechanosensitive channels. *J Cell Sci* 121:496-503.

Helmuth J.A., Burckhardt C.J., Koumoutsakos P., Greber U.F.,Sbalzarini I.F. 2007. A novel supervised trajectory segmentation algorithm identifies distinct types of human adenovirus motion in host cells. *Journal of Structural Biology* 159:347-358.

Hu S., Chen J., Fabry B., Numaguchi Y., Gouldstone A., Ingber D.E., Fredberg J.J., Butler J.P.,Wang N. 2003. Intracellular stress tomography reveals stress focusing and structural anisotropy in cytoskeleton of living cells. *Am J Physiol Cell Physiol* 285:C1082-1090.

Langhorst M.F., Solis G.P., Hannbeck S., Plattner H.,Stuermer C.A.O. 2007. Linking membrane microdomains to the cytoskeleton: Regulation of the lateral mobility of reggie-1/flotillin-2 by interaction with actin. *Febs Letters* 581:4697-4703.

Lester H., Arridge S., Jansons K., Lemieux L., Hajnal J.,Oatridge A. (1999). Non-linear registration with the variable viscosity fluid algorithm. In *Information Processing in Medical Imaging*, pp. 238-251.

Manderson A.P., Kay J.G., Hammond L.A., Brown D.L.,Stow J.L. 2007. Subcompartments of the macrophage recycling endosome direct the differential secretion of il-6 and tnf alpha. *Journal of Cell Biology* 178:57-69.

Maniotis A.J., Chen C.S.,Ingber D.E. 1997. Demonstration of mechanical connections between integrins cytoskeletal filaments, and nucleoplasm that stabilize nuclear structure. *Proceedings of the National Academy of Sciences of the United States of America* 94:849-854.

Qian H. 2000. Single-particle tracking: Brownian dynamics of viscoelastic materials. 79:137-143.

Saxton M.J.,Jacobson K. 1997. Single-particle tracking:Applications to membrane dynamics. *Annual Review of Biophysics and Biomolecular Structure* 26:373-399.

Sbalzarini I.F.,Koumoutsakos P. 2005. Feature point tracking and trajectory analysis for video imaging in cell biology. *Journal of Structural Biology* 151:182-195.

Schnapp B.J., Gelles J.,Sheetz M.P. 1988. Nanometer-scale measurements using video light microscopy. *Cell Motility and the Cytoskeleton* 10:47-53.

Sengers B.G., Taylor M., Please C.P.,Oreffo R.O.C. 2007. Computational modelling of cell spreading and tissue regeneration in porous scaffolds. *Biomaterials* 28:1926-1940.

Wang N., Tytell J.D., Ingber D.E. 2009. Mechanotransduction at a distance: Mechanically coupling the extracellular matrix with the nucleus. 10:75-82.

Zhang F., Crise B., Su B., Hou Y., Rose J., Bothwell A.,Jacobson K. 1991. Lateral diffusion of membrane-spanning and glycosylphosphatidylinositol- linked proteins: Toward establishing rules governing the lateral mobility of membrane proteins. *J. Cell Biol.* 115:75-84.

Zitova B.,Flusser J. 2003. Image registration methods: A survey. *Image and Vision Computing* 21:977-1000.

Chapter 4

Effect of Cytoskeletal Disruption on Force Transmission and Cell Stiffness

4.1 Introduction

In Chapter 3, mitochondrial displacements were shown to significantly increase following AFM indentation. The question being asked now is what caused this increase in displacement, or, which cellular element is responsible for transmitting the local forces applied by the AFM, resulting in displacements of mitochondria at the far reaches of the cell (of an average distance of ~25 μm from the point of indentation)? An obvious candidate for force transmission would be the cytoskeleton. However, it is plausible that the observed mitochondrial displacement result from deformations or displacements in other components, such as the plasma membrane or the cytoplasm, or might even be an artefact caused by movement of the glass substrate to which the cells adhere (although the latter is highly unlikely when dealing with loads as small as 10 nN, especially when the cantilever is not even in direct contact with the substrate). In order to test this hypothesis and establish the cytoskeleton as the medium that is responsible for the observed force transmission, we used the cytoskeletal active drugs, nocodazole and cytochalasin D (CytD), to disrupt the integrity of either the microtubule or actin network, respectively. We then carried out particle tracking experiments using the feature-point tracking algorithm, as described in Chapter 3.

The cytoskeletal disrupting drugs Cytochalasin D (CytD) and nocodazole are frequently used in cell biology. CytD is a member of the fungal metabolites *cytochalasins*. By binding to the barbed end of actin filaments, CytD prevents both association and dissociation of actin monomers at the end of the filament (Cooper, J., 1987). Treatments with CytD have previously been shown to reduce cell stiffness in 3T3 fibroblasts by up to

a factor of 3, depending on concentration and incubation times (Rotsch, C. & Radmacher, M., 2000). Nocodazole interferes with microtubule dynamics by inhibiting tubulin polymerisation (Vasquez, R. *et al.*, 1997). Treatments with nocodazole have previously been shown to reduce cell stiffness in 3T3 fibroblasts (Pelling, A.E. & Dawson, D.W. *et al.*, 2007)

The experiments described here were carried on a large population of cells and involved the tracking of over 300 separate mitochondrial trajectories for each drug treatment. In the same fashion as described in Chapter 3, herein there was also a built-in control for each experimental system: the natural movement of mitochondria was recorded and quantified in addition to the force-induced movement. Using this method and having both the control and force-induced movement recorded in the same cell and within a 1-second interval, ensures validity of the results in spite of the natural diversity and variance between cells. The experiments gave us two sets of data: one set allows us to compare the natural, basal motility of mitochondria, between untreated and drug-treated cells, and to learn more about the cytoskeleton's role in facilitating mitochondria transportation through the cell. The second set of data, which is more important to our study, allows us to compare the force-induced movement of mitochondria in untreated cells with that observed in drug-treated cells. Force-induced movement of mitochondria was showed to be ~40% higher than their natural movement (Chapter 3). If our hypothesis about the role of the cytoskeleton in intracellular force transmission is correct, then we would predict that this increase in mitochondrial movement following indentation in the cells that were treated with cytoskeletal drugs will be blunted.

4.2 Materials and Methods

4.2.1 Cell Culture

NIH-3T3 Fibroblasts were cultured in DMEM GlutaMAX media supplemented with 10% fetal bovine serum (both obtained from Invitrogen, Paisley, UK), 100 IU/mL penicillin and 100 μg/mL streptomycin (Invitrogen), and were maintained at 37 °C and 5% CO_2. Cells were plated into 50 mm glass-bottom FluoroDish™ culture dishes (World Precision Instruments, Inc., UK) one day prior to the experiment.

4.2.2 Treatment with cytoskeleton-disrupting drugs

Cells were incubated with CytD (5 μM), nocodazole (10 μM) or both drugs together, 20 min prior to the experiment. Media were not replaced during the indentation experiment in order to maintain the effect of the drug throughout the experiment.

4.2.3 Immunofluorescence and Imaging

For demonstrating the effects of CytD and nocodazole on the actin filaments and microtubules, drug-treated cells were stained for actin, tubulin and the nucleus. Prior to fluorescence staining, cells were washed with warm PBS, fixed with 3.5% paraformaldehyde, 2% sucrose (10 min) and permeabilsed with 0.1% Triton-X (3 min) at room temperature. Actin filaments were stained at room temperature by incubating with Phalloidin Alexa Fluor 546 (Invitrogen, Paisley, UK) for 20 min followed by a 15 min wash. Microtubules were then stained on ice by incubating cells with mouse monoclonal anti α-tubulin conjugated to FITC (Abcam, Cambridge, UK) for 30 min followed by 15

min wash on ice. Finally, nuclei were stained by incubation with DAPI (Invitrogen, Paisley, UK) on ice for 10 min, followed by a final 10 min wash with PBS. Images were acquired on an Olympus FV1000 laser scanning confocal microscope (Olympus, UK).

4.2.4 Live-cell mitochondrial dye and displacement experiments

Cells were incubated with MitoTracker Red at 100 nM for 10 min, before replacing with fresh media. Cells were then left to equilibrate for further 30 min prior to experiment. Mitochondrial displacements experiments were conducted as described previously (Chapter 3) by acquiring fluorescence images at 1 sec intervals prior and post-AFM indentation, with the control being mitochondrial displacements between two consecutive images taken prior to indentation. Trajectories of mitochondria were analysed using the feature point tracking algorithm.

4.2.5 AFM indentation and extraction of Young's modulus

Cells plated in cell culture dishes were placed in a combined AFM-fluorescence microscope (Olympus IX71 inverted optical microscope and JPK NanoWizard® I AFM). The temperature controlled stage was maintained at 37°C for the duration of the experiment. MSCT-AUWH cantilevers (Veeco) with pyramidal-shaped tips were calibrated and the spring constant was experimentally determined to be 0.05 ± 0.01 N/m (Levy, R. & Maaloum, M., 2002). Single, live interphase cells were chosen optically and the AFM cantilever was positioned above the nucleus. Force-distance measurements were initiated with a maximum force of 2nN. Individual cells were selected randomly from across the tissue culture dish and 24 cells were tested for each of the drug treatment experiments and controls. 8 force curves were recorded over the nucleus of each cell at 1

Hz. The data was then fitted for an indentation of 200nm using the Hertz model for either conical or spherical indenters (Pelling, A.E. & Nicholls, B.M. *et al.*, 2007; Radmacher, M. *et al.*, 1995)

$$\mathbf{1.}\ F_{cone} = \frac{2}{\pi}\frac{E}{(1-\nu^2)}\tan(\alpha)\delta^2$$

$$\mathbf{2.}\ F_{sphere} = \frac{4}{3}\frac{E}{(1-\nu^2)}\sqrt{R}\delta^{3/2}$$

Where is ν is Poisson's ratio, α the half opening angle of the tip in the case of cone indentation (1), R is the sphere radius in the case of sphere indentation (2), δ is the indentation depth of the tip and *E* is the Young's modulus.

4.2.6 Preparation of spherical indenters

Polystyrene microspheres (Bangs Laboratories Inc., Fishers, IN) of ~19 μm diameter were glued onto tipless cantilevers (CSC 12 rectangular beam, MikroMasch, Estonia, 350 um long, 35 μm wide and 1.0 μm thick, spring constants about 0.03 N/m) using a small amount of epoxy resin (UHUÒ plus Schnellfest, UHU GmbH & Co. KG, Germany). Spring constants of each individual cantilever were determined as described before (Levy, R. & Maaloum, M., 2002) and the exact size of each sphere was measured using optical and scanning electron microscopy. The particles were washed in Decon 90 (Decon Laboratories Limited, UK), rinsed in an excess of deionised water, and subsequently treated in an O_2 plasma for 100 s. Probes were stored in nitrogen atmosphere before use. Tips were calibrated before each experiment and the spring constant was determined to be 0.06 ± 0.01 N/m (Levy, R. & Maaloum, M., 2002).

4.2.7 Statistical Methods

Data are presented as mean ± standard error of the mean (s.e.m), unless stated otherwise. Measurements were analysed using unpaired or paired Student's *t* tests with significance at $P < 0.05$ or lower, as stated in the text.

4.3 Results and Discussion

4.3.1 Effect of cytoskeletal disruption on natural mitochondrial motility

Figure 4-1 demonstrates the effect of the cytoskeletal drugs CytD and nocodazole on the actin and microtubule networks.

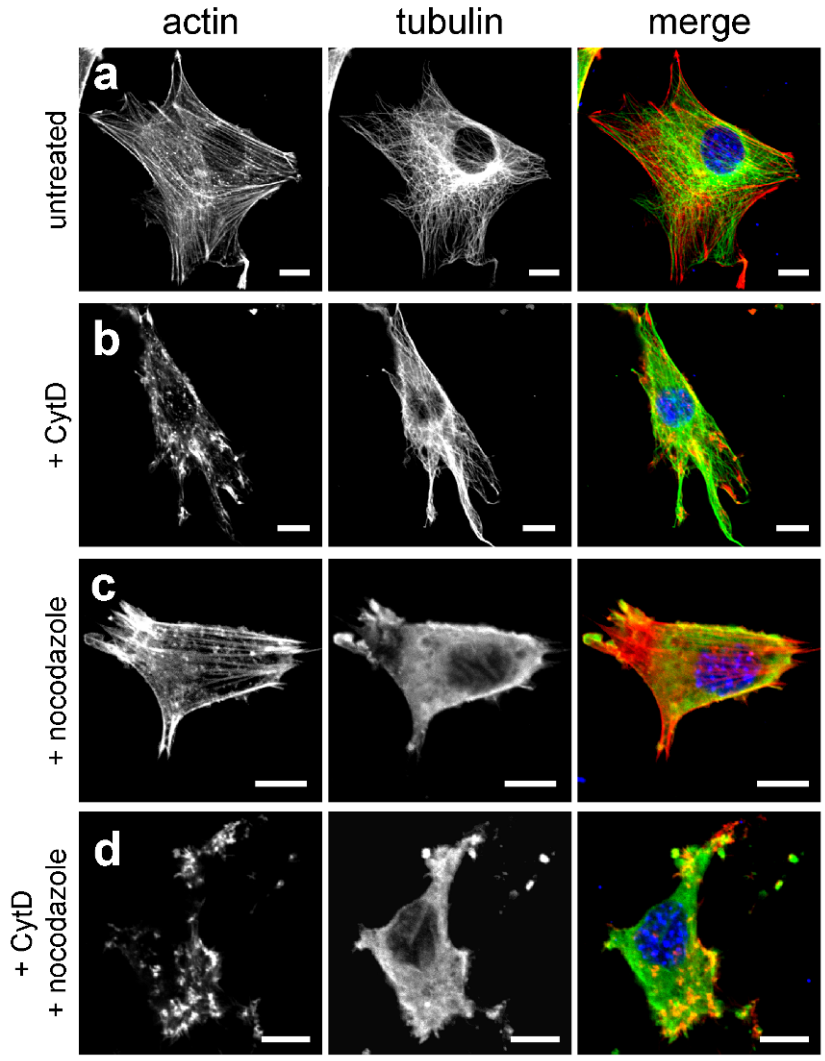

Figure 4-1. The effect of cytoskeletal drugs on the actin and microtubule networks. Cell were incubated with either CytD (5 μM), nocodazole (10 μM) or both drugs together for 20 minutes, and then fixed and stained as described in 4.2.3. The left column shows the actin filaments, the middle shows the microtubules and the right column is a merge of the actin (red), microtubules (green) and nucleus (blue). CytD-treated cells (b) show severely fragmented actin cytoskeleton, though microtubules can still be distinguished. Nocodazole-treated cells (c) show an intact actin cytoskeleton but microtubules are highly disrupted. Treatment with both drugs disrupts both cytoskeletal networks (d). Scale bars are 10 μm.

Figure 4-2 shows phase-contrast images of the cells (left column) and fluorescence images of mitochondria (middle column), together with overlay of the two (right column), for the different drug treatments. Although the optical images show cell morphology to be affected by treatments with either CytD or nocodazole, mitochondria are still dispersed throughout the cell, and individual structures that are further away from the indentation point (>20 μm) can be chosen for tracking analysis (Figure 4-2a and b; white arrows). Treatment with CytD and nocodazole in combination usually caused adverse effects, which often led to lose of plasma membrane integrity and further 'balling up' of the cells (Figure 4-2c). Quantifying mitochondrial movement here was not possible as mitochondria aggregated around the nucleus forming a dense mesh, making it difficult to distinguish and track individual structures (Figure 4-2c, right). Similar changes in mitochondria morphology following both actin and microtubule disruption has been observed previously (Kabashima, K. *et al.*, 2007; Knowles, M.K. *et al.*, 2002). We therefore analysed mitochondrial displacements in cells treated with either CytD or nocodazole, and compared the results to those of untreated cells.

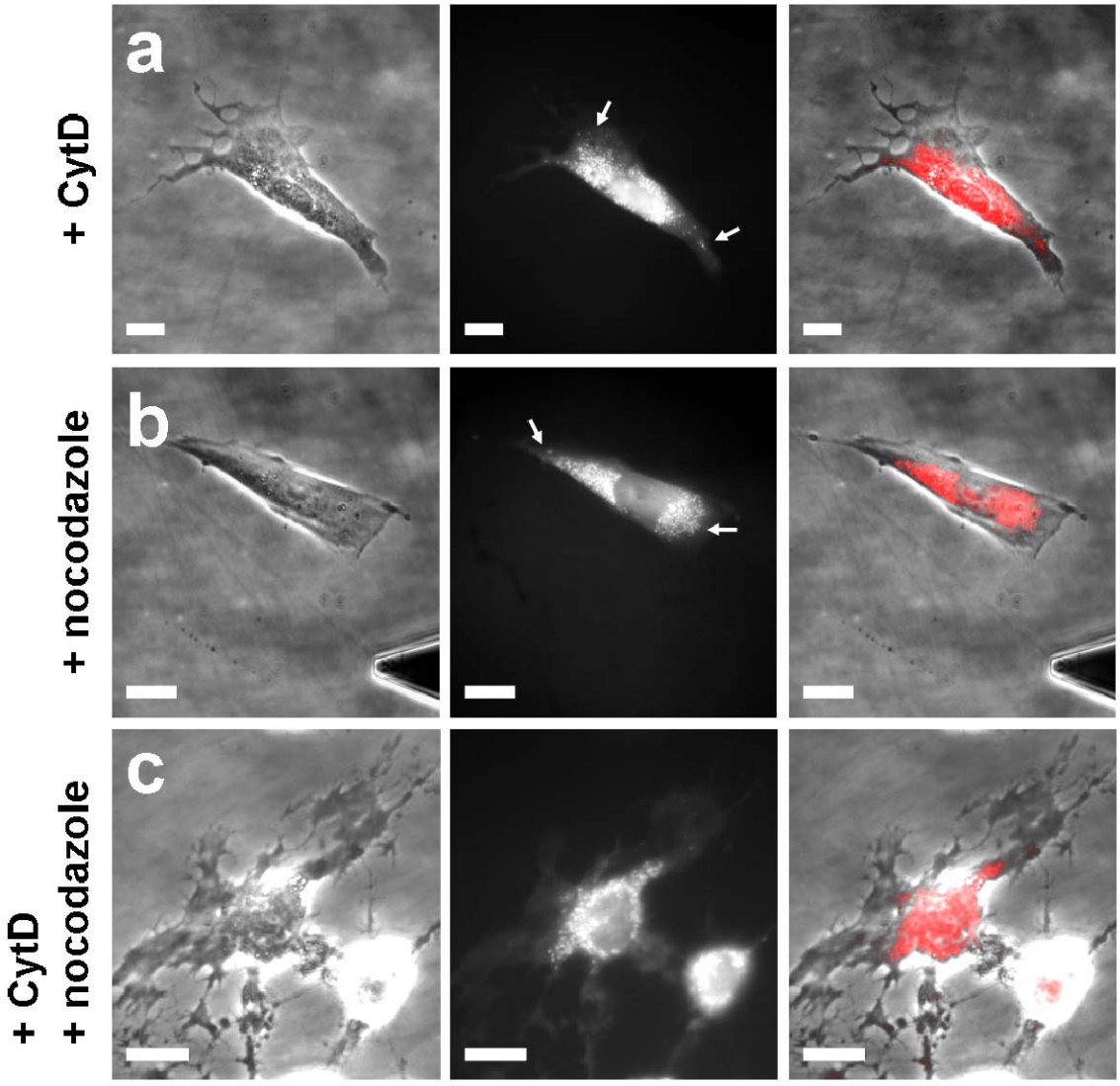

Figure 4-2. Cytochalasin D and nocodazole effect on cell and mitochondria morphology.

(a) Phase-contrast (left) and fluorescence image of mitochondria (middle), together with an overlay of the two images (right), in live 3T3 cells, after incubation with CytD (5 μM) for 20 min. (b) same as (a), after incubation with nocodazole (10 μM) for 20 min. The triangular cantilever tip can be seen in the lower-right corner. (c) Treatment with both drugs together. Scale bars are all 10 μm.

First, we compared the natural movement of mitochondria (i.e., with no AFM intervention), between untreated and drug-treated cells. 3T3 fibroblasts were treated with either CytD or nocodazole prior to indentation experiments, as described in 4.2.2. Figure 4-3 shows the mean mitochondrial displacement for untreated cells (n = 21 cells), CytD-treated (n = 17 cells) and nocodazole-treated (n = 13 cells). In each case over 300 trajectories of individual mitochondria were analysed. The mean displacement in untreated cells was 114 ± 6 nm. Cells treated with the actin-disrupting drug CytD displayed an average mitochondrial displacement of 56 ± 3 nm, and cells treated with the microtubule-disrupting drug nocodazole showed an average mitochondrial displacement of 57 ± 2 nm (mean ± s.e.m).

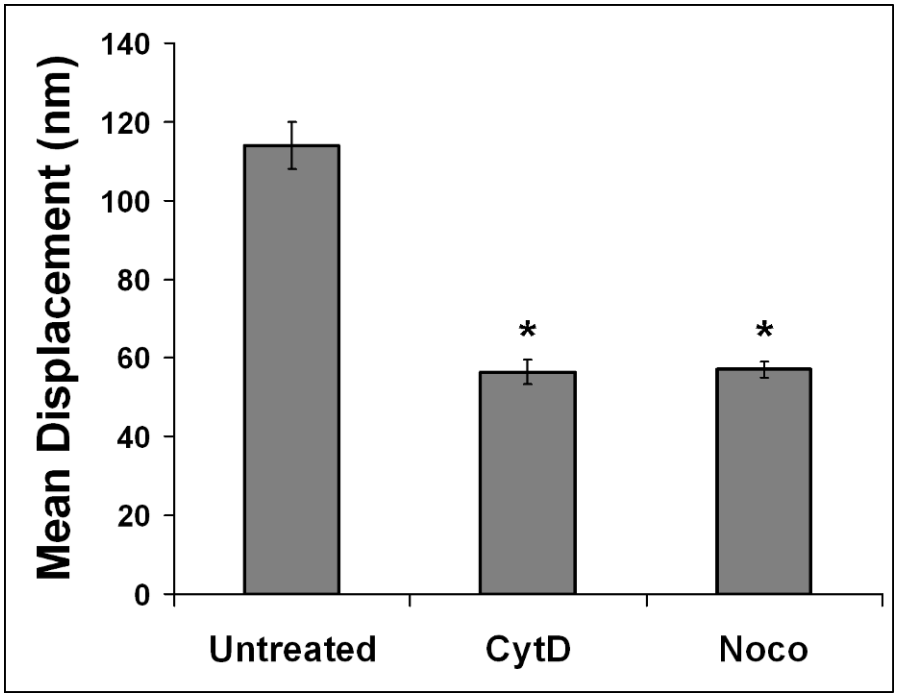

Figure 4-3. The effect of cytoskeleton disrupting drugs on mitochondria motility.
The mean displacement of mitochondria was reduced in ~50% for cells treated with either CytD (56 ± 3 nm) or nocodazole (57 ± 2), compared to untreated cells (114 ± 6 nm; mean ± s.e.m). *P < 0.001, control *versus* drug-treated, unpaired *t* test)

These results shows that natural mitochondrial motion is strongly dependent on both intact actin filaments and the microtubule network, confirming prior findings on the role of the cytoskeleton in mitochondrial transport (Brady, S. *et al.*, 1982; Heggeness, M.H. *et al.*, 1978; Rudiger Suelmann, R.F., 2000). Incubation with either CytD or nocodazole led to a decrease of ~50% in mitochondrial movement, compared to untreated cells (*$P < 0.001$, untreated *versus* each drug treatment; unpaired *t* test). This observed decrease in mitochondrial motility following CytD and nocodazole treatments has been previously reported in neuronal (Lee A. Ligon, O.S., 2000) and osteosarcoma cells, where treatment with the drugs led to a decrease in mitochondria mobility by a factor of 2-3 (Knowles, M.K. *et al.*, 2002). Mitochondrial dynamics were thoroughly described by the measurement of both the time- and length-scale dependent diffusion coefficients. It is important to note that the study showed that mitochondria still had enhanced mobilities relative to the diffusive limit; thus mitochondrial movement on the filaments still occurred, but at a much slower rate. These movements could be passive displacements of mitochondria that result from, for example, cytoplasmic flow or CSK remodelling.

4.3.2 Effect of cytoskeletal disruption on force-induced displacement

In order to establish the role of the cytoskeleton in force transmission, as indicated by the measured mitochondrial displacements after AFM indentation, we compared the effect on mitochondrial displacements in untreated cells with those treated with CytD and nocodazole. The indentation experiments followed the same protocol as described earlier in 3.2.2 and 3.3.2. Figure 4-4 shows the natural displacement next to the force-induced displacement, in each of the cases.

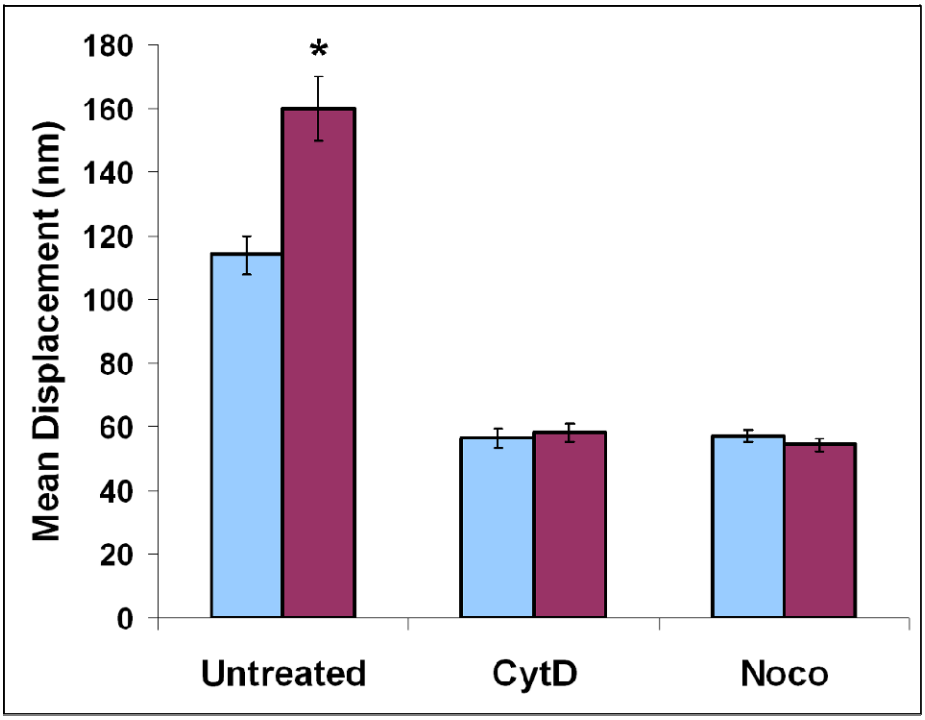

Figure 4-4. Cytoskeleton disruption effect on force-induced mitochondrial motility. For each case, the blue bar represents the mean natural displacement (nm) of mitochondria in a one-second interval. The red bar represents the mean displacement of mitochondria in the consecutive one-second interval, in which AFM indentation took place. The displacement of mitochondria following indentation did not show a significant increase (P = 0.62 for CytD treatments; P = 0.31 for nocodazole treatments), in comparison to the ~40% increase that was observed for untreated cells (*P < 0.001, control *versus* post-indentation displacement).

For CytD-treated cells, indentation increased from 56 ± 3 to 58 ± 3 nm (P = 0.62) and for nocodazole-treated indentation decreased from 57 ± 2 to 54 ± 2 nm (P = 0.31). Therefore, after either drug treatment, AFM indentation did not lead to a significant change in mitochondrial displacement, compared to the ~40% increase shown for untreated cells.

The results clearly show that indentation has no effect on mitochondrial displacements when the cell's cytoskeletal infrastructure is disrupted, and an intact cytoskeleton is essential for the transmission of long-distance forces throughout the cell. Furthermore, disrupting either the microtubule or the actin network led to a similar result, suggesting that an intact presence of both cytoskeletal elements is needed to produce the observed force-induced displacements of mitochondria.

4.3.3 Effect of cytoskeletal disruption on cell stiffness

Young's modulus (YM) was derived from force curves measured on untreated, CytD-treated and nocodazole-treated cells, as described in 4.2.5 and 4.2.6. 24 cells were analysed in each case, with approximately 8 force curves obtained and analysed for each cell. Figure 4-5 shows typical force-indentation curves (derived from AFM force-displacement curves that were measured with a conical indenter), for untreated and treated cells.

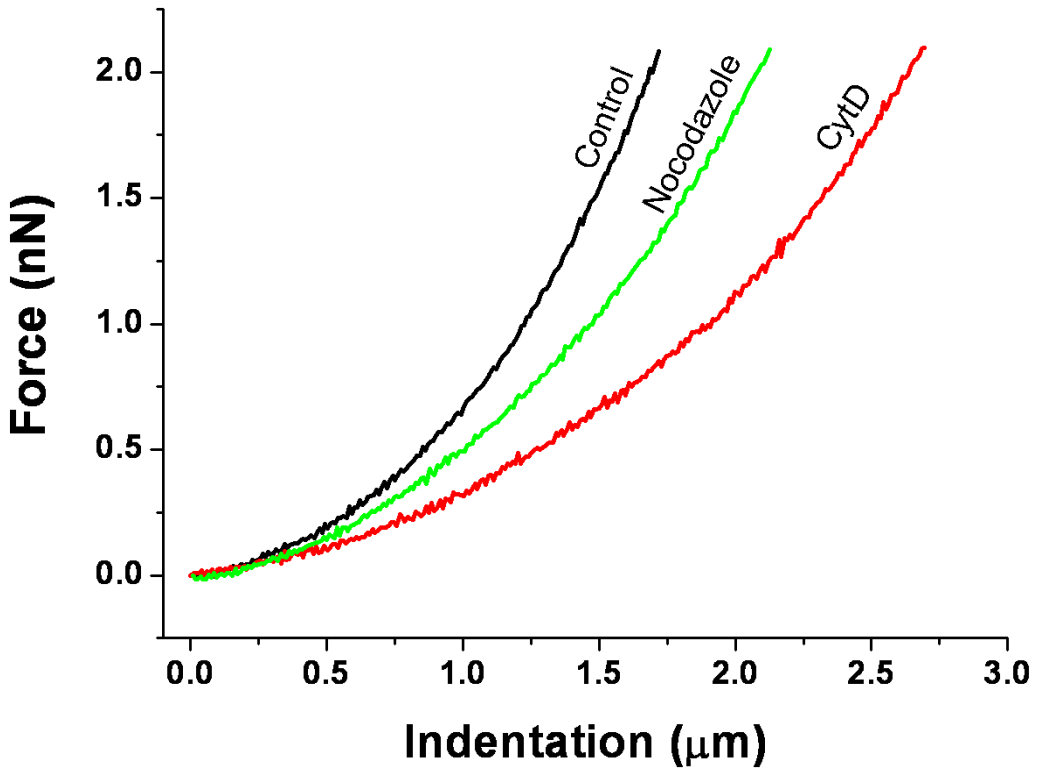

Figure 4-5. Force-indentation curves for cells treated with CytD and nocodazole. Force-indentation curves were derived from force-distance AFM measurements, by fitting to the Hertz model for a cone. Contact points were estimated by fitting for a 200 nm indentation (as described in 3.2.1). Treatment with CytD (red line) showed the strongest effect on cell stiffness, as seen above: cells were softer and an applied force of 2 nN led to an indentation of ~2.7 μm, compared to ~1.7 μm in untreated cells (black line).

From the force-indentation curves, the effect of the drugs on cell stiffness is clear. The strongest effect was observed for cells treated with CytD. Here, cells were softer, and the applied force of 2 nN led to an indentation of ~2.7 μm (Figure 4-5, red line), in comparison with untreated cells where an indentation of ~1.7 μm was observed (black line). Figure 4-6 shows the average YM calculated for untreated and treated cells. For untreated cells the average YM was 3.4 ± 0.2 kPa, for CytD-treated cells 1.5 ± 0.2 kPa

and for nocodazole-treated cells 2.4 ± 0.3 kPa (mean ± s.e.m). Hence, treatment with CytD and nocodazole led to a decrease in cell stiffness of ~55% and ~30%, respectively.

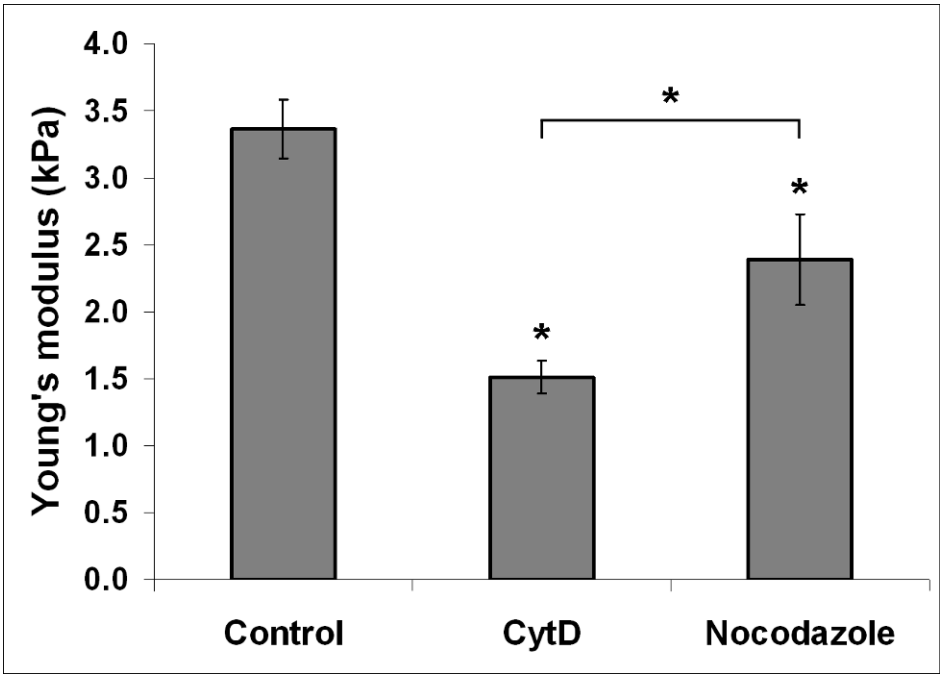

Figure 4-6. Young's modulus of cells treated with CytD and nocodazole.
Average YM calculated from force-curves measured with a conical indenter for untreated cells, CytD-treated cells and nocodazole-treated cells (n = 24 cells in each case, ~8 force curves obtained and averaged for each cell). The average YM for control was 3.4 ± 0.2 kPa, for CytD-treated cells 1.5 ± 0.2 kPa and for nocodazole-treated cells 2.4 ± 0.3 kPa (mean ± s.e.m). *P < 0.001, drugs *versus* control and CytD *versus* nocodazole.

Similar decrease in YM following treatments with CytD and nocodazole in 3T3 fibroblasts were previously observed (Pelling, A.E. & Dawson, D.W. *et al.*, 2007; Rotsch, C. & Radmacher, M., 2000). It is interesting to note the similarity between YM (Figure 4-6) and mitochondrial displacement measurements (Figure 4-3) for the drug-treated cells and in particularly for CytD, where both cell stiffness and the average mitochondrial motility were reduced by ~50% in comparison with the control. In the case of nocodazole,

though, the decrease in cell stiffness was smaller (in line with previous observations), but mitochondrial motility decreased in a similar manner to that observed for CytD treatments.

In order to compare local and global variations in stiffness, all YM measurements were repeated with a cantilever tip to which a polystyrene bead of ~19μm diameter was attached (A-Hassan, E. *et al.*, 1998; Charras, G.T. & Horton, M.A., 2002a), as described in 4.2.6. Spherical indentation has a much larger surface area (>10 μm^2 for a 200 nm indentation) when compared to conical indentation where the contact surface area for a 200 nm indentation is < 100 nm^2. The experiments were carried out in the same fashion as described for conical indentation. Figure 4-7 shows the average YM measured for the different treatments. The average YM for untreated cells was 1.0 ± 0.05 kPa, 0.42 ± 0.05 kPa for CytD-treated cells and 0.57 ± 0.03 kPa for nocodazole-treated cells (mean ± s.e.m; $*P < 0.001$, drugs versus control and CytD versus nocodazole). Thus, 58% decrease in stiffness following CytD treatment and 42% decrease following nocodazole treatment. These results indicate a similar reduction in cell stiffness over both global and local scales.

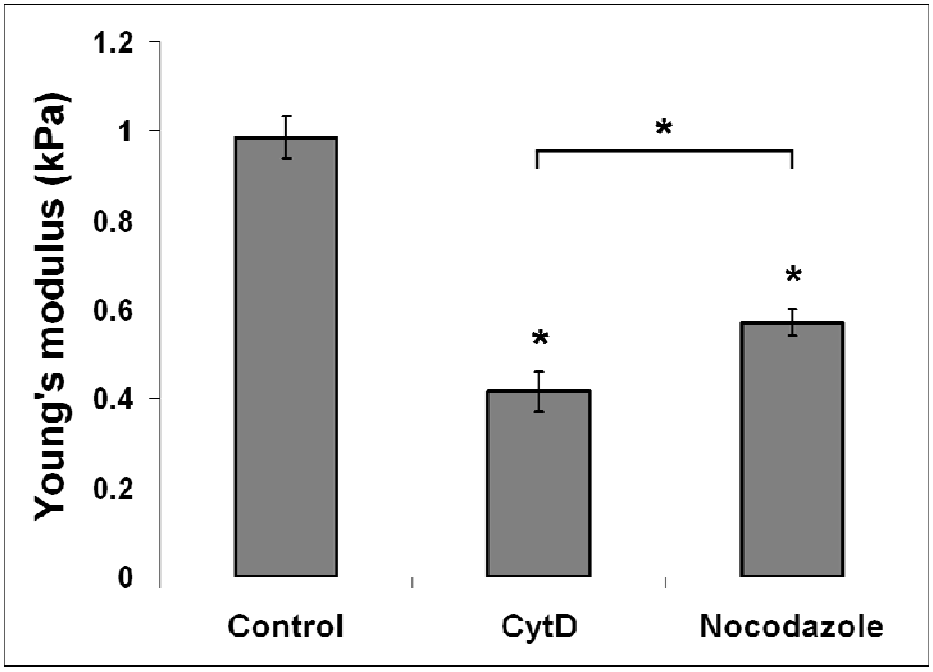

Figure 4-7. Young's modulus of cells treated with CytD and nocodazole (spherical indentation).

Average YM calculated for untreated cells, CytD-treated cells and nocodazole-treated cells, using a ~19μm polystyrene probe (n = 24 cells in each case, ~8 force curves obtained and averaged for each cell). The average YM was 1.0 ± 0.05 kPa for control, 0.42 ± 0.05 kPa for CytD-treated cells and 0.57 ± 0.03 kPa for nocodazole-treated cells (mean ± s.e.m). *P < 0.001, drugs *versus* control and CytD *versus* nocodazole.

The absolute YM values obtained using conical tips have been observed previously to be higher than those obtained with spherical tips (Radmacher, M. *et al.*, 1995). This is mainly due to the small contact area of the conical tip with the sample, where the tip is almost in direct contact with single actin filaments and is influenced by their high YM of around ~2 GPa (Kojima, H. *et al.*, 1994), and thus force is dissipated directly into the cytoskeleton. On the other hand, the spherical beads have a large contact area with the cell and are more highly influenced by the cell membrane and cytoplasm as

it flows through the cytoskeleton in response to the applied force. Force is mainly dissipated into the cytoplasm and membrane.

Although the absolute values for YM differed significantly between the two indentation methods, the important point to note is that the relative change in YM, when comparing control to treated cells, was similar for both forms of indentation. These results show that the decrease in membrane stiffness, which followed the drug treatments, is measureable both at the local nano-scale (<100 nm^2) and at the global micro-scale (>10 μm^2) and appear to be correlated to the measured mitochondrial displacements.

4.3.4 Membrane damage control experiments

Cells used in this study were typically 5-8 μm in height and an applied force of 10 nN, as used in the mitochondrial displacements experiments, will produce a large indentation into the cell of ~2 μm (or 25-40% of cell height). It was important to ensure that the applied force was not damaging the cell membrane, thus indirectly influencing mitochondrial behaviour. Force curves were measured over the nucleus under conditions similar to our experiment (1Hz, with a maximum applied force of 10 nN). It is clear from the measured force curve (Figure 4-8a) that no discontinuities or significant adhesion events occurred before or after the application of 10nN force, in agreement with previous work in which the membrane was purposely damaged (Obataya, I. *et al.*, 2005).

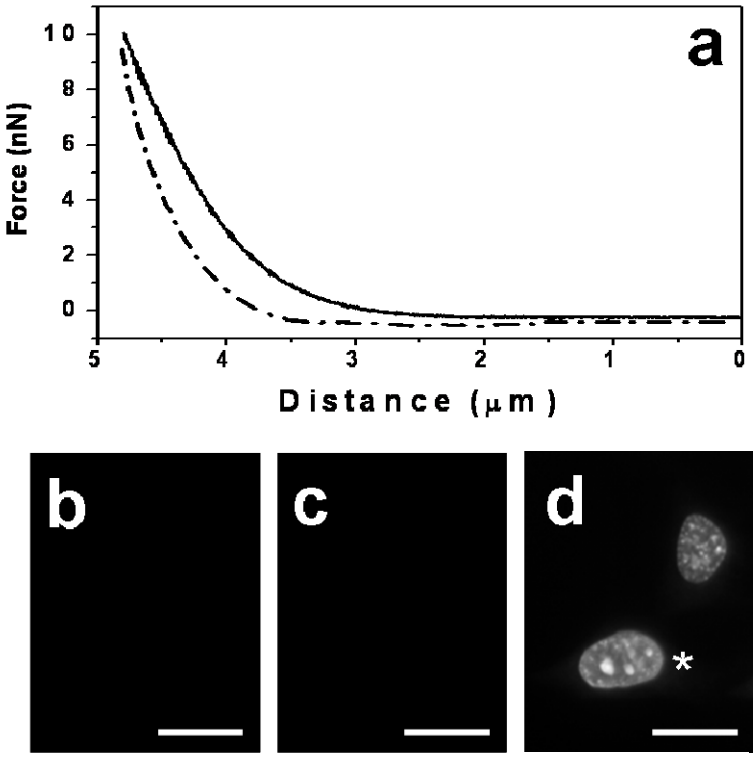

Figure 4-8. Membrane damage control experiment.

(a) A typical force-distance curve measured on a live cell with a maximum force of 10nN (straight line = approach; dashed line = retract). No discontinuities were observed in the approach portion of the force curve, and no significant adhesion events were observed in the retract portion of the curve. This suggests that there was no penetration of the AFM tip through the membrane. (b-d) In a second control experiment, the membrane-impermeable nuclear dye propidium iodide (PI) was added to the medium prior to perturbation at 10nN force. Fluorescent images were obtained 1 minute (b), and 20 minutes (c) after perturbation. As a positive control Triton X-100, a membrane-permeabilizing agent, was added to the medium and an image obtained 20 sec afterwards (d). In comparison to post-AFM perturbation images (b, c) where there was no staining observed, PI quickly localized in the nucleus after Triton X-100 exposure, producing a strong, well-defined, fluorescent signal (* shows the nucleus of the cell that was perturbed with the AFM tip). Scale bars: 20 μm

As a second control, propidium iodide (PI) was introduced into the medium during an AFM indentation experiment. PI is a membrane impermeable DNA

intercalating fluorescent dye which is routinely used to check for cell membrane damage or rupture during apoptosis. If membrane damage occurs, PI enters the cell and will quickly localize in the nucleus that becomes fluorescent; otherwise, PI remains outside the cell and does not fluoresce. With PI in the medium, fluorescence imaging before and after membrane indentation will reveal any damage to the cell membrane. In our study, we observed no evidence of membrane damage as there was no PI fluorescence immediately after perturbation and up to 20 minutes later (Figure 4-8b, c). As a positive control, we also added 0.5% Triton-X100 to the medium to purposefully damage the membrane. Upon addition of Triton-X100, PI immediately localized in the nucleus producing bright fluorescence, which can be seen as a well defined image of round and intact nuclei (Figure 4-8d). Taken together, these results confirm that the perturbation by the AFM tip does not damage the cell membrane of NIH3T3 fibroblasts or induce any longer term damage within the timeframe or conditions of our experiments. Therefore, any observed rearrangement of mitochondria in this study is due to the local perturbation by the AFM tip.

4.4 Conclusions

Here, the role of the cytoskeleton in transmission of mechanical forces over long distances was investigated. The methodology described here was used to evaluate the cytoskeleton's role in cellular force transmission by measuring force-induced displacements of mitochondria. Here, we used a natural cellular component as a marker for force transduction, eliminating the need for interference, such as by injection of microbeads or quantum dots into the cell. Two important observations were made:

1. The basal motility of mitochondria relies on an intact cytoskeleton. Disruption of either the microtubules or the actin cytoskeleton resulted in a ~50% decrease in the average mitochondrial motility;
2. AFM indentation, which led to a rapid increase of ~40% in mitochondrial displacement in untreated cells, did not have any effect on mitochondrial displacement when either the actin network or microtubules were disrupted using cytoskeletal drugs, showing the requirement of both cytoskeletal frameworks for the effective transmission of forces through the cell.

These findings have implications on our understanding of the connectivity of the different cytoskeletal networks in the cell and their relative impact on both cell stiffness and on the long distance propagation of forces through the cell. The importance of the cytoskeletal drug experiments performed here is the fact that they prove the cytoskeleton as the facilitator of the large increase in mitochondrial displacements that was observed in untreated cells following AFM indentation. Propagation of forces through the cell at

such high speeds may have a crucial role in the way cells adapt to their surrounding and interact with the ECM and neighbouring cells. As mechanical connections have previously been shown to exist between cytoskeletal filaments and the nucleus (Maniotis, A.J. *et al.*, 1997), this mechanism of force transduction might also be used to relay mechanical cues directly to the nucleus, directly affecting gene transcription (Hu, S.H. *et al.*, 2005; Ingber, D.E., 1993).

4.5 References

A-Hassan E., Heinz W.F., Antonik M.D., D'Costa N.P., Nageswaran S., Schoenenberger C.-A.,Hoh J.H. 1998. Relative microelastic mapping of living cells by atomic force microscopy. *Biophys. J.* 74:1564-1578.

Brady S., Lasek R.,Allen R. 1982. Fast axonal transport in extruded axoplasm from squid giant axon. *Science* 218:1129-1131.

Charras G.T.,Horton M.A. 2002. Determination of cellular strains by combined atomic force microscopy and finite element modeling. *Biophys. J.* 83:858-879.

Cooper J. 1987. Effects of cytochalasin and phalloidin on actin. *J. Cell Biol.* 105:1473-1478.

Heggeness M.H., Simon M.,Singer S.J. 1978. Association of mitochondria with microtubules in cultured cells. *PNAS* 75:3863-3866.

Hu S.H., Chen J.X., Butler J.P.,Wang N. 2005. Prestress mediates force propagation into the nucleus. *Biochemical and Biophysical Research Communications* 329:423-428.

Ingber D.E. 1993. Cellular tensegrity - defining new rules of biological design that govern the cytoskeleton. *Journal of Cell Science* 104:613-627.

Kabashima K., Matsuzaki M.,Suzuki H. 2007. Both microtubules and microfilaments mutually control the distribution of mitochondria in two-cell embryos of golden hamsters. *Journal of Mammalian Ova Research* 24:120-125.

Knowles M.K., Guenza M.G., Capaldi R.A.,Marcus A.H. 2002. Cytoskeletal-assisted dynamics of the mitochondrial reticulum in living cells. *Proceedings of the National Academy of Sciences of the United States of America* 99:14772-14777.

Kojima H., Ishijima A.,Yanagida T. 1994. Direct measurement of stiffness of single actin filaments with and without tropomyosin by in vitro nanomanipulation. *Proceedings of the National Academy of Sciences of the United States of America* 91:12962-12966.

Lee A. Ligon O.S. 2000. Role of microtubules and actin filaments in the movement of mitochondria in the axons and dendrites of cultured hippocampal neurons. *The Journal of Comparative Neurology* 427:351-361.

Levy R.,Maaloum M. 2002. Measuring the spring constant of atomic force microscope cantilevers: Thermal fluctuations and other methods. *Nanotechnology* 13:33-37.

Maniotis A.J., Chen C.S.,Ingber D.E. 1997. Demonstration of mechanical connections between integrins cytoskeletal filaments, and nucleoplasm that stabilize nuclear structure. *Proceedings of the National Academy of Sciences of the United States of America* 94:849-854.

Obataya I., Nakamura C., Han S., Nakamura N.,Miyake J. 2005. Nanoscale operation of a living cell using an atomic force microscope with a nanoneedle. *Nano Letters* 5:27-30.

Pelling A.E., Dawson D.W., Carreon D.M., Christiansen J.J., Shen R.R., Teitell M.A.,Gimzewski J.K. 2007. Distinct contributions of microtubule subtypes to cell membrane shape and stability. *Nanomedicine* 3:43-52.

Pelling A.E., Nicholls B.M., Silberberg Y.R.,Horton M.A. (2007). Approaches for investigating mechanobiological dynamics in living cells with fluorescence and atomic force microscopies. In *Modern research and educational topics on microscopy* (Méndez-Vilas, A. & Díaz, J., eds.), Vol. 3, pp. 3-10. Formatex.

Radmacher M., Fritz M.,Hansma P.K. 1995. Imaging soft samples with the atomic-force microscope - gelatin in water and propanol. *Biophysical Journal* 69:264-270.

Rotsch C.,Radmacher M. 2000. Drug-induced changes of cytoskeletal structure and mechanics in fibroblasts: An atomic force microscopy study. *Biophys. J.* 78:520-535.

Rudiger Suelmann R.F. 2000. Mitochondrial movement and morphology depend on an intact actin cytoskeleton in aspergillus nidulans. *Cell Motility and the Cytoskeleton* 45:42-50.

Vasquez R., Howell B., Yvon A., Wadsworth P.,Cassimeris L. 1997. Nanomolar concentrations of nocodazole alter microtubule dynamic instability in vivo and in vitro. *Mol. Biol. Cell* 8:973-985.

Chapter 5

Effect of Retinol and Conjugated Linoleic Acid (CLA) on Focal Adhesions and Cell Mechanics

Abstract

Retinol and Conjugated Linoleic Acid (CLA) have previously been shown to have an important role in gene expression and various cellular processes, including differentiation, proliferation and cell death. Here, we have investigated the effect of retinol and CLA, both individually and in combination, on the intracellular cytoskeleton, focal adhesions (FAs) and on the mechanical properties of 3T3 fibroblasts. We observed a dose-dependent decrease in the formation of FAs following treatment with either compound, which was directly correlated to an increase in cell height (>30%) and a decrease in the measured Young's modulus (~28%). Furthermore, treatments with both compounds demonstrated an increased, additive effect and led to a reduction of >70% in the average number of FAs per cell and a decrease of >50% in average cell stiffness. In addition, by quantifying displacements of mitochondria in response to applied AFM perturbations, force propagation through the cytoskeleton was shown to be strongly blunted in retinol- and CLA-treated cells. These data reveal that retinol and CLA disrupt FA formation, leading to an increase in cell height and a significant decrease in stiffness. These results may broaden our understanding of the interplay between cell mechanics and cellular contact with the external microenvironment, and help to shed light on the important role of retinoids and CLA in health and disease.

5.1 Introduction

Retinoids are naturally occurring derivatives of retinol (vitamin A) and have an important role in gene regulation and control in a variety of cellular and tissue processes, including proliferation, cell differentiation and apoptosis (Chambon, P., 1996; Napoli, J.L., 1996). They play an important role in tissue development, such as the nervous system and neurite growth (Margaret Clagett-Dame, E.M.M., Parag D. Muley,, 2006) and limb formation (Benoît Robert, Y.L., 2006). Retinoids are also potent inhibitors of carcinogenesis (Spom, M.B. & Roberts, A.B., 1983); for example, retinoic acid was found to prevent mammary carcinogenesis in rats (Anzano, M.A. *et al.*, 1994) and has also been used for the treatment of leukemia and other cancers in humans (Huang, M. *et al.*, 1988; Jing, Y. & Waxman, S., 2007; Lotan, R., 1996; Marill, J. *et al.*, 2003). These compounds also have wider functions reflected in their diverse effects on the regulation of specific genes (Balmer, J.E. & Blomhoff, R., 2002), including impacting on cell adhesion mediated by integrin cell adhesion receptors (Carla Rozzo, V.C., Gianluca Caridi, Gabriella Pagnan, Mirco Ponzoni,, 1997). Retinoic acid (RA) has been previously shown to stimulate keratinocyte growth in culture and also to inhibit the extracellular matrix (ECM) molecules fibronectin (FN) and thrombospondin (TSP) production (Varani, J. *et al.*, 1989). Similar results on FN inhibition were observed on 3T3 fibroblasts (Scita, G. *et al.*, 1996). Adhesion to the substrate was also reduced following treatments with RA, together with a decrease in ability of cells to reattach and spread (Varani, J. *et al.*, 1989).

Retinol and RA has also shown to have direct effect on skin conditions and appearance. Photoaging (also termed 'premature ageing') describes the sun-induced damage caused by UV irradiation to the skin. Unlike chronological ageing, which is affected only by the passage of time, photoaging relies upon the degree of sun exposure and skin pigmentation. Extracellular matrix degradation caused by solar irradiation contributes to the wrinkle phenotype of skin ageing (Fisher, G.J. *et al.*, 1996). A large number of controlled clinical studies has shown RA to improve the appearance of photoaged skin (Fisher, G.J. *et al.*, 2002; Weiss, J.S. *et al.*, 1988). It was suggested that this is related to the induction of TGF-β in mouse cells, which is a known inducer for the production of type I and III procollagen and other components of the dermal ECM (Glick, A.B. *et al.*, 1989; Kim, H.J. *et al.*, 1992). A dose-dependent decrease in the collagen-inductive effects of TGF-β following incubation with RA was also observed in fibroblasts (Redlich, C. *et al.*, 1995). Besides the effect on collagen, it is likely that other dermal components are affected by RA. One example is the UV irradiation-induced protein c-Jun, which is a known inhibitor of types I and III procollagen and which accumulation was shown to be blocked by RA treatment (Fisher, G.J. *et al.*, 2002).

Clinical vehicle-controlled studies also show that retinol can be used to improve naturally-aged skin. Retinol application significantly reduced the fine wrinkling in chronologically aged skin (skin located at the upper inner arms) and induced type I procollagen (Kafi, R. *et al.*, 2007). In these studies retinol was favourably used over retinoic acid, as it was found to penetrate the skin and cause RA-like effects, with a much less degree of skin irritation, compared to RA (Kang, S.W. *et al.*, 1995)

Retinol can enter the cell passively by diffusion through the plasma membrane or via active transport by a membrane-bound retinol-binding protein (RBP) (Napoli, J., 1996) (Figure 5-1). Once in the cell, retinol binds to cellular retinol-binding protein (CRBP) which serves as a substrate for retinol conversion into retinoic acid (RA), the biologically active form of retinol (Napoli, J., 1996). RA then enters the nucleus, most likely with the assistance of one of the cellular RA binding proteins (CRABPs) (Ward, S.J. & Morriss-Kay, G.M., 1997). In the nucleus, RA acts as a ligand to activate the transcription factors RA-receptor (RAR) and retinoid X receptor (RXR). Together, they influence the transcription of various genes by binding to retinoic acid response elements (RARE) that are downstream of those genes (Levin, A.A. *et al.*, 1992; Napoli, J.L., 1996). Figure 5-1 shows the metabolic pathways of retinol and the mechanism through which it influences gene expression.

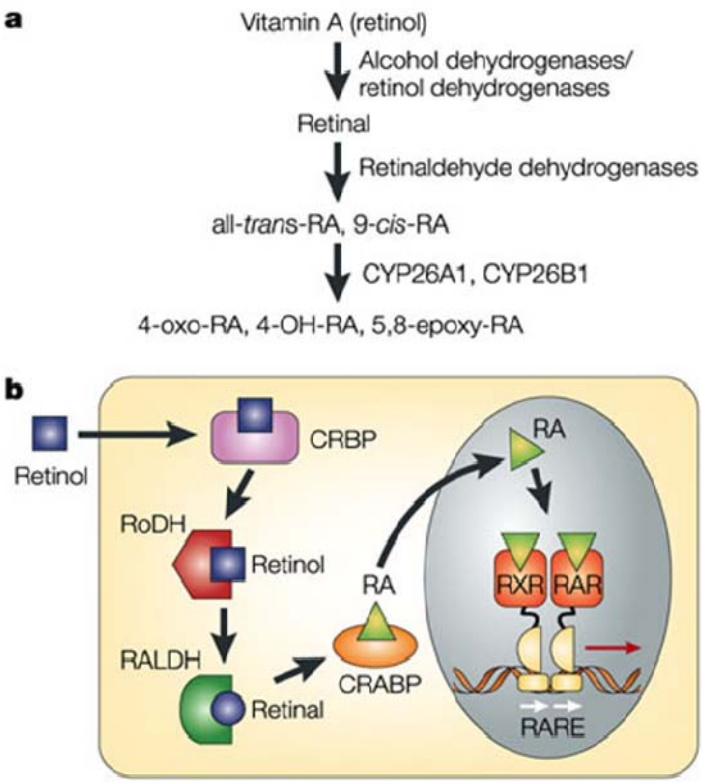

Figure 5-1. Retinol: metabolic pathways and mechanism of action.

(a) Metabolic pathway for retinol conversion into various forms of RA. (b) The cellular pathway of RA action. In the cytoplasm retinol is bound to CRBP and undergoes conversion into RA. With the assistance of CRABPs it enters the nucleus and activates transcription factors RAR and RXR, together with which it binds to RARE elements of the DNA, affecting gene transcription (from (Maden, M., 2002)

Conjugated Linoleic Acid (CLA) is a general term for a family of linoleic acid isomers, found mainly in beef, milk and other dairy products (Pariza, M.W. *et al.*, 2000). Recent research shows that retinol levels increase in the breast, liver and plasma in proportion to CLA intake (Banni, S. *et al.*, 1999; Carta, G. *et al.*, 2002). As such, CLAs affect fat metabolism and hence body composition (DeLany, J.P. & West, D.B., 2000; Evans, M.E. *et al.*, 2002) and are anti-adipogenic and impact insulin resistance. CLA has a broad range of physiological effects and, as with retinoids, CLA exposure produces diverse effects on gene regulation (Moya-Camarena, S.Y. & Belury, M.A., 1999). Previous research found CLA to be a potent inhibitor of various pathological processes, including atherosclerosis, inflammatory responses, osteoporosis and carcinogenesis (Bhattacharya, A. *et al.*, 2006; Butz, D.E. *et al.*, 2007; Das, U.N., 2000; O'Shea, M. *et al.*, 2004; Pariza, M.W. *et al.*, 2000; Song, H.J. *et al.*, 2005; Toomey, S. *et al.*, 2006; Watkins, B.A. & Seifert, M.F., 2000; Whigham, L.D. *et al.*, 2000; Zulet, M.A. *et al.*, 2005). Regarding the latter, both animal and *in-vitro* data suggest that CLA possesses anti-carcinogenic characteristics, including an increase in retinol concentrations, inhibition of tumor growth and suppression of metastasis of cancer cells (Whigham, L.D. *et al.*, 2000). Of particular relevance to the present work, CLA can impact cell adhesion at several levels: extracellular matrix synthesis and degradation (Hubbard, N.E. *et al.*, 2007; Ringseis, R. *et al.*, 2008), intracellular signaling (Song, H.J. *et al.*, 2004), and cell-cell and cell-matrix interactions (Chen, B.-Q. *et al.*, 2004; Sneddon, A.A. *et al.*, 2006). Moreover, the capacity of CLA to increase retinol levels in different tissues could be related to the known ability of CLA to activate peroxisome proliferator activated receptors (PPARs) (Lampen, A. *et al.*, 2005). A suggested route might be the activation

of PPAR-alpha by CLA, which is a known transcription factor for CRBP, the cellular retinol-binding protein. CRBP acts as a substrate for the conversion of retinol into RA, hence increasing the concentration of CRBP would lead to increased synthesis of RA (Carta, G. *et al.*, 2002; Napoli, J., 1996).

One of the proteins in which expression is known to be affected by RA is fibronectin (FN), a dimeric protein that plays an important role in cell attachment to the extracellular matrix (ECM) at cellular focal adhesions. FN is bound by integrin receptors on the cell through specialized protein domains and amino-acid sequences, such as the arginine-glycine-aspartate (RGD sequence), and ECM components such as collagen, heparin and fibrin (Hynes, R.O., 1992; Pankov, R. & Yamada, K.M., 2002). In vertebrates, FN exists in one of two forms: as an abundant soluble constituent of plasma (at a concentration of about 300 μg/ml) and other body fluids, and in the insoluble extracellular matrix. Soluble FN dimers are secreted by various cells, mainly fibroblasts, and then assembled into an insoluble matrix as part of the ECM (Pankov, R. & Yamada, K.M., 2002). Retinoic acid has previously been shown to reduce cellular fibronectin mRNA and protein levels in primary hepatocytes (Kim, H. & Wolf, G., 1987). More recently, RA was found to significantly reduce the levels of intracellular FN in NIH-3T3 fibroblasts, in a dose-dependant manner (Scita, G. *et al.*, 1996; Scita, G. & Wolf, G., 1994). RA did not alter the levels of FN transcripts and was proposed to act on FN at a post-transcriptional level (Luigi M. De Luca, G.S., Jun Takatsuka,, 1997).

Focal adhesions (FAs) are specialised sites of adhesion between the cell and the ECM and appear in many cell types, including fibroblasts (Burridge, K. & Chrzanowska-Wodnicka, M., 1996). They consist of a complex of proteins, including integrin cell

adhesion receptors that interact with the ECM externally and with the actin cytoskeleton on the inside of the cell. Integrins are heterodimeric cell surface receptors composed of two non-covalently associated transmembrane subunits, α and β, which in addition to connecting adhesive proteins in the ECM to the cytoskeleton are also involved in intracellular signal transduction (Hynes, R.O., 1992). The cytoplasmic part of the integrin dimer interacts with various intracellular proteins, most notably talin and vinculin (Miyamoto, S. *et al.*, 1995). Vinculin is an intracellular protein that controls and regulates the formation of FAs by directly interacting with actin and other proteins that are involved in FAs formation (Humphries, J.D. *et al.*, 2007).

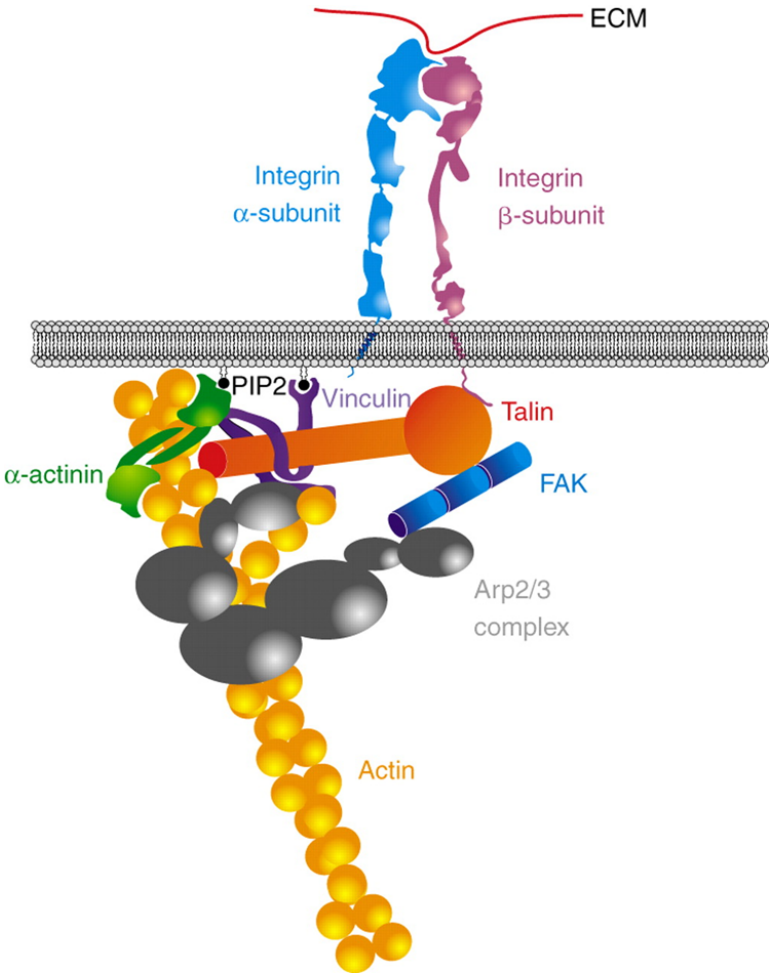

Figure 5-2. The various proteins involved in focal adhesions.

The complex assembly of proteins involved in the linking of the membrane-spanning integrins to the actin cytoskeleton. Integrins can bind directly to the talin head domain. Through its tail domain, talin can bind directly to the actin, as well as to other protein that are involved in the FA such as vinculin. Vinculin can also directly bind actin and is also anchored to the membrane (from (Vicente-Manzanares, M. *et al.*, 2009)

Acting as the point of contact between the cell and the extracellular matrix, integrins have been shown to be mechanically coupled to the cytoskeleton filaments, the nucleus and the ECM (Maniotis, A.J. *et al.*, 1997). Acting as mechanoreceptors, integrins mediate the transfer of extracellular mechanical stresses into the cytoskeleton and nucleus (Ingber, D.E., 2003b; Wang, N. *et al.*, 1993). Conversely, tensional forces generated within the cytoskeleton are directed towards the cell substrate and ECM through FAs to affect cell shape and motility (Polte, T.R. *et al.*, 2004). FAs also play a crucial role in the ability of cells to generate and transmit forces to the ECM (Balaban, Nathalie Q. *et al.*, 2001; Burridge, K. & Chrzanowska-Wodnicka, M., 1996) and to maintain an internal prestress in cells (Ingber, D., 1991; Wang, N. *et al.*, 1993). Furthermore, the magnitude of local forces exerted by the cell have been linearly correlated to the intensity and surface area of the corresponding FAs (Balaban, N. Q. *et al.*, 2001).

Here, we have treated fibroblast cells with retinol and CLA in order to examine their effect on the intracellular cytoskeleton, cell adhesion and the nanomechanical properties of living cells. We have found a dose-dependent decrease in the average number of FAs per cell following retinol and CLA treatments. The loss of FAs was also followed by an increase of up to 30% in the average cell height. This directly correlated to a decrease in cell stiffness, determined on local (<100 nm^2) and global (>10 μm^2, using fabricated colloidal probes) areas of the cell membrane by AFM measurements of Young's modulus (YM). In addition, a combination treatment of both retinol and CLA was shown to have a cooperative effect and led to a decrease in the average number of FAs per cell and a >50% decrease in average cell stiffness, supporting previous evidence of CLA role as an enhancer of retinol levels (Carta, G. *et al.*, 2002). Our results reveal

that retinol and CLA treatments disrupt intact FA formation and cell adhesion, leading to a concomitant increase in cell height and changes to the nanomechancial properties of the cell membrane. Therefore, understanding the interplay between retinol and CLA with cell adhesion and cellular mechanics may help to illuminate some of the underlying mechanisms linked to these vital biological pathways in normal physiology and the development of a range of diseases.

5.2 Materials and Methods

5.2.1 Cell Culture

NIH-3T3 Fibroblasts were cultured in DMEM GlutaMAX media supplemented with 10% fetal bovine serum (both obtained from Invitrogen, Paisley, UK), 100 IU/mL penicillin and 100 μg/mL streptomycin (Invitrogen), and were maintained at 37 °C and 5% CO_2. Cells were plated into 50 mm glass-bottom FluoroDish™ culture dishes (World Precision Instruments, Inc., UK) one day prior to the experiment.

5.2.2 Retinol and CLA

Retinol and CLA were obtained from Sigma-Aldrich Company Ltd., Dorset, UK. Synthetic crystalline retinol (>95% HPLC) was dissolved in ethanol at 3 mM. Conjugated Linoleic acid (CLA) containing a mixture of *cis*-9, *trans*-11 CLA and *trans*-10, *cis*-12 CLA, was dissolved in ethanol at 71 mM. All stock solutions were stored at -20ºC until used. Retinol was used at final concentrations of 10 μM and 20 μM, and CLA was used at final concentrations of 50 μM and 100 μM. At higher concentrations of the two compounds there was an apparent toxic effect with changes in cell proliferation and hence the lower concentrations were used throughout this study. The ethanol solutions of the compounds were dissolved in the culture media and cells were left for incubation for 24 hr prior to the experiment. Controls were incubated for 24 hr with an equal dose of ethanol as the highest compound-treated cells were incubated with. For comparisons of drug effect, in some cases cells were incubated with the actin depolymerisation drug

Cytochalasin D (5μM, Sigma, UK) for 30 min prior to elasticity measurement experiments (Pelling, A.E. & Veraitch, F.S. *et al.*, 2007).

5.2.3 Immunofluorescence and Imaging

Prior to fluorescence staining, cells were washed with warm PBS, fixed with 3.5% paraformaldehyde, 2% sucrose (10 min) and permeabilsed with 0.5% Triton-X (3 min) at room temperature. FAs were stained at room temperature by incubating cells with mouse monoclonal anti-vinculin (Abcam, Cambridge, UK) for 30 min followed by Alexa 546 rabbit-anti-mouse immunoglobulins (Invitrogen, Paisley, UK) for 30 min with a 15 min wash after each incubation. Actin filaments were then stained by incubating at room temperature with Phalloidin Alexa Fluor 488 (Invitrogen, Paisley, UK) for 20 min followed by a 15 min wash. Finally, nuclei were stained by incubation with DAPI (Invitrogen, Paisley, UK) on ice for 10 min, followed by a final 10 min wash with PBS. Images were acquired on an Olympus FV1000 laser scanning confocal microscope (Olympus, UK).

5.2.4 AFM indentation and extraction of Young's modulus

Cells plated in cell culture dishes with 3 ml of buffered (10 mM Hepes) media were placed in a combined AFM-fluorescence microscope (Olympus IX71 inverted optical microscope and JPK NanoWizard® I AFM). Using a temperature-controlled stage, the culture media was maintained at 37°C for the duration of the experiment. For each culture dish, the experimental time was less than half an hour, which prevented significant evaporation of the culture media. MSCT-AUWH cantilevers (Veeco) with

pyramidal-shaped tips were calibrated and the spring constant was experimentally determined to be 0.05 ± 0.01 N/m (Levy, R. & Maaloum, M., 2002). Single, live interphase cells were chosen optically and the AFM cantilever was positioned above the nucleus. Force-distance measurements were initiated with a maximum force of 2nN. Individual cells were selected randomly from across the tissue culture dish and 24 cells were tested for each of the drug treatment experiments and controls. All AFM measurements were made over the nucleus for two reasons: First, to act as a constant reference point, as cell shape can vary greatly. Secondly, to avoid the effect of the hard glass substrate that the cells were adhering to - AFM material properties would artificially be higher if the cell edges of spread cells were used. 10 force curves were recorded over the nucleus of each cell at 1 Hz. The data was then fitted for an indentation of 200nm using the Hertz model for either conical or spherical indenters (Pelling, A.E. & Nicholls, B.M. *et al.*, 2007; Radmacher, M. *et al.*, 1995)

$$\textbf{1.}\quad F_{cone} = \frac{2}{\pi}\frac{E}{(1-\nu^2)}\tan(\alpha)\delta^2$$

$$\textbf{2.}\quad F_{sphere} = \frac{4}{3}\frac{E}{(1-\nu^2)}\sqrt{R}\delta^{3/2}$$

Where is ν is Poisson's ratio, α the half opening angle of the tip in the case of cone indentation (1), R is the sphere radius in the case of sphere indentation (2), δ is the indentation depth of the tip and *E* is the Young's modulus.

5.2.5 Preparation of spherical indenters

Polystyrene microspheres (Bangs Laboratories Inc., Fishers, IN) of ~19 μm diameter were glued onto tipless cantilevers (CSC 12 rectangular beam, MikroMasch, Estonia, 350

um long, 35 μm wide and 1.0 μm thick, spring constants about 0.03 N/m) using a small amount of epoxy resin (UHUÒ plus Schnellfest, UHU GmbH & Co. KG, Germany). Spring constants of each individual cantilever were determined as described before (Levy, R. & Maaloum, M., 2002) and the exact size of each sphere was measured using optical and scanning electron microscopy. The particles were washed in Decon 90 (Decon Laboratories Limited, UK), rinsed in an excess of deionised water, and subsequently treated in an O_2 plasma for 100 s. Probes were stored in nitrogen atmosphere before use. Tips were calibrated before each experiment and the spring constant was determined to be 0.06 ± 0.01 N/m (Levy, R. & Maaloum, M., 2002).

5.2.6 Statistical Methods

Data are presented as mean ± standard error of the mean (s.e.m), unless stated otherwise. Measurements were analysed using unpaired or paired Student's *t* tests with significance at $P < 0.05$ or lower, as stated in the text.

5.3 Results and Discussion

5.3.1 Effect of retinol and CLA on focal adhesions formation

Cells were incubated for 24h with either retinol, CLA, or retinol and CLA together, at various concentrations and then fixed and stained for vinculin, actin filaments and the nucleus (see Materials & Methods).Figure 5-3 shows results for the following treatments: untreated control, 10 μM retinol, 50 μM CLA and a combination of 10 μM retinol and 50 μM CLA. Images reveal the structure of the nucleus (blue), focal adhesions (FAs) (red) and actin filaments (green). The right column of images shows only the nucleus and FAs, for clarity. FAs are clearly visible at the cell periphery and in much greater number in the control (Figure 5-3, b; white arrows) when compared to the retinol- and CLA-treated cells (Figure 5-3, d and f). The combination of retinol and CLA resulted in a further reduction of discrete FAs (Figure 5-3, h) are only apparent at the cell periphery.

In order to assess the effect retinol and/or CLA had on the spatial distribution of FAs, the morphology and total number of discrete FAs were analysed for 30 cells along a cross section of the culture dish for the controls and each compound. A significant decrease in the number of individual FAs per cell for the treated cells was observed. Figure 5-4 shows the average number of FAs per cell (n = 30 cells for control and each of the treatments).

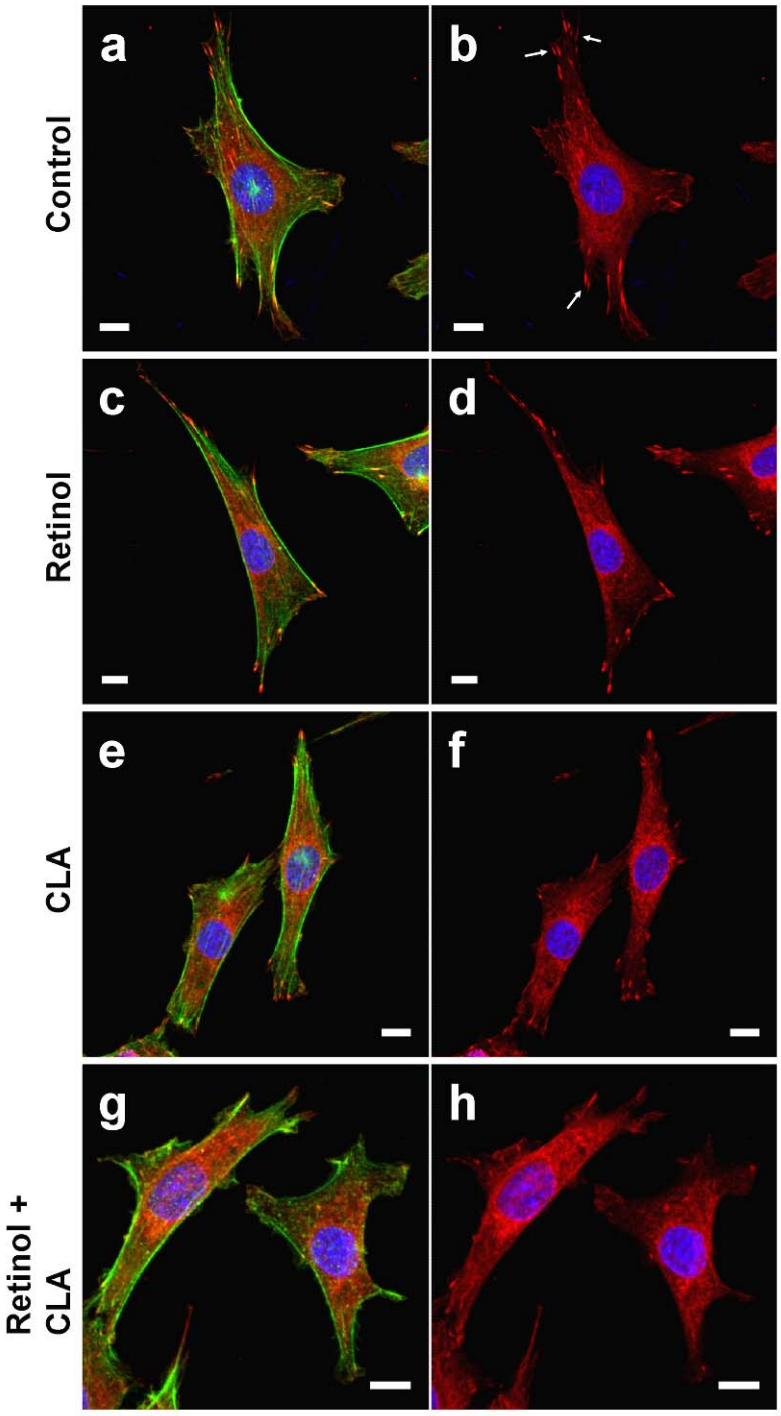

Figure 5-3. Reduction in focal adhesions following treatments with retinol and CLA

NIH-3T3 fibroblasts were treated at the lower-end concentrations of retinol (10 μM) and CLA (50 μM) for 24h prior to staining, individually and in combination of the two compounds. Cells were then fixed and stained for nucleus (blue), actin filaments (green) and FAs (red). The left column shows all three dyes, and the right column shows only the nucleus and FAs, for clarity. Discrete FAs are clearly visible in large numbers at the cell periphery for the control (b, white arrows). Fewer FAs are seen for the retinol- and CLA-treated cells (d and f, respectively) and are much less apparent in the case of combination treatment of the two compounds (h). The actin cytoskeleton does not seem to be greatly affected and cell integrity is maintained after treatments (a, c, e, h). Scale-bars are all 10μm.

For control cells, 19.8 ± 1.2 discrete FAs were observed per cell, while in treated cells the number showed a dose and compound dependent significant decrease of 22% to 70% (Figure 5-4). The lowest doses of retinol (10 μM) and CLA (50 μM) resulted in a reduction of 22% and 23%, respectively. Doubling the dose led to a further decrease in the average number of FAs per cell of 47% for retinol and 44% for CLA. Interestingly, a combination of retinol and CLA treatments, even at the low doses, led to a decrease of more than 50%, showing an additive effect of the two drugs. The highest dose combination gave rise to the greatest decrease (70%; $*P < 0.01$, control *versus* each treatment).

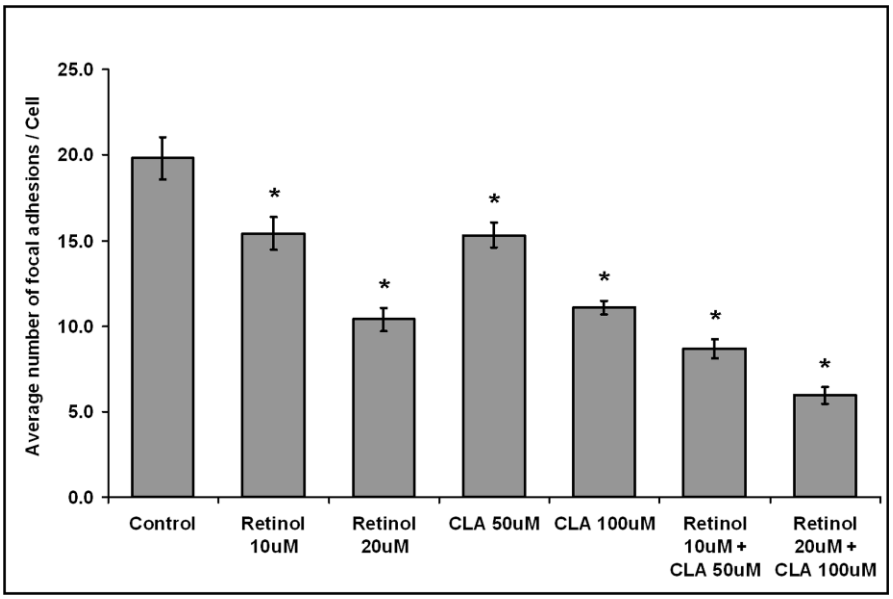

Figure 5-4. The effect of retinol and CLA treatments on focal adhesions.

The number of FAs per cell was averaged along a cross section of the dish (n = 30 cells in each treatment). For control, there was an average of 19.8 ± 1.2 discrete FAs per cell. The lowest doses of retinol and CLA (10μM and 50μM, respectively) resulted in similar reductions (22% and 23%, respectively). Doubling the doses of retinol and CLA led to a decrease of 47% and 44%, respectively. Treatment with both drugs, in combination, at their lower concentration, led to a decrease of 56% and at their higher concentration to a decrease of 70% in the average number of FAs. $*P < 0.01$ for control *versus* each treatment.

In addition to a decrease in the number of FAs a change in cell height was observed, as determined by confocal microscopy. Treated cells were also higher than control, with an average height of 7.7 μm ± 0.6 μm for cells treated with retinol and CLA (at concentrations of 20 μM and 100 μM, respectively; n = 20 cells), compared to an average height of 5.8 μm ± 0.6 μm (n = 14 cells) for controls (*P < 0.005). Thus, an increase of >30% in the average cell height following the treatment. The decrease in FAs formation and the subsequent increase in cell height raised the question of whether these biological effects have a significant impact on the nanomechanical properties of the treated cells.

5.3.2 Effect of retinol and CLA on cell stiffness

Prior to Young's modulus (YM) measurements, 3T3 fibroblasts were plated and incubated with the retinol or CLA for 24h as described above. Figure 5-5 shows typical AFM force-indentation plots that were derived from force curves produced for control and for the different treatments, using either conical (Figure 5-5a) or spherical (Figure 5-5b) indenters.

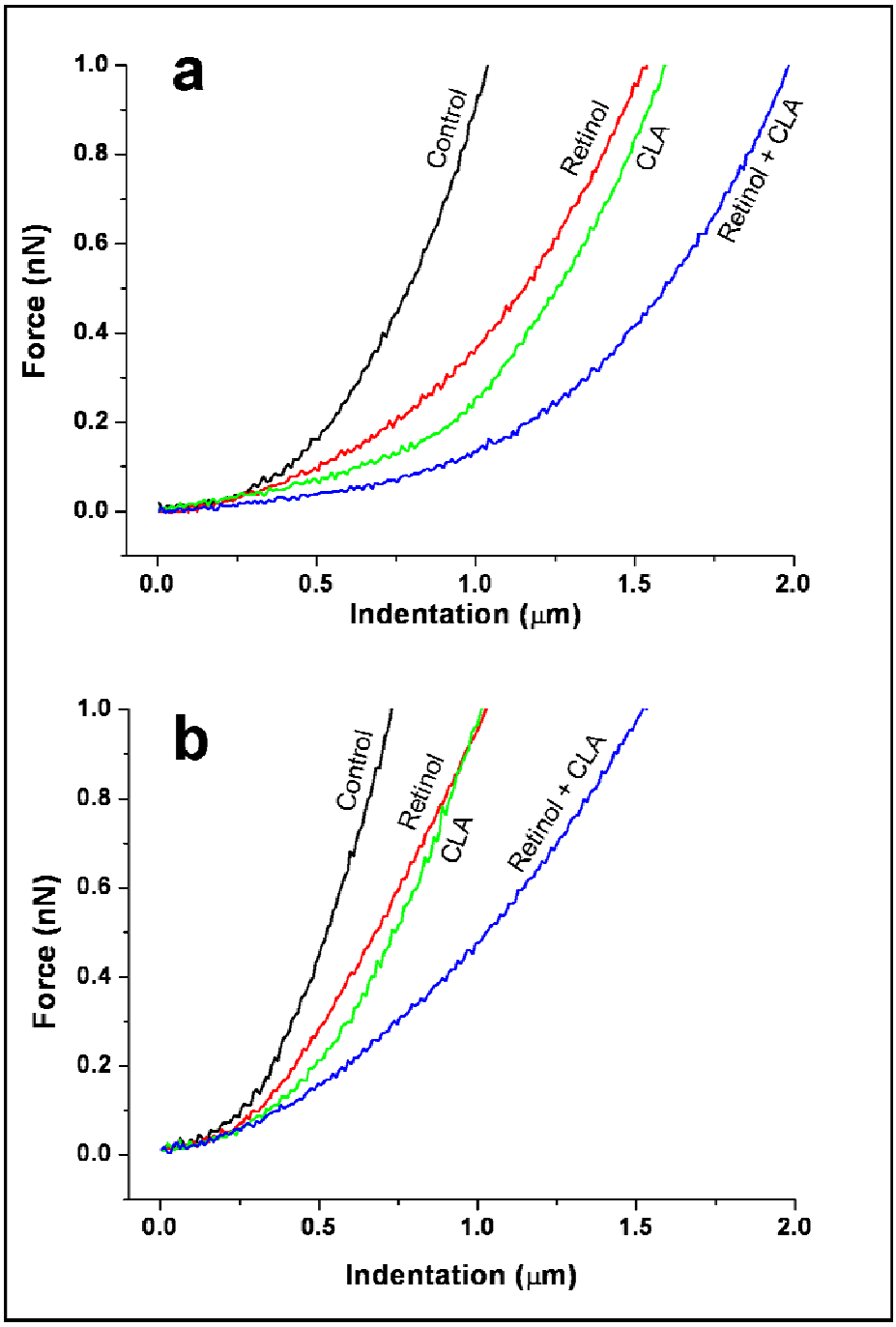

Figure 5-5. Force-indentation plots for cells treated with retinol and CLA.

AFM force-indentation plots that were derived from force curves produced for control and for the different treatments, using either conical (a) or spherical (b) AFM indenters. For the same magnitude of force, the indentation of the AFM into treated cells is greater than that of control, demonstrating the decrease in Young's modulus following treatments with retinol and CLA.

The effect of compounds on cell material properties was first examined by using standard AFM cantilevers with nominally cone-shaped tips. Figure 5-6 shows the dose-dependant decrease in cell stiffness in retinol and CLA-treated cells.

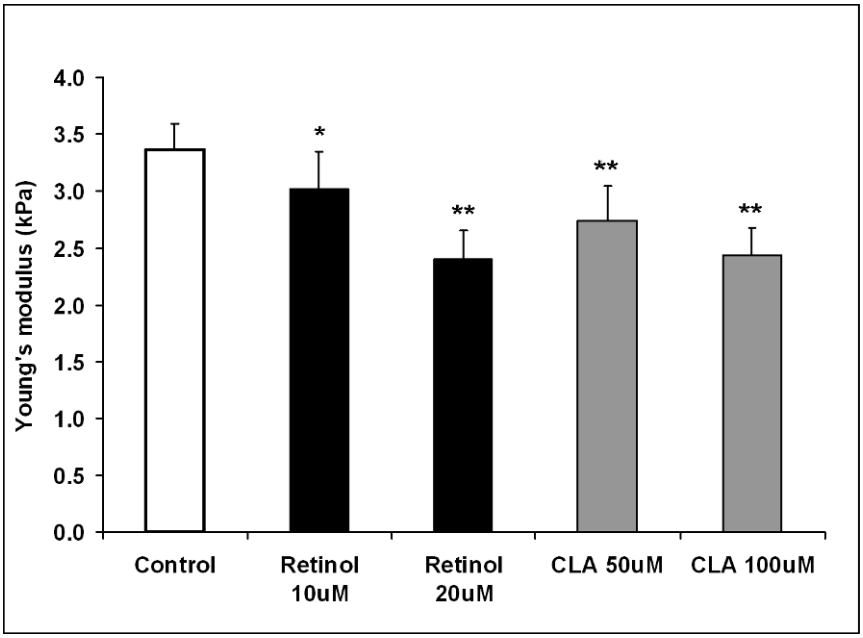

Figure 5-6. Young's modulus of retinol- and CLA-treated fibroblasts.

Cells were incubated with either retinol or CLA for 24h prior to force measurements. For the control, the measured YM was 3.4 ± 0.2 kPa; for 10μM retinol, YM was 3.0 ± 0.3 kPa and for 20μM retinol, the measured YM was 2.4 ± 0.35 kPa. Thus, a decrease of 10% and 29%, respectively, in comparison to the control. Following incubation with 50μM CLA the measured YM was 2.7 ± 0.3 kPa and for 100μM CLA the measured YM was 2.4 ± 0.2 kPa. Thus, a decrease was observed of 19% and 28%, respectively, in comparison to the control. $*P < 0.05$; $**P < 0.005$ (control versus drug treated; n = 24 cells for each treatment).

For the control, untreated cells, the average measured YM was 3.4 ± 0.2 kPa. For 10 μM retinol treatment the measured YM was 3.0 ± 0.3 kPa ($*P < 0.05$ *versus* control; n = 24 cells, 10 measurements per cell as described in the Materials and Methods) and for 20 μM the YM was 2.4 ± 0.3 Pa ($**P < 0.005$ *versus* control; n = 24 cells). Thus, a decrease

of 10% and 29%, respectively, in comparison to the control. Treatments with CLA showed a similar dose-dependent decrease in stiffness, as shown in the case of retinol. For 50 μM CLA, the measured YM was 2.7 ± 0.3 kPa and for 100 μM CLA the measured YM was 2.4 ± 0.2 kPa (**$P < 0.005$ *versus* control; n=24 cells). Therefore, there was a decrease of 19% and 28%, for each treatment respectively, in comparison to the control.

In order to investigate the effect of retinol and CLA in combination, cells were incubated with the two: at either a concentration of 10 μM retinol and 50 μM CLA, or twice that at a concentration of 20 μM and 100 μM. Figure 5-7 shows the results of YM measurements for these treatments. Incubation with a combination at the lower concentrations led to a significant decrease of ~50% in stiffness compared to the control. Thus, the drug combination resulted in a greater decrease than in each of the individual cases (**$P < 0.005$ for all drug combinations; n = 24 cells for each treatment), showing a cooperative effect of the two drugs on cell stiffness. When retinol and CLA concentrations were doubled, the decrease was similar to that with the lower concentration (data not shown). Cytochalasin D (CytD) interferes with actin filament polymerisation/depolymerisation, disrupting the cytoskeleton, and was used to examine the effects of disrupting the actin cytoskeleton. Treatment with CytD (for 20 min at concentration of 5 μM) caused a reduction in cell stiffness of 55% (Figure 5-7). As treatment with a combination of retinol and CLA, on the other hand, did not show disruption to the actin cytoskeleton (Figure 5-3g), but nonetheless resulted in a similar decrease in stiffness, a different mechanism is to be considered (see Discussion, below).

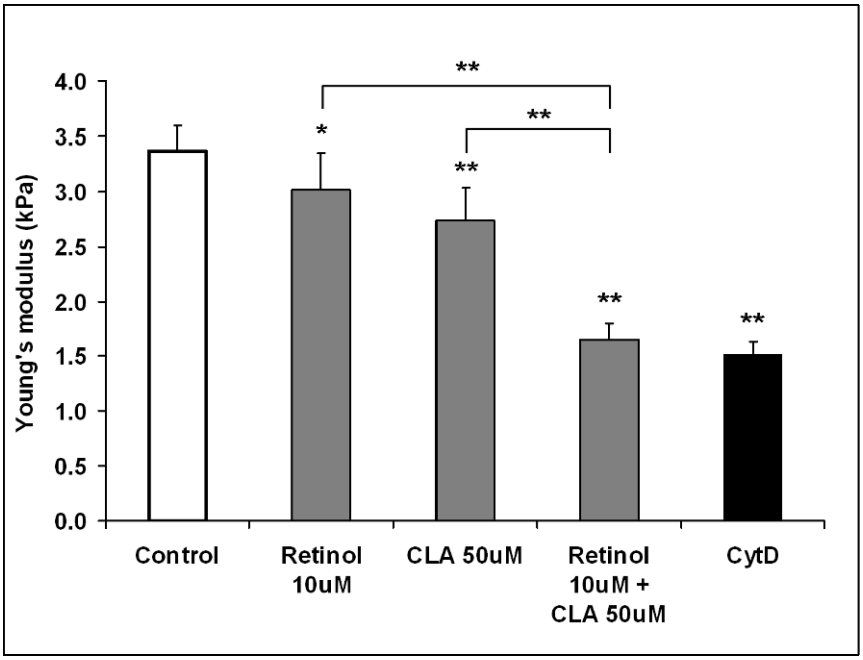

Figure 5-7. Young's modulus following combination treatments with retinol and CLA.

When cells were incubated with both retinol and CLA, a decrease in stiffness of ~50% was observed. This decrease is larger than that observed for the individual drugs, and is similar to the decrease observed when cells were incubated with the actin polymerisation inhibitor, CytD (5μM, 20 min). Error bars are mean ± s.e.m; **P* < 0.05, ***P* < 0.005 (control *versus* drug-treated and individual treatments *versus* the combination treatment).

To examine the effect of local versus global force curve measurements on the observed Young's modulus, all experiments were repeated with a cantilever tip to which a polystyrene bead of ~19 μm diameter was attached (A-Hassan, E. *et al.*, 1998; Charras, G.T. & Horton, M.A., 2002a). A spherical indentation differs from a conical indentation in both the contact area and indentation profile. Spherical indentation has a much larger surface area (>10 μm^2 for a 200 nm indentation) when compared to conical indentation where the contact surface area for a 200 nm indentation is < 100 nm^2. Figure 5-8 shows the YM results for spherical indentations in the different treatments. The results here

were similar to those obtained with a conical indenter, and revealed a decrease of 44% in cell stiffness for the lower-concentration combination treatment and a decrease of 53% in stiffness for the higher-concentration combination treatment ($p < 0.005$ for both cases when comparing untreated versus treated and individual drugs versus the combination).

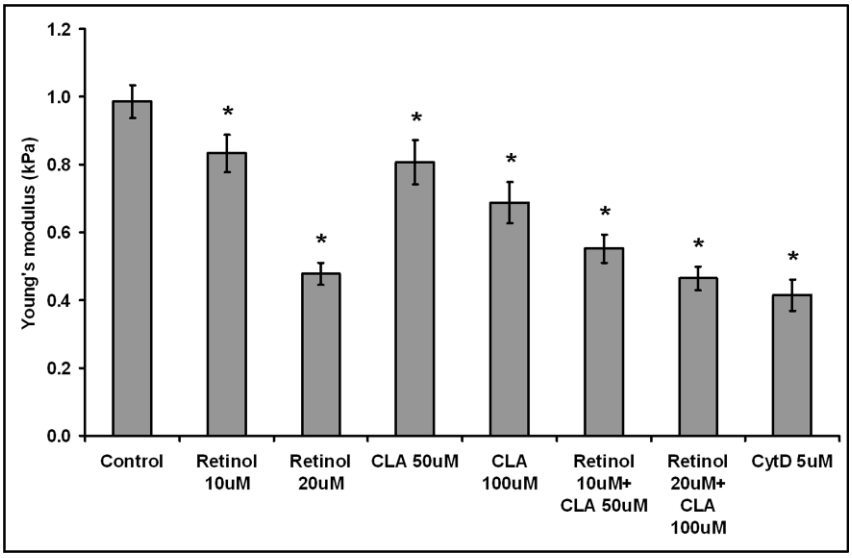

Figure 5-8. Young's modulus for retinol/CLA treatments using a spherical indenter.

Changes in cell stiffness following treatments with retinol and CLA, measured with a spherical indenter (polystyrene bead, 19μm diameter), showed a similar trend to the ones measured using a conical indenter (Figure 5-6 and Figure 5-7). Treatment with the actin polymerisation inhibitor CytD (5μM, 30min) led to a decrease of 58% in YM. This decrease in YM was similar to that observed for a combination treatment of retinol and CLA (20μM and 100μM, respectively), where a decrease of 53% was observed.

Although the absolute values for YM differed significantly between conical and spherical indentations, it is important to note that the relative change in YM, when comparing control to treated cells for each of the two indentation methods, is similar (see discussion in 4.3.3). These results show that a decrease in membrane stiffness that follows drug treatments is measureable both at the local nano-scale (<100 nm^2) and at the

global micro-scale (>10 μm^2) and appears to be correlated to the number and distribution of FAs per cell.

5.3.3 Effect of retinol and CLA on force-induced displacements of mitochondria

As a final step for the investigation of retinol and CLA effects on the cell, mitochondrial displacements experiment were conducted for all of the different treatment combinations, in a similar way as was done for CytD- and nocodazole-treated cells in Chapter 4. Fluorescence images were acquired at 1 sec intervals prior and post-AFM indentation, with the control being mitochondrial displacements between two consecutive images taken prior to indentation. Trajectories of mitochondria were analysed using the feature point tracking algorithm. For each of the treatments, 10 cells were examined with a total of ~200 mitochondrial trajectories analysed. Figure 5-9 shows the natural displacement (white) next to the force-induced displacements (green) for each of the treatments.

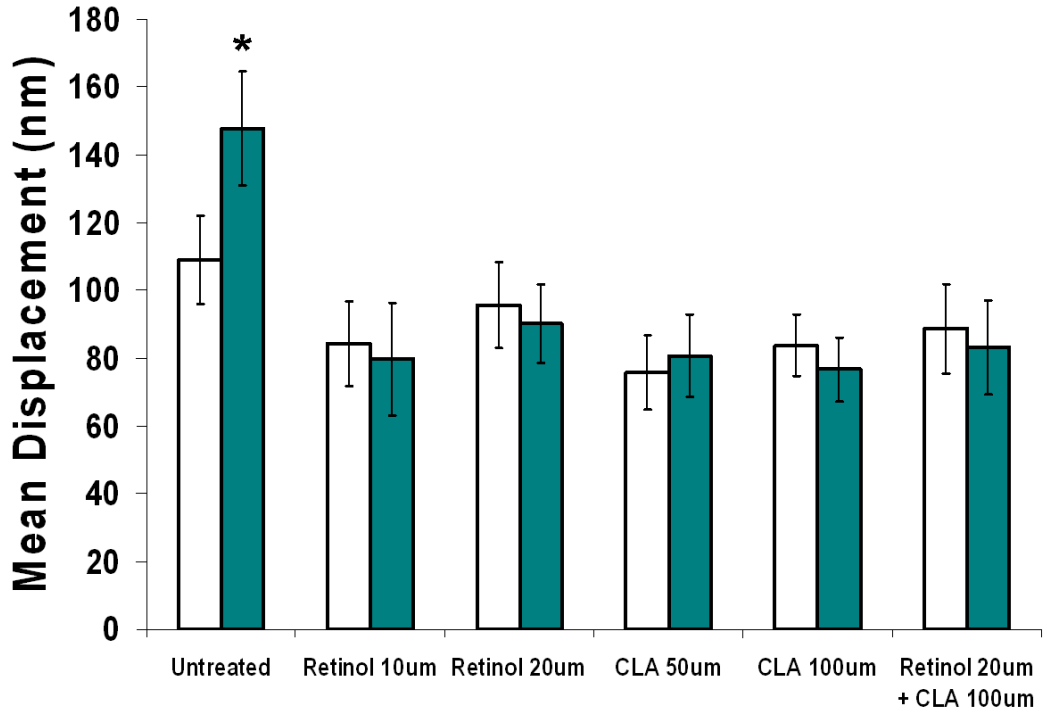

Figure 5-9. Effect of retinol and CLA on the force-induced displacement of mitochondria.

For each case, the white bar represents the mean natural displacement (nm) of mitochondria in a one-second interval. The green bar represents the mean displacement of mitochondria in the consecutive one-second interval, in which AFM indentation took place. The displacement of mitochondria following indentation did not show a significant increase in any of the treatments ($P > 0.1$), in comparison to the ~35% increase that was observed for untreated cells (*$P < 0.001$, control *versus* force-induced displacement).

Natural mitochondrial motility of compound-treated cells showed no significant difference from that of untreated cells ($P > 0.1$). Interestingly, the mean displacement of mitochondria following indentation also did not show a significant increase in any of the treatments ($P > 0.1$ for all treated cells; natural *versus* force-induced displacement). In comparison, untreated cells showed an increase of ~35% in the force-induced

displacement (*$P < 0.001$). A similar effect on force transmission was observed in cells treated with cytoskeleton-disrupting drugs (Chapter 4). However, unlike treatments with CytD and nocodazole, treatments with retinol did not show an adverse effect on the cytoskeleton (compare retinol/CLA-treated cells in Figure 5-3 with CytD/nocodazole-treated cells, Figure 4.1 in Chapter 4).

5.4 Conclusions

In this study, we examined the effect of two compounds, retinol and CLA, alone and in combination, on the number of intact FAs in the cell as well as cell stiffness in 3T3 fibroblasts. Both retinol and CLA were shown to have a similar dose-dependant impact on the number of FAs present at the cell periphery and on the stiffness of 3T3 fibroblasts. At lower doses of the two drugs, a decrease of ~20% in FAs was observed, and this decrease rose to ~45% when the concentrations were doubled. Interestingly, a combination treatment of the two drugs, even in the lower concentrations, led to a decrease of ~50% in the number of FAs. This decrease in the number of FAs at the cell periphery might have led to an observed increase in cell height of more than 30%, which, in turn, led to a significant decrease in the measured YM for the treated cells. Lower-dose treatments with the individual compounds led to a decrease of up to ~20% in the measured YM, and a combination of the two led to a significant decrease in cell stiffness of ~50%. In addition, by quantifying mitochondrial displacements in response to applied AFM perturbations, force propagation through the cytoskeleton was shown to be strongly attenuated in retinol- and CLA-treated cells. This correlation between the reduction in the number of FAs, the decrease in the measured YM and the lack of significant force-induced mitochondrial displacements, may point to the importance of FAs in maintaining the mechanical prestress in the cell, and the direct effect that retinol and CLA have on it.

The findings from treatments with a combination of retinol and CLA support the view that CLA acts by enhancing the effects of retinol. Previous studies have shown that CLA treatment can lead to an increase in retinol levels (Carta, G. *et al.*, 2002). Thus,

exposure to CLA could act to enhance levels of cellular retinol and we suggest that this could explain the additive effect of the treatment with a combination of the two compounds.

The significant decrease in YM following the treatments was also observed when using a spherical indenter rather than a pyramidal tip, where indentation with a sphere covers a larger surface area (>10 μm^2). The results were similar to those of pyramidal tip indentation, showing that the decrease in stiffness following the treatments is measurable. The decrease in the average number of FAs per cell has clear impacts on the mechanical properties of the cell over a range of spatial scales. Reduction in cell stiffness can be attributed to several factors, including changes in cell shape, the plasma membrane or cytoskeleton (or combinations thereof). Previous studies have shown that treatment with the actin-disrupting drug, CytD, leads to a significant decrease in cell stiffness as well as changes in cell morphology (Charras, G.T. & Horton, M.A., 2002b; Pelling, A.E. & Veraitch, F.S. *et al.*, 2007; Rotsch, C. & Radmacher, M., 2000). However, retinol and CLA treatments in our study did not show an obvious disruption of the actin cytoskeleton, yet led to a similar decrease in cell stiffness. The decrease in cell stiffness was therefore driven by a concomitant increase in cell height and a decrease in the number of FAs per cell. Staining for FAs showed a significant decrease in their number per cell. This relationship between FAs and cell stiffness may point to the important role FAs have on governing cell adhesion and consequently the material properties of the cell. The loss of FAs, which are mechanically linked to actin stress fibres, could lead to a reduction in actin tension and an increase in cell height which drives a decrease in the observed cell stiffness. This was followed by a decrease in the efficacy of force propagation through

the cytoskeleton, as was evident from the measurements of mitochondrial displacements following AFM indentations. A complex interplay between cell morphology, mechanics and adhesion was previously shown, where in a feedback-like mechanism an increase in cytoskeleton tension was correlated with induced assembly of FAs and cell spreading (Chen, C.S. *et al.*, 2003)

Although the exact mechanism in which retinol acts to disrupt FA formation is unclear, a possible route that has been previously suggested is the effect it has on fibronectin synthesis: RA has been shown to inhibit the synthesis of fibronectin in 3T3 fibroblasts in a dose-dependent manner (Luigi M. De Luca, G.S., Jun Takatsuka,, 1997; Scita, G. *et al.*, 1996) . In addition, adhesion to the substrate was also reduced following treatments with RA, together with a decrease in ability of cells to reattach and spread (Varani, J. *et al.*, 1989). This decrease in fibronectin secretion by the cell could lead to reduction in FAs, which would then lead to the mechanical effects observed here. Previous studies observed various biological effects of retinol on the living cell. Here, by employing a combination of AFM and fluorescence microscopy, we have shown how treatments with retinol and CLA have implications not only on cell biology and gene expression, but also a direct effect on the mechanical properties of treated cells. Retinol has an effect on proliferation, differentiation and apoptosis (Chambon, P., 1996; Napoli, J.L., 1996), which have also been linked to cell mechanics and the mechanical properties of the microenvironment (Engler, A.J. *et al.*, 2006; Paszek, M.J. *et al.*, 2005). Therefore, understanding the interplay between retinol and cell nanomechanics may help to illuminate some of the underlying nanomechanical mechanisms linked to these vital biological pathways.

Our results reveal a mechanistic understanding of how these naturally occurring compounds may regulate the cell adhesion cascade and their possible role in governing tissue function. Their roles in the pathogenesis of several diseases suggest that exploring the link between cell adhesion and disease, via the manipulation of the CLA-retinol pathway, may be a valuable route to the development of new therapeutics. This is particularly so for those conditions in which a mechanical element is apparent in the regulation of normal tissue physiology and disease pathogenesis such as vascular and bone diseases and tumour cell spread.

5.5 References

A-Hassan E., Heinz W.F., Antonik M.D., D'Costa N.P., Nageswaran S., Schoenenberger C.-A.,Hoh J.H. 1998. Relative microelastic mapping of living cells by atomic force microscopy. *Biophys. J.* 74:1564-1578.

Anzano M.A., Byers S.W., Smith J.M., Peer C.W., Mullen L.T., Brown C.C., Roberts A.B.,Sporn M.B. 1994. Prevention of breast-cancer in the rat with 9-cis-retinoic acid as a single-agent and in combination with tamoxifen. *Cancer Research* 54:4614-4617.

Balaban N.Q., Schwarz U.S., Riveline D., Goichberg P., Tzur G., Sabanay I., Mahalu D., Safran S., Bershadsky A., Addadi L.,Geiger B. 2001. Force and focal adhesion assembly: A close relationship studied using elastic micropatterned substrates. 3:466-472.

Balaban N.Q., Schwarz U.S., Riveline D., Goichberg P., Tzur G., Sabanay I., Mahalu D., Safran S., Bershadsky A., Addadi L.,Geiger B. 2001. Force and focal adhesion assembly: A close relationship studied using elastic micropatterned substrates. *Nature Cell Biology* 3:466-472.

Balmer J.E.,Blomhoff R. 2002. Gene expression regulation by retinoic acid. *J. Lipid Res.* 43:1773-1808.

Banni S., Angioni E., Casu V., Melis M.P., Scrugli S., Carta G., Corongiu F.P.,Ip C. 1999. An increase in vitamin a status by the feeding of conjugated linoleic acid. *Nutrition and Cancer-an International Journal* 33:53-57.

Benoît Robert Y.L. 2006. Anteroposterior patterning in the limb and digit specification: Contribution of mouse genetics. *Developmental Dynamics* 235:2337-2352.

Bhattacharya A., Banu J., Rahman M., Causey J.,Fernandes G. 2006. Biological effects of conjugated linoleic acids in health and disease. *The Journal of nutritional biochemistry* 17:789-810.

Binnig G., Quate C.F.,Gerber C. 1986. Atomic force microscope. *Physical Review Letters* 56:930-933.

Burridge K.,Chrzanowska-Wodnicka M. 1996. Focal adhesions, contractility, and signaling. *Annual Review of Cell and Developmental Biology* 12:463-518.

Butz D.E., Li G., Huebner S.M.,Cook M.E. 2007. A mechanistic approach to understanding conjugated linoleic acid's role in inflammation using murine

models of rheumatoid arthritis. *American Journal of Physiology-Regulatory Integrative and Comparative Physiology* 293:R669-R676.

Carla Rozzo V.C., Gianluca Caridi, Gabriella Pagnan, Mirco Ponzoni,. 1997. Induction of apoptosis in human neuroblastoma cells by abrogation of integrin-mediated cell adhesion. *International Journal of Cancer* 70:688-698.

Carta G., Angioni E., Murru E., Melis M.P., Spada S.,Banni S. 2002. Modulation of lipid metabolism and vitamin a by conjugated linoleic acid. *Prostaglandins, Leukotrienes and Essential Fatty Acids* 67:187-191.

Chambon P. 1996. A decade of molecular biology of retinoic acid receptors. *FASEB J.* 10:940-954.

Charras G.T.,Horton M.A. 2002a. Determination of cellular strains by combined atomic force microscopy and finite element modeling. *Biophys. J.* 83:858-879.

Charras G.T.,Horton M.A. 2002b. Single cell mechanotransduction and its modulation analyzed by atomic force microscope indentation. *Biophys. J.* 82:2970-2981.

Chen B.-Q., Yang Y.-M., Wang Q., Gao Y.-H., Liu J.-R., Zhang J.-S., Wang X.-L.,Liu R.-H. 2004. Effects of c9,t11-conjugated linoleic acid on adhesion of human gastric carcinoma cell line sgc-7901. *World J Gastroenterol* 10:

Chen C.S., Alonso J.L., Ostuni E., Whitesides G.M.,Ingber D.E. 2003. Cell shape provides global control of focal adhesion assembly. *Biochemical and Biophysical Research Communications* 307:355-361.

Das U.N. 2000. Essential fatty acids and osteoporosis. *Nutrition (Burbank, Los Angeles County, Calif.)* 16:386-390.

DeLany J.P.,West D.B. 2000. Changes in body composition with conjugated linoleic acid. *J Am Coll Nutr* 19:487S-493.

Engler A.J., Sen S., Sweeney H.L.,Discher D.E. 2006. Matrix elasticity directs stem cell lineage specification. *Cell* 126:677-689.

Evans M.E., Brown J.M.,McIntosh M.K. 2002. Isomer-specific effects of conjugated linoleic acid (cla) on adiposity and lipid metabolism. *The Journal of nutritional biochemistry* 13:508-516.

Fisher G.J., Datta S.C., Talwar H.S., Wang Z.-Q., Varani J., Kang S.,Voorhees J.J. 1996. Molecular basis of sun-induced premature skin ageing and retinoid antagonism. 379:335-339.

Fisher G.J., Kang S., Varani J., Bata-Csorgo Z., Wan Y., Datta S.,Voorhees J.J. 2002. Mechanisms of photoaging and chronological skin aging. *Arch Dermatol* 138:1462-1470.

Glick A.B., Flanders K.C., Danielpour D., Yuspa S.H.,Sporn M.B. 1989. Retinoic acid induces transforming growth factor-beta-2 in cultured keratinocytes and mouse epidermis. *Cell Regulation* 1:87-97.

Haupt B.J., Pelling A.E.,Horton M.A. 2006. Integrated confocal and scanning probe microscopy for biomedical research. *TheScientificWorldJOURNAL* 6:1609-1618.

Huang M., Ye Y., Chen S., Chai J., Lu J., Zhoa L., Gu L.,Wang Z. 1988. Use of all-trans retinoic acid in the treatment of acute promyelocytic leukemia. *Blood* 72:567-572.

Hubbard N.E., Lim D.,Erickson K.L. 2007. Conjugated linoleic acid alters matrix metalloproteinases of metastatic mouse mammary tumor cells. *J. Nutr.* 137:1423-1429.

Humphries J.D., Wang P., Streuli C., Geiger B., Humphries M.J.,Ballestrem C. 2007. Vinculin controls focal adhesion formation by direct interactions with talin and actin. *J. Cell Biol.* 179:1043-1057.

Hynes R.O. 1992. Integrins: Versatility, modulation, and signaling in cell adhesion. *Cell* 69:11-25.

Ingber D. 1991. Integrins as mechanochemical transducers. *Current Opinion in Cell Biology* 3:841-848.

Ingber D.E. 2003. Tensegrity ii. How structural networks influence cellular information processing networks. *Journal of Cell Science* 116:1397-1408.

Jing Y.,Waxman S. (2007). The design of selective and non-selective combination therapy for acute promyelocytic leukemia. In *Acute promyelocytic leukemia: Molecular genetics, mouse models and targeted therapy*, Vol. 313, pp. 245-269. SPRINGER-VERLAG BERLIN, Berlin.

Kafi R., Kwak H.S.R., Schumacher W.E., Cho S.Y., Hanft V.N., Hamilton T.A., King A.L., Neal J.D., Varani J., Fisher G.J., Voorhees J.J.,Kang S.W. 2007. Improvement of naturally aged skin with vitamin a (retinol). *Archives of Dermatology* 143:606-612.

Kang S.W., Duell E.A., Fisher G.J., Datta S.C., Wang Z.Q., Reddy A.P., Tavakkol A., Yi J.Y., Griffiths C.E.M., Elder J.T.,Voorhees J.J. 1995. Application of retinol to human skin in-vivo induces epidermal hyperplasia and cellular retinoid-binding proteins characteristic of retinoic acid but without measurable retinoic acid levels or irritation. *Journal of Investigative Dermatology* 105:549-556.

Kim H.,Wolf G. 1987. Vitamin a deficiency alters genomic expression for fibronectin in liver and hepatocytes. *J. Biol. Chem.* 262:365-371.

Kim H.J., Bogdan N.J., Dagostaro L.J., Gold L.I.,Bryce G.F. 1992. Effect of topical retinoic acids on the levels of collagen messenger-rna during the repair of uvb-

induced dermal damage in the hairless mouse and the possible role of tgf-beta as a mediator. *Journal of Investigative Dermatology* 98:359-363.

Kojima H., Ishijima A.,Yanagida T. 1994. Direct measurement of stiffness of single actin filaments with and without tropomyosin by in vitro nanomanipulation. *Proceedings of the National Academy of Sciences of the United States of America* 91:12962-12966.

Lampen A., Leifheit M., Voss J.,Nau H. 2005. Molecular and cellular effects of cis-9, trans-11-conjugated linoleic acid in enterocytes: Effects on proliferation, differentiation, and gene expression. *Biochimica et Biophysica Acta (BBA) - Molecular and Cell Biology of Lipids* 1735:30-40.

Levin A.A., Sturzenbecker L.J., Kazmer S., Bosakowski T., Huselton C., Allenby G., Speck J., ratzeisen C., Rosenberger M., Lovey A.,Grippo J.F. 1992. 9-cis retinoic acid stereoisomer binds and activates the nuclear receptor rxr[alpha]. 355:359-361.

Levy R.,Maaloum M. 2002. Measuring the spring constant of atomic force microscope cantilevers: Thermal fluctuations and other methods. *Nanotechnology* 13:33-37.

Lotan R. 1996. Retinoids in cancer chemoprevention. *FASEB J.* 10:1031-1039.

Luigi M. De Luca G.S., Jun Takatsuka,. 1997. Retinoic acid downregulates growth, fibronectin and rar-alpha: In 3t3 cells: Ha-ras blocks this response and ra metabolism. *Journal of Cellular Physiology* 173:297-300.

Maden M. 2002. Retinoid signalling in the development of the central nervous system. *Nature Reviews Neuroscience* 3:843-853.

Maniotis A.J., Chen C.S.,Ingber D.E. 1997. Demonstration of mechanical connections between integrins cytoskeletal filaments, and nucleoplasm that stabilize nuclear structure. *Proceedings of the National Academy of Sciences of the United States of America* 94:849-854.

Margaret Clagett-Dame E.M.M., Parag D. Muley,. 2006. Role of all-trans retinoic acid in neurite outgrowth and axonal elongation. *Journal of Neurobiology* 66:739-756.

Marill J., Idres N., Capron C.C., Nguyen E.,Chabot G.G. 2003. Retinoic acid metabolism and mechanism of action: A review. *Current Drug Metabolism* 4:1-10.

Miyamoto S., Teramoto H., Coso O., Gutkind J., Burbelo P., Akiyama S.,Yamada K. 1995. Integrin function: Molecular hierarchies of cytoskeletal and signaling molecules. *J. Cell Biol.* 131:791-805.

Moya-Camarena S.Y.,Belury M.A. 1999. Species differences in the metabolism and regulation of gene expression by conjugated linoleic acid. *Nutrition Reviews* 57:336-340.

Napoli J. 1996. Retinoic acid biosynthesis and metabolism. *FASEB J.* 10:993-1001.

Napoli J.L. 1996. Biochemical pathways of retinoid transport, metabolism, and signal transduction. *Clinical Immunology and Immunopathology* 80:S52-S62.

O'Shea M., Bassaganya-Riera J.,Mohede I.C.M. 2004. Immunomodulatory properties of conjugated linoleic acid. *American Journal of Clinical Nutrition* 79:1199S-1206S.

Pankov R.,Yamada K.M. 2002. Fibronectin at a glance. *J Cell Sci* 115:3861-3863.

Pariza M.W., Park Y.,Cook M.E. 2000. Mechanisms of action of conjugated linoleic acid: Evidence and speculation. *Proc Soc Exp Biol Med* 223:8-13.

Paszek M.J., Zahir N., Johnson K.R., Lakins J.N., Rozenberg G.I., Gefen A., Reinhart-King C.A., Margulies S.S., Dembo M., Boettiger D., Hammer D.A.,Weaver V.M. 2005. Tensional homeostasis and the malignant phenotype. *Cancer Cell* 8:241-254.

Pelling A.E., Dawson D.W., Carreon D.M., Christiansen J.J., Shen R.R., Teitell M.A.,Gimzewski J.K. 2007. Distinct contributions of microtubule subtypes to cell membrane shape and stability. *Nanomedicine* 3:43-52.

Pelling A.E., Nicholls B.M., Silberberg Y.R.,Horton M.A. (2007). Approaches for investigating mechanobiological dynamics in living cells with fluorescence and atomic force microscopies. In *Modern research and educational topics on microscopy* (Méndez-Vilas, A. & Díaz, J., eds.), Vol. 3, pp. 3-10. Formatex.

Pelling A.E., Veraitch F.S., Chu C.P.K., Nicholls B.M., Hemsley A.L., Mason C.,Horton M.A. 2007. Mapping correlated membrane pulsations and fluctuations in human cells. *Journal of Molecular Recognition* 20:467-475.

Polte T.R., Eichler G.S., Wang N.,Ingber D.E. 2004. Extracellular matrix controls myosin light chain phosphorylation and cell contractility through modulation of cell shape and cytoskeletal prestress. *Am J Physiol Cell Physiol* 286:C518-528.

Radmacher M., Fritz M.,Hansma P.K. 1995. Imaging soft samples with the atomic-force microscope - gelatin in water and propanol. *Biophysical Journal* 69:264-270.

Redlich C., Delisser H.,Elias J. 1995. Retinoic acid inhibition of transforming growth factor-beta-induced collagen production by human lung fibroblasts. *Am. J. Respir. Cell Mol. Biol.* 12:287-295.

Ringseis R., Gahler S.,Eder K. 2008. Conjugated linoleic acid isomers inhibit platelet-derived growth factor-induced nf-îºb transactivation and collagen formation in human vascular smooth muscle cells. *European Journal of Nutrition* 47:59-67.

Rotsch C.,Radmacher M. 2000. Drug-induced changes of cytoskeletal structure and mechanics in fibroblasts: An atomic force microscopy study. *Biophys. J.* 78:520-535.

Scita G., Darwiche N., Greenwald E., Rosenberg M., Politi K.,De Luca L.M. 1996. Retinoic acid down-regulation of fibronectin and retinoic acid receptor alpha proteins in nih-3t3 cells. *J. Biol. Chem.* 271:6502-6508.

Scita G.,Wolf G. 1994. Retinoic acid and beta-carotene inhibit fibronectin synthesis and release by fibroblasts; antagonism to phorbol ester. *Carcinogenesis* 15:1043-1048.

Sneddon A.A., McLeod E., Wahle K.W.J.,Arthur J.R. 2006. Cytokine-induced monocyte adhesion to endothelial cells involves platelet-activating factor: Suppression by conjugated linoleic acid. *Biochimica Et Biophysica Acta-Molecular and Cell Biology of Lipids* 1761:793-801.

Song H.J., Grant I., Rotondo D., Mohede I., Sattar N., Heys S.D.,Wahle K.W.J. 2005. Effect of cla supplementation on immune function in young healthy volunteers. *European Journal of Clinical Nutrition* 59:508-517.

Song H.J., Sneddon A.A., Barker P.A., Bestwick C., Choe S.N., McClinton S., Grant I., Rotondo D., Heys S.D.,Wahle K.W.J. 2004. Conjugated linoleic acid inhibits proliferation and modulates protein kinase c isoforms in human prostate cancer cells. *Nutrition and Cancer-an International Journal* 49:100-108.

Spom M.B.,Roberts A.B. 1983. Role of retinoids in differentiation and carcinogenesis. *Cancer Res* 43:3034-3040.

Toomey S., Harhen B., Roche H.M., Fitzgerald D.,Belton O. 2006. Profound resolution of early atherosclerosis with conjugated linoleic acid. *Atherosclerosis* 187:40-49.

Varani J., Nickoloff B.J., Dixit V.M., Mitra R.S.,Voorhees J.J. 1989. All-trans retinoic acid stimulates growth of adult human keratinocytes cultured in growth factor-deficient medium, inhibits production of thrombospondin and fibronectin, and reduces adhesion. *Journal of Investigative Dermatology* 93:449-454.

Vicente-Manzanares M., Choi C.K.,Horwitz A.R. 2009. Integrins in cell migration - the actin connection. *J Cell Sci* 122:199-206.

Wang N., Butler J.P.,Ingber D.E. 1993. Mechanotransduction across the cell-surface and through the cytoskeleton. *Science* 260:1124-1127.

Ward S.J.,Morriss-Kay G.M. 1997. The functional basis of tissue-specific retinoic acid signalling in embryos. *Seminars in Cell & Developmental Biology* 8:429-435.

Watkins B.A.,Seifert M.F. 2000. Conjugated linoleic acid and bone biology. *Journal of the American College of Nutrition* 19:478S-486S.

Weiss J.S., Ellis C.N., Headington J.T., Tincoff T., Hamilton T.A.,Voorhees J.J. 1988. Topical tretinoin improves photoaged skin. A double-blind vehicle-controlled study. *JAMA* 259:527-532.

Whigham L.D., Cook M.E.,Atkinson R.L. 2000. Conjugated linoleic acid: Implications for human health. *Pharmacological Research* 42:503-510.

Zulet M.A., Marti A., Parra M.D.,Martinez J.A. 2005. Inflammation and conjugated linoleic acid: Mechanisms of action and implications for human health. *Journal of Physiology and Biochemistry* 61:483-494.

Chapter 6

Conclusions and Future Prospects

In this thesis I presented quantitative approaches for investigating and evaluating force transmission in live cells. The use of single particle tracking techniques to measure intracellular displacements and reorganisations in response to extracellular perturbations, combined with real-time information about local and global stiffness variations, not only will allow better understanding of force transmission in live, normal cells but may also prove useful for diagnosis of the cell 'state' in health and disease. The correlation between force transmission, cell stiffness and adhesion emphasizes the dependency of the different cellular components on each other and the complex interplay between them.

Chapters 2 and 3 presented the techniques and methodology used for visualising deformations of the intracellular cytoskeleton and displacements of organelles in response to local indentations applied by the AFM. Two different approaches for the quantification of intracellular displacements were presented: the fluid registration analysis and the feature point tracking algorithm. The application of local AFM perturbations were found to increase mitochondrial displacement by ~40% compared to their basal displacement, demonstrating the effect of force transmission in live cells.

In Chapter 4 I combined information from stiffness measurements (both localised and global) together with single particle tracking in order to investigate the role of the cytoskeleton in the long-distance propagation of forces through the cell. The lack of increase in mitochondrial displacements following AFM indentation in cells where the cytoskeleton was disrupted pointed out the essential role an intact cytoskeletal network

has in the propagation of stress. Moreover, similar results were observed for both microtubule disruption and actin cytoskeleton disruption, suggesting that both cytoskeletal components are equally essential for effective force propagation.

In Chapter 5 I investigated the effect retinol and conjugated linoleic acid (CLA) have on various cellular properties: stiffness of the cell was evaluated by measuring the change in Young's modulus following treatments with the compounds; adhesion to the substrate was assessed by staining and quantifying of focal adhesions and measurements of cell height; finally, the ability of the cells to propagate forces was evaluated by tracking displacements of mitochondria in response to perturbations. Treatment of the two compounds in combination proved to be highly effective in both reducing the stiffness of treated cells (~50%) and in attenuating the displacement of mitochondria in response to applied force. These two observations were similar to those seen for cells treated with cytoskeletal disrupting drugs CytD and nocodazole (Chapter 4). However, the mechanism of action is different, as the cytoskeleton was not disrupted in this case. Rather, a decrease in FAs was observed. These results suggest that the existence of cytoskeletal network by itself might not be enough for intracellular force transmission; the crucial role of focal adhesions in maintaining the adherence of the cell to the surface may also have a direct effect on the transduction and propagation of force through the cytoskeleton, perhaps by helping to keep it under constant prestress. However, more research needs to be done in order to understand the interrelations between the different cellular components.

Future prospects

The methodology presented in this study employs a quantitative single particle tracking techniques to measure intracellular reorganisation in response to extracellular perturbation, combined with real-time information about the local and global variations in stiffness. This study demonstrated a correlation between the decrease in organelle displacement (both natural and force-induced movement) and the reduction in cell stiffness. This technique might provide useful insights into the way forces are transmitted through the cell and perhaps enable a way to evaluate cytoskeletal integrity and tension by way of its effectiveness to transmit force and from the correlation to the measured variations in cell stiffness. It might also prove useful in the diagnosis of cellular conditions in health and disease, where correlations between cell state and organelle motility may be made.

Quantifying the direction of mitochondrial displacements in respect to the nucleus (the point of indentation) can give an indication of the directionality of force propagation in the cell (after subtracting the baseline of basal mitochondrial displacement). Also, quantifying the displacement as function of distance from the indentation point can give indication of the transduction efficacy and degree of force dissipation. It would be very interesting to compare force-induced displacements of mitochondria with that of fluorescent beads or quantum dots on or inside the same cell. Another interesting experiment would be to compare the displacement of force-induced mitochondria with that of embedded beads in a flexible substrate (such as in the traction force microscopy technique). This could be used to investigate the proportion of force that is transmitted through the cell compared with that exerted by the cell onto the extracellular matrix. In

other words, how much of the mechanical force received by the cell is propagated onwards to surrounding cells or the ECM.

The methodology presented here, being relatively straight forward to implement, could eventually be up-scaled and used for diagnosis of multi-cellular aggregates and whole tissues: combining single particle tracking of fluorescent markers, or even non-invasive indicators such as surface-bound beads, together with localised stiffness measurement (a single indentation could be used both for exerting a perturbation and for measuring Young's modulus), may provide important information about cell and tissue condition and integrity. Combining AFM with high-speed confocal microscopy imaging will allow real-time 3D visualization of the distribution and propagation of forces through the living cell, which can then be fitted with mechanical models of the cell and significantly contribute to our understanding of cell biophysics.